SR-Site Data report

THM modelling of buffer, backfill and other system components

Mattias Åkesson, Lennart Börgesson, Ola Kristensson
Clay Technology AB

March 2010

SKB

SR-Site Data report

THM modelling of buffer, backfill and other system components

Mattias Åkesson, Lennart Börgesson, Ola Kristensson
Clay Technology AB

March 2010

Update notice

The original report, dated March 2010, was found to contain both factual and editorial errors which have been corrected in this updated version. The corrected factual errors are presented below.

Updated 2013-12

Location	Original text	Corrected text
Page 87, Reference Dueck 2004	Hydro-mechanical properties of a water-unsaturated sodium bentonite. Lund University.	Hydro-mechanical properties of a water unsaturated sodium bentonite. Laboratory study and theoretical interpretation. Ph. D. thesis, Lund University, Sweden.
Page 88, Reference Johannesson et al. 2010	Deep repository – Engineered barrier systems. Characterization of backfill candidate material, IBECO-RWC-BF. Baclo project – phase 3, Laboratory tests.	Characterization of backfill candidate material, IBECO-RWC-BF. Baclo project – phase 3, Laboratory tests.

Abstract

This report is a supplement to the SR-Site data report and has been prepared in agreement with the SKB quality assurance instruction. Based on the issues raised in the Process reports concerning THM processes in buffer, backfill and other system components, 22 modelling tasks have been identified, representing different aspects of the repository evolution. The purpose of this data report is to provide parameter values for the materials included in these tasks. Two codes, Code_Bright and Abaqus, have been employed for the tasks. The data qualification has focused on the bentonite material for buffer, backfill and the seals for tunnel plugs and bore-holes. All these system components have been treated as if they were based on MX-80 bentonite.

The sources of information and documentation of the data qualification for the parameters for *MX-80* have been listed. A substantial part of the refinement, especially concerning parameters used for Code_Bright, is presented in the report. The data qualification has been performed through a motivated and transparent chain; from measurements, via evaluations, to parameter determinations. The measured data was selected to be as recent, traceable and independent as possible. The data sets from this process are thus regarded to be qualified.

The *conditions* for which the data is supplied, the *conceptual uncertainties*, the *spatial and temporal variability* and *correlations* are briefly presented and discussed. A more detailed discussion concerning the *data uncertainty due to precision, bias and representativity* is presented for measurements of swelling pressure, hydraulic conductivity, shear strength, retention properties and thermal conductivity.

The *results from the data qualification* are presented as a detailed evaluation of measured data. In order to strengthen the relevance of the parameter values and to confirm previously used relations, either newer or independent measurements have been taken into account in the parameter value evaluation. Previously used relations for swelling pressure, hydraulic conductivity and shear strength have been re-evaluated from more recent measurements, and this have basically confirmed the previously used relations for these parameters. Independent measurements of retention properties and thermal conductivity have demonstrated the coherence of the measured data sets on which the used parameters values and tables are based. These parameters are highly significant for calculations of the hydration process, homogenisation and peak temperatures. Special emphasis has been put on the adoption of BBM mechanical parameters used in Code_Bright. The aim has been to develop a general and clear-cut method to quantify the parameters for all relevant dry densities.

Data for *other materials* (copper, cast iron, rock, EDZ, crushed rock and concrete) are more or less well defined. The main documents for the adoption of parameter values for these other material have been listed in report, but no extensive qualification process has been pursued due to the various degrees of definition for these materials. It should be noted that the modeling tasks are generally not site-specific and the variability of some parameters is handled through sensitivity analyses.

Data recommended for use in the SR-Site modelling are compiled in tables at the end of the report.

Sammanfattning

Denna rapport är ett supplement till datarapporten för SR-Site och har tagits fram i enlighet med SKB:s kvalitetssäkringsinstruktion. 22 modelleringsuppgifter som representerar olika aspekter av förvarsutvecklingen har identifierats utifrån de frågeställningar som har lyfts fram i process-rapporten för THM processer i buffert, återfyllnad och andra systemkomponenter. Syftet med denna datarapport är att tillhandahålla parametervärden för de material som ingår i dessa uppgifter. Två koder, Code_Bright och Abaqus, har använts för uppgifterna. Datakvalificeringen har fokuserat på bentonitbaserade material för buffert, återfyllnad och tätningar för tunnelpluggar och borrhål. Alla dessa systemkomponenter har behandlats som om de var baserade på MX-80 bentonit.

Informationskällorna och dokumentationen för datakvalificeringen av parametrarna för MX-80 har listats. En betydande del av utvärderingen presenteras i rapporten, i synnerhet för parametrar som används i Code_Bright. Datakvalificeringen har utförts genom en motiverad och transparant kedja; från mätningar, via utvärderingar, till parameterbestämningar. Urvalet av mätdata gjordes så att dessa är så nya, spårbara och oberoende som möjligt. Datamängderna från denna process betraktas som kvalificerade.

Villkoren för vilka data tillhandahålls, *konceptuella osäkerheter, variationer i tid och rum samt korrelationer* presenteras och diskuteras kortfattat. En mer detaljerad diskussion angående *data-osäkerhet på grund av precision, systematiska fel och representativitet* presenteras för mätningar av svälltryck, hydraulisk konduktivitet, skjuvhållfasthet, vattenhållande egenskaper och termisk konduktivitet.

Resultaten från datakvalificeringen presenteras som en detaljerad utvärdering av mätdata. Nyare eller oberoende mätningar har beaktats i utvärderingen för att på så sätt styrka relevansen för parametervärdena och för att bekräfta tidigare använda samband. Tidigare använda samband för svälltryck, hydraulisk konduktivitet och skjuvhållfasthet har utvärderats på nytt från nyare mätningar, och detta har i stort sett bekräftat tidigare använda samband för dessa parametrar. Oberoende mätningar av vattenhållande egenskaper och termisk konduktivitet har visat sig vara samstäm-miga med de datamängder på vilka de använda parametervärdena och tabellerna baseras. Dessa parametrar är av stor betydelse för beräkningar av vattenmättnadsprocessen, homogeniseringen och temperaturutvecklingen. Särskild vikt har lagts på tilldelningen av mekaniska parametrar för BBM modellen, vilken används i Code_Bright. Målet har varit att utveckla en allmän och entydig metod för att kvantifiera parametrarna för alla relevanta torrdensiteter.

Data för *andra material* (koppar, gjutjärn, berg, EDZ, krossat berg och betong) är mer eller mindre väldefinierade. Huvuddokumenten för tilldelningen av parametervärden för dessa material har listats i rapporten, men ingen omfattande kvalificeringsprocess har fullföljts eftersom vissa av dessa material inte är tydligt definierade. Det bör noteras att modelleringsuppgifterna generellt inte är platsspecifika och att variationen hos vissa parametrar hanteras genom känslighetsanalys.

Data som rekommenderas för användning inom modelleringen för SR-Site är sammanställd i tabeller i slutet av rapporten.

Contents

1   Modelling in SR-Site

This report is a supplement to the SR-Site data report /SKB 2010/. The text has been prepared in agreement with the SKB quality assurance instruction "Supplying data for the SR-Site data report", which is found in Section 2.2 of the SR-Site data report.

Based on the issues raised in the Process reports concerning THM processes in buffer, backfill and other system components, a number of modelling tasks have been identified, representing different aspects of the repository evolution. In total, 22 modelling tasks have been identified. The overall topics and objectives of these models are summarized in Table 1-1. These tasks are described in more detail in the following sections. It should be noted that these descriptions were prepared before the data qualification process and do not necessarily correspond exactly to the actual modeling work. See also Appendix A.

The purpose of this data report is to provide parameter values for these tasks. An overview of the constitutive laws used in the different tasks is shown in Table 1-2. More detailed information about the different parameters used in the different constitutive laws is given in Chapter 10. A summary of the different materials included in the different modelling tasks is given in Table 1-3.

Table 1-1. Overall topics and objectives of modelling tasks.

Topics	Modelling tasks
Homogenization models	5, 6, 7, 16, 17, 19, 20, 21, 22
Hydration calculations	2, 3,12, 14, 15
Large-scale mechanical buffer models (upward swelling, canister sinking, rock shearing)	8, 9, 10
Piping and erosion	11, 18
Sealing ability	13
Dry rock condition	4
Peak temperature calculations	1

Table 1-2. Summary of constitutive laws used in the different modelling tasks.

Task	Therm. cond.	Hydr. Cond.	Vap. diff.	Water retention curve	BBM* param.	Porous elastic & Drucker-Prager	Code*	Other models
1	X						CB	
2		X		X	(X)		CB	
3	X	X	X	X			CB	
4	X	X	X	X			CB	
5	X	X	X	X	X	X	CB/A	
6		X				X	A	
7		X		X	X		CB	
8		X		X		X	A	
9		X				X	A	Creep model
10						X	A	Shear rate model
11								Empirical model
12		X		X			CB	
13		X					CB	
14		X		X			CB	
15		X		X			CB	
16		X		X	X		CB	
17		X				X	A	
18								Special analysis
19		X				X	A	
20								Special analysis
21								Special analysis
22								Special analysis

* BBM: Barcelona Basic Model; CB: Code_Bright; A: Abaqus.

Table 1-3. Summary of materials included in the different modelling tasks.

Task	Bentonite buffer	Bentonite backfill and tunnel seal	Bentonite bore-hole seal	Concrete	Crushed rock	Rock/EDZ	Copper/ Cast iron
1	X					X	X
2		X				X	
3	X	X				X	X
4	X	X				X	X
5	X						
6	X						
7		X					
8	X	X					
9	X	X					
10	X						X*
11	X						
12		X		X	X	X	
13		X		X	X	X	
14		X			X	X	
15			X			X	
16		X		X	X		
17		X		X	X		
18	X						
19	X	(X)		X			
20			X				
21			X				
22		X					

* The mechanical properties of the canister are described in the data report for the canister.

It should be noted that the models used in the different tasks are deterministic rather than probabilistic. And the general approach to address variability is to perform sensitivity analyses of boundary conditions and single parameters rather than to vary all parameters simultaneously.

1.1 Peak temperature calculations

The objective of this task is to estimate the peak temperature in the buffer.

The criterion for a peak temperature in the bentonite of 100°C will have a large impact on the design of the entire repository since it affects the canister spacing and deposition tunnel spacing.

It will be the hottest canisters in each domain that determine the minimum canister spacing. These canisters will be found in deposition holes that are:

1. Completely dry.
2. Located in the central parts of the deposition areas.
3. Located in volumes dominated by rock with low thermal conductivity.

A thorough discussion of the buffer peak temperature calculation approach is performed in the report "*Strategy for thermal dimensioning of the final repository for spent nuclear fuel*" (the STD report), /Hökmark et al. 2009/.

Site-specific simulations, using model properties corresponding to the different sites, will be reported in the Site Engineering Reports (SER) and additional examples will be found in the Geosphere THM report. No additional peak temperature calculations will be done in this project.

In short, the approach used for determining the buffer peak temperature, T_b, uses superposition of the solutions of two sub-problems. The objective of the first sub-problem is to calculate the rock wall temperature at canister mid height T_{rw}, (see Figure 1-1). In the second sub-problem, which
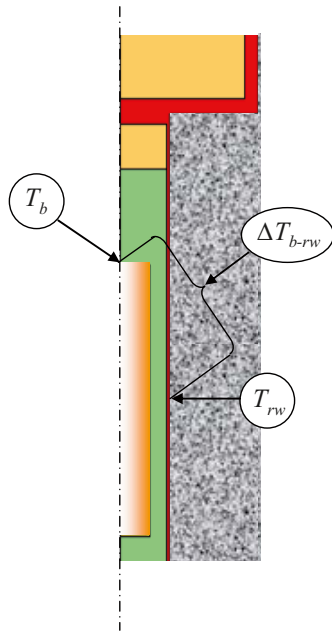
Figure 1-1. *Temperatures and temperature-difference identified when calculating the buffer peak temperature.*

connects to Task 4 in the present report, the objective is to calculate the temperature difference between the rock wall at canister mid height and the buffer at the top of the canister ΔT_{b-rw}, see (Figure 1-1).

This temperature difference, ΔT_{b-rw}, is calculated using thermal axis-symmetric 2D Code_Bright models with relevant values of thermal conductivity for the buffer. Some models use a hetero-geneous thermal conductivity field in the buffer which is evaluated from the analyses of moisture redistribution in a deposition hole situated in dry rock performed in Task 4.

In SR-Can, the corresponding problem was modelled as a radial heat flow with a constant buffer thermal conductivity and a 5 mm air-filled gap.

1.2 Analysis of time-scale of backfill hydration

The objective of this task is to analyze the time-scale to saturate the backfill. The task will be modelled with different hydraulic Code_Bright models. In the primary variation, four different geometries will be used: one 1D axis-symmetric geometry, two 2D axis-symmetric geometries with different fracture distances (6 m and 24 m), and one 2D plane geometry (PS). Two different tunnel sections will be considered: a theoretical section (Th) and a maximum fallout (MF) section. Two different approaches will be considered for the filling of the tunnels: with block and pellets materials (B&P), and with homogenized (Hom) material. Finally a number of fracture transmissivities will be considered. In the secondary variation, the effect of an EDZ, tunnel ventilation, alternative rock properties, the absence of fracture and trapped air will be investigated. An attempt to include the mechanical processes will also be made.

In SR-Can, the corresponding problem was modelled with Abaqus for a similar geometry, for similar conditions and with a similar conceptual model (the Abaqus code uses the same conceptual models for pure hydraulic problems). The modelled backfill was different than the one considered in SR-Site and three types were modelled: 30/70, Friedland and sandwich. In addition, a hydraulic axis-symmetric 1D Code_Bright model was used for analyzing the effect of trapped air.

Geometry 1: 1D axisymmetric

Symmetry axis

2.86 m

2.31 m

Geometry 2: 2D axisymmetric; 6 m fracture

Symmetry axis

10 m

3 m

2.31 m

2.86 m

Symmetry plane

Geometry 3: 2D axisymmetric; 24 m fracture

Symmetry axis

10 m

12 m

2.31 m

2.86 m

Symmetry plane

Geometry 4: 2D plane model

Symmetry plane

Fracture

120 m

20 m
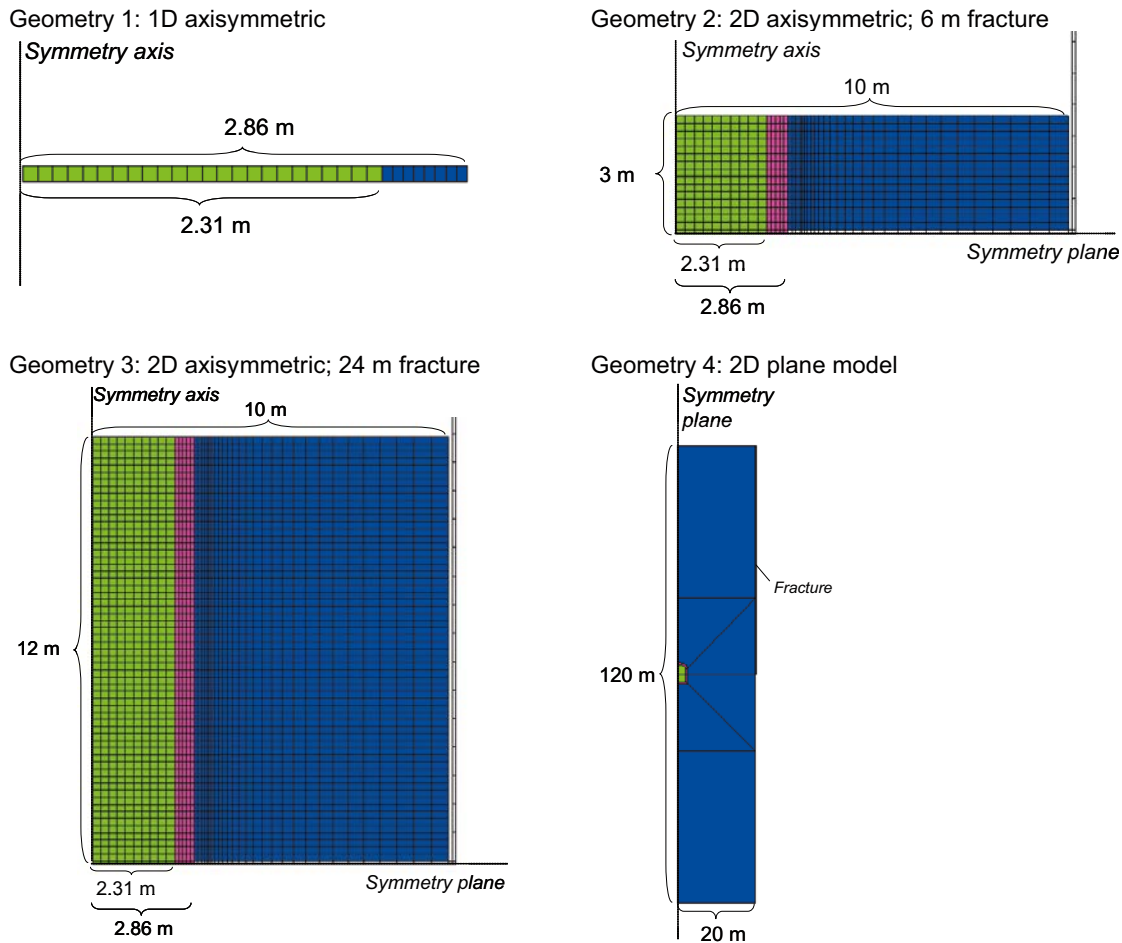
Figure 1-2. Backfill model geometries.

1.3 Analysis of time-scale of buffer hydration

The objective of this task is to estimate the time until saturation for the buffer.

The time until full water saturation approximates to the time when full swelling pressure (full sealing capacity) occurs in the buffer. The swelling pressure is an important property in this sense. Factors that may affect the time to full saturation are:

1. Fractures (transmissivity and position).
2. Rock properties (hydraulic conductivity and retention).
3. Presence of an EDZ at the bore-hole wall.
4. The initial hydraulic state at the installation of the buffer.

2D axisymmetric TH-models will be used to study the buffer hydration in a deposition hole. The geometric representation of the deposition hole is shown in Figure 1-3.

Two mechanically extreme cases will be analyzed to simplify the simulations:

1. Using initial densities for block and pellets.
2. Using a homogenized density.

This approach makes it possible to consider the influence from the mechanical process explicitly, using TH-models only, since the used extreme cases bounds the "actual" evolving mechanical state.

Two different positions of a horizontal fracture will be analyzed:

1. At canister mid-height.
2. At the tunnel.
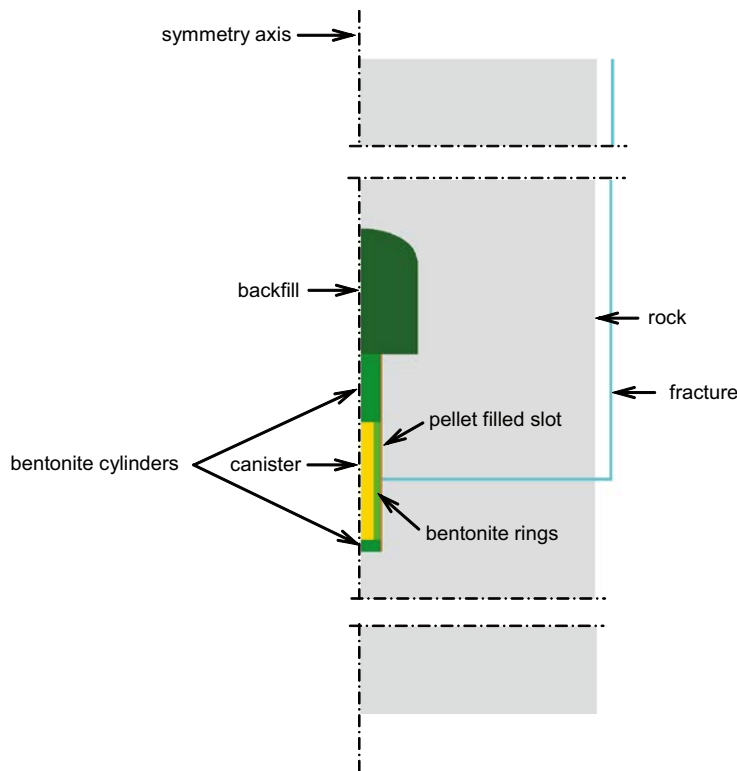
Figure 1-3. *Buffer hydration model geometry.*

The hydraulic conductivity in the rock will also be altered. The fractures will be allotted with two different transmissivities. The first tranmissivity will be calibrated to give the maximum allowed deposition hole inflow ($Q = 0.1$ l/min) and the second choice will be one tenth of the first choice. The primary variations of the models are compiled in Table 1-4.

Also some secondary cases will be investigated. The rock retention will be altered. The inflow from the fracture will also be allowed to be of a more diffuse character incorporating a more permeable layer close to the hole wall (an EDZ). Also, the initial saturation in the rock before the installation will be investigated. A prescribed RH in the tunnel will determine the initial saturation in the host rock. The secondary variations of the models are compiled in Table 1-5.

In SR-Can, the corresponding problem was modelled with Abaqus for a similar geometry and for similar conditions. The buffer was modelled to be homogenized from the beginning. In addition, the outer 10 cm of the buffer was modelled to be water saturated from the beginning. The conceptual model for vapour flow used for the Abaqus model in SR-Can, is quite different than the conceptual model that will be used for the Code_Bright model in SR-Site.

Table 1-4. Primary variations.

Buffer representation	Homogenized state (H)	Initial state (I)
Fracture position	Canister Mid Height (CMH)	Tunnel (T)
Rock conductivity	K_{high}	K_{low}
Fracture transmissivity	$T_1 = T_{0.1}$ $T_{0.1}$: $Q = 0.1$ l/min	$T_2 = T_{0.1}/10$

Table 1-5. Secondary variations.

Rock retention
Diffuse inflow (EDZ)
RH in tunnel before installation

1.4   Analysis of moisture re-distribution in dry rock

The objective of this task is two-fold:

1. To provide moisture redistribution data and thermal conductivity distributions for peak-temperature calculations.
2. To investigate the dehydration of the rock due to the ventilation of the tunnels.

A dry rock may cause drying of the buffer and subsequent wetting of the upper part of the buffer or the backfill. An important effect may be a change in thermal properties of the buffer. The resulting thermal conductivities for the buffer are used in the peak temperature calculations (Task 1). One important question is whether significant amounts of water can be lost to the rock. One approach may be to investigate what rock properties are required in order to result in significant dehydration of the buffer.

In the first subtask, the effects of a case with dry rock will be analyzed with a number of thermo-hydraulic axis-symmetric 2D Code_Bright models of the buffer and backfill with a geometric representation according to Figure 1-4.

The second subtask will be investigated through analyzing steady-state pore water pressure profiles resulting from radial inflow into a cylindrical tunnel, see Figure 1-5. Such a profile corresponds to a certain gas-filled pore volume for a given canister spacing. And if this volume is significantly smaller than the water volume in one installed buffer, then the potential dehydration of the buffer can be neglected. This analysis can be performed for a large number of parameter values describing the rock and boundary conditions.

This problem with possible drying of the buffer was not addressed in SR-Can.
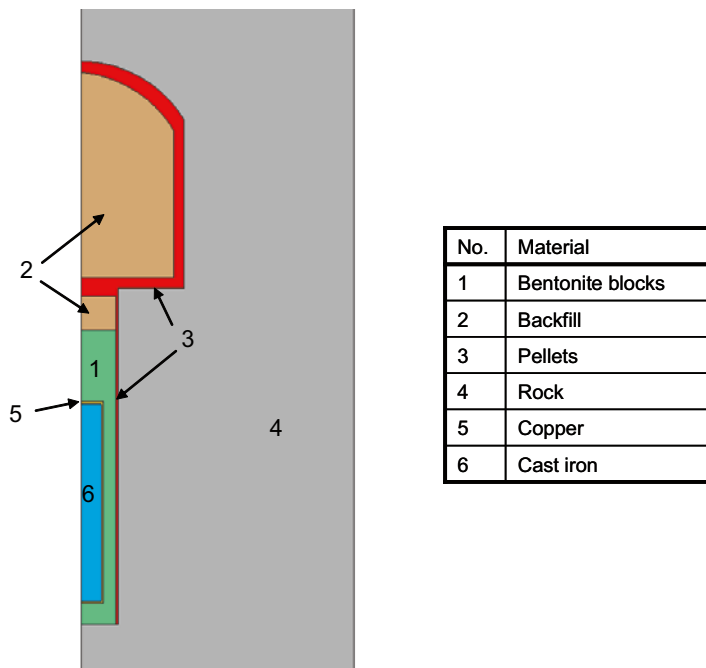

No.	Material
1	Bentonite blocks
2	Backfill
3	Pellets
4	Rock
5	Copper
6	Cast iron

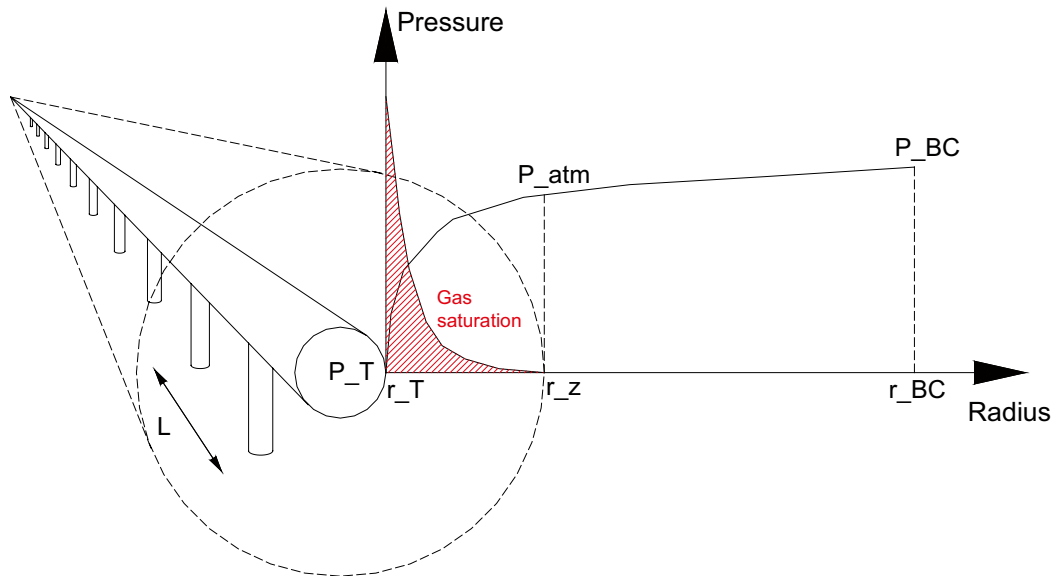**Figure 1-4.** *Geometry of dry rock model used in the first subtask.*

Figure 1-5. *Axisymmetric representation of dehydration of rock surrounding tunnel used in the second subtask. The red area represents the degree of gas saturation given by the capillary pressure (P_{atm}-P) and the retention properties.*

1.5   Natural buffer homogenisation

The objective of this task is to investigate the mechanical homogenization process when the density of the buffer homogenize due to swelling of the bentonite block, which leads to filling the inner slot and compression of the pellet filled slot. Influences of different properties of the model on the homogenization will be studied.

The Canister Retrieval Test (CRT) will here be used as the problem to model, since sensor data is available from this test and the final state (after excavation) of the experiment is also known. The CRT geometry was designed close to the present KBS-3 specifications and CRT is therefore also a suitable case to study.

In the CRT water inflow was controlled by filter-mats at the deposition hole wall, and within the canister an arrangement of heaters simulated the thermal response of spent fuel elements. After that the outer slot was filled with pellets and the filled slot subsequently filled with water. Sensor data from positions in the bentonite block close to the canister shows that the water, used when filling the pellet slot, penetrated through the block-interfaces and therefore the inner slot has some water initially.

Here the investigations will be focused on the buffer (open slot, bentonite block and pellet slot) at canister mid-height, where the processes to the greatest extent are radial. Experimental data also indicate that the processes were close to axisymmetric.

To model the canister mid-height section of the CRT, axisymmetric 1D THM models will be used, see Figure 1-6. Both Code_Bright and Abaqus will be used to obtain solutions.

The boundary pressure at the rock wall side is prescribed according to the filter pressure protocol obtained from the experiment. The thermal boundary conditions are obtained from a thermal 3D simulation made for the Engineered Barrier System (EBS) Task-Force.

Modelling the CRT experiment has been one of the assignments (assignment 2.2) considered in the EBS Task-Force project, and a Code_Bright model and an Abaqus model , both using material parameters that differ from those provided by the Data report, already exists. A model using the parameters provided by the Data report will be developed and the results from this will be compared with the existing EBS Task-Force models.
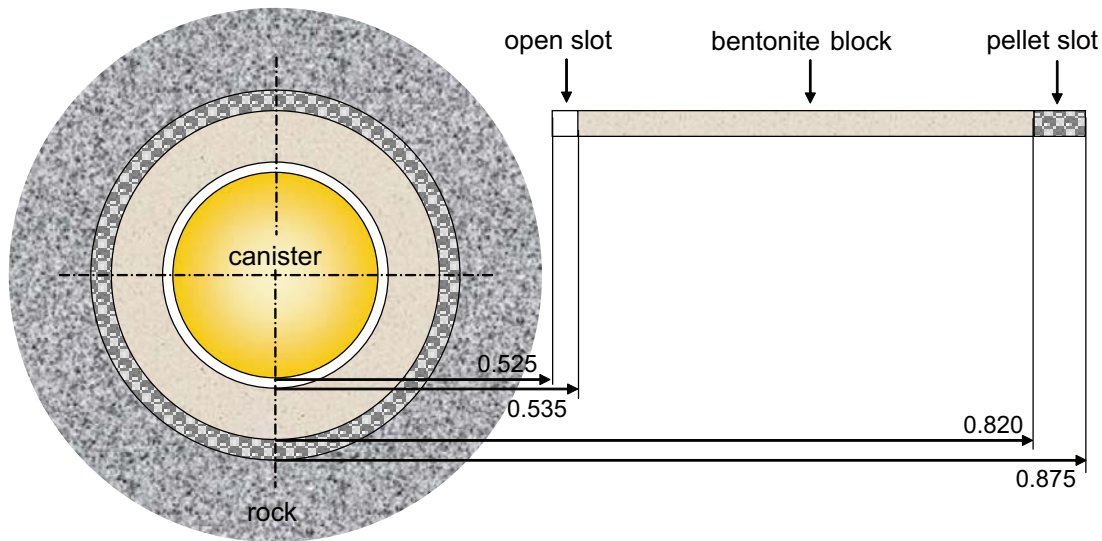
Figure 1-6. *Geometry of homogenisation models.*

In the work performed in the EBS project investigations of how different alterations of material parameters affect the solution have been performed, some of these results will be shown.

The variations of the new Code_Bright model, using the Data report parameters, concern geometry, where the difference in response from using the largest and smallest ring shaped block allowed will be studied.

In Abaqus 2D axial symmetric model will be used to study the full test. Although CRT was interrupted before full water saturation was reached above the canister, the calculation will be extended until full saturation. Since the lid on the test hole is made to displace upwards at high pressure the effect of upwards swelling will also be simulated. This case is further analysed in Task 8.

This problem was not addressed in SR-Can.

1.6   Homogenisation of erosion damages

Loss of buffer may occur both during the installation period (mechanical erosion) and in the long term via chemical erosion in fractures. The ability of the buffer to homogenise after such damage will be investigated by mainly H-M modelling of a water saturated buffer material.

Such calculations were done in SR-Can /Börgesson and Hernelind 2006B/ but the models will be checked and improved by ongoing laboratory tests if they are finished in time. Otherwise the old model will be used.

A number of new calculations will be done whereby the results of Task 11 (Piping and erosion) will be used for estimating the maximum total weight of eroded bentonite.

The homogenisation process after loss of bentonite due to erosion will be modelled with the material model of the buffer at full water saturation, i.e. the material lost will be modelled as a hole in the buffer with the volume that correspond to the dry mass lost divided to the average dry density of the buffer (1,560 kg/m^3). Several hole geometries will be modelled (entire bentonite ring, half sphere, half pipe and small pipe) via 2D-rotational symmetry models. The eroded hole will be modelled as filled with water and the calculation run until pore water equilibrium in the model is reached.

1.7   Backfill homogenisation

The objective of this task is to analyze the homogenisation of the backfill during hydration.

The task is modelled with a number of hydro-mechanical axis-symmetric 1D Code_Bright models (see Figure 1-2). The backfill consists of blocks and pellets. Two tunnel sections are considered: one with a theoretical section and one with maximum fallout. Analyses are made for cases with control-led suction evolution and, if possible, for cases with a hydraulic boundary. The influence of the shear strength will be investigated.

This problem was not modelled in SR-Can.

1.8   Buffer upward swelling

One of the main design requirements of the backfill is to keep the buffer in place and prevent it from swelling upwards so that the buffer will not loose too much of its density. Some upwards swelling is expected since the backfill has a lower swelling pressure than the buffer and a compressibility.

For SR-Can both finite element modelling and analytical calculations of this process have been performed (see e.g. /Börgesson and Johannesson 2006, Börgesson and Hernelind 2006A, Börgesson et al. 2006/), but the reference backfill considered in those calculations was an in-situ compacted mixture of 30/70 bentonite/crushed rock.

For SR-Site the new reference backfill (compacted blocks and pellets of Milos backfill) will be considered. This backfill behaves very differently in dry and wet conditions. Both cases will be modelled.

3D models of the deposition hole and the tunnel will be used. Figure 1-7 shows an example of such a model. Only a ¼ of the hole and tunnel will be included in the model since the remaining ¾ will be mirrored with symmetry planes.
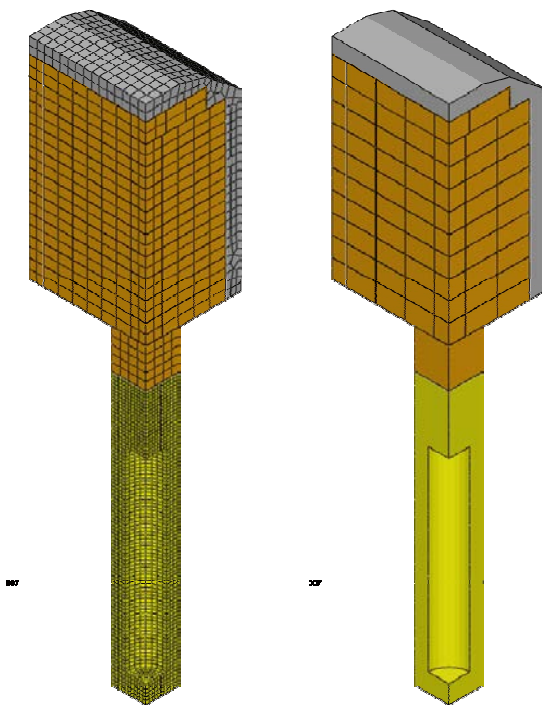

Figure 1-7. *Model geometries. Element mesh (left) and applied block configuration in the backfill (right).*

The following simplified extreme cases will be modelled:

1. Initially wet and homogeneous buffer and backfill. This case is assumed to model the final state of equilibrium after full saturation and homogenisation and does not take into account the wetting and homogenisation processes.

2. Initially wet and homogenised buffer and dry backfill. This models the extreme case that the backfill will stay dry during the entire calculation and does not take into account the wetting and homogenisation processes.

If possible, a modelling example of how the wetting and homogenisation process may affect the results will also be done. In addition, the influence of the simplified technique to have an initially saturated and homogenised buffer compared to the actual case will be done but not in these models. Instead the model used for case 5 that is also used to model the full deposition hole in the CRT (2D axial symmetric) will be used and the calculated axial plug displacement compared.

The mechanical interaction between the buffer/backfill and the rock is modelled with friction elements. The joints between the backfill blocks are modelled with 4 mm thick joint elements. The calculation is coupled hydro-mechanical without considering the thermal effects.

1.9 Canister sinking

The canister movements caused by the weight of the canister and the upward swelling of the buffer was analyzed in SR-Can /Börgesson and Hernelind 2006A/. This study is judged to be sufficient also for SR-Site so no further analyses are planned.

1.10 Rock shear through a deposition hole

When a fracture intersecting a deposition hole is affected by a nearby earthquake the fracture may slip and cause a shearing of the buffer and the enclosed canister. The magnitude of such a rock shear and the rate of rock shear displacement have been estimated to be at maximum 5 cm and 1 m/s respectively, which are stipulated as dimensioning values.

During a rock shear through a deposition hole the buffer material plays an important role to cushion the stress transfer to the canister since the buffer material is much softer than both the rock and the canister. Since the stiffness and the shear strength of the buffer material is rather low the most stressed parts of the buffer close to the shear plane will plasticize and thus only transfer a small fraction of the rock displacements to the canister. However, those properties are very sensitive to the density of the bentonite and also within the relatively small density interval accepted for the buffer material ($1,950 \text{ kg/m}^3 < \rho_m < 2,050 \text{ kg/m}^3$) the stiffness and shear strength and thus also the effect on the canister can vary substantially.

Several investigations and reports regarding the consequences of a rock shear on the canister have been made (see e.g. /Börgesson 1986, Börgesson et al. 2003, Börgesson and Hernelind 2006C/). The rock shear calculations for SR-Site are performed in a separate project as part of the safety analyses for the canister and will be reported separately. A more detailed description is given in the Task description of modelling tasks for the canister.

The material of the bentonite and the canister are modelled with von Mises' stress as a function of the strain (stress-strain model). The model is elastic-plastic with an E-modulus that determines the behaviour until the material starts yielding whereupon the plastic strain is modelled as a function of von Mises' stress and added to the elastic strain.

The rock, buffer and canister are modelled in 3D with an axial symmetry plane mirroring half the model along the canister axis. Several models with different shear plane inclinations are used. Figure 1-8 shows an example of an element model with the shear plane inclination 22.5° against the canister axis. The canister is modelled in great detail in order to catch local stresses. The shear is modelled by successively displacing the upper part of the rock along the shear plane until at least 10 cm displacement is reached. The effect of creep in the copper is also modelled using the external final stresses on the canister after completed shear as a starting point for the analysis.
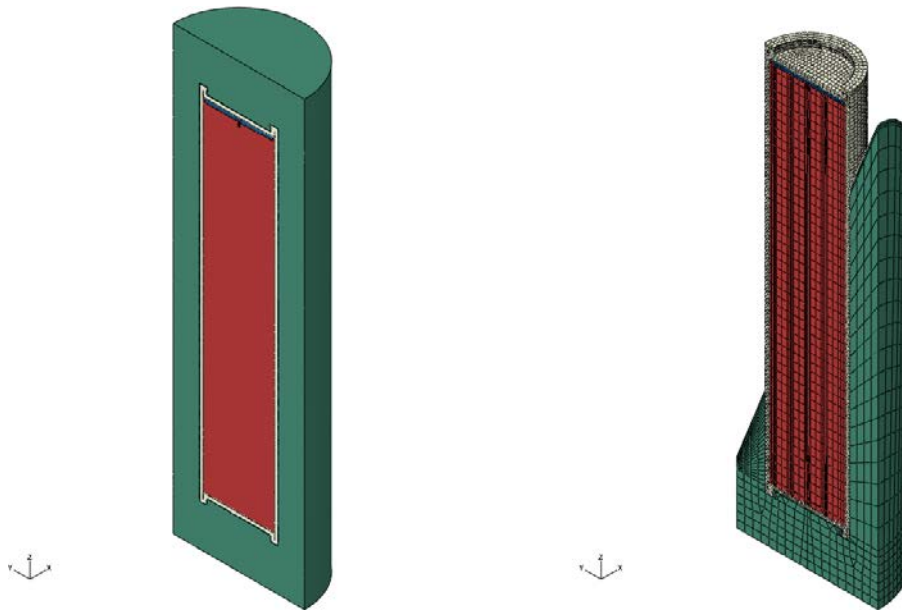
Figure 1-8. *Plot of geometry for rock shear inclined 22.5 degrees to axis of canister (left) and the element mesh with shearing part removed (right).*

1.11 Piping and erosion

Piping and subsequent erosion cannot be prevented by the pellets filling in the bufffer or the backfill. HM modelling of these processes cannot be performed due to lack of models and tools. However, ongoing measurements show that limits can be set to the effect of the erosion. A model of the erosion rate is under development and will be used to estimate the maximum erosion for different cases.

In SR-Can no calculations were done and only a brief description of the processes has been given /Börgesson and Sandén 2006/. 1–10 g dry mass of bentonite per litre eroding water was used as an estimate. The results of the new calculations will be used as basis for Task 6 (homogenisation of erosion damages).

Two main experiences are guiding the calculation of the erosion damages in the buffer and the backfill:

1. The flow pipes, resulting from piping during water inflow from the rock, will not be sealed and the flow cannot be stopped until
   a. the plug at the end of the deposition tunnel has been built and prevents outflow from the tunnel,
   b. the tunnel has been filled with water and the water pressure gradient is located across the plug.
2. There is a relation between water inflow and the amount of eroded material with decreasing erosion rate with time. This relation is derived from laboratory tests.

The dry weight of lost bentonite in both the buffer and the backfill will be calculated for different inflow scenarios.

1.12 Analysis of time-scale of plug hydration

The objective of this task is to analyze the time-scale to saturate the tunnel plug.

The time-scale to saturate the tunnel plug in general, and the seal in particular, is expected to be complex and dependent on piping and the frequency and transmissivity of fractures along the tunnel upstream the seal and the plug. However the time-scale from filling of the filter to full saturation of the seal is, on the other hand, a fairly simple and well-defined problem.
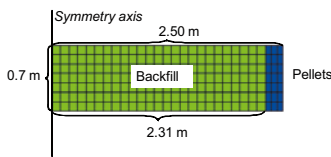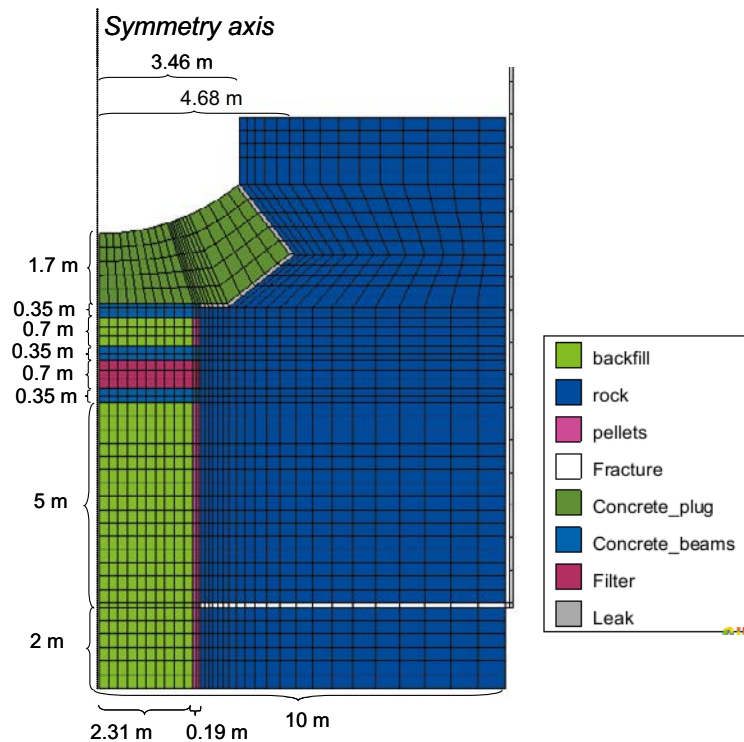
Figure 1-9. *Tunnel plug model geometries (hydraulic tasks).*

The chosen approach is therefore to calculate the time to saturate the seal, given that the filter has been filled. This is a plane 1D hydraulic problem. The block in the seal is expected to be saturated from both sides, at least to some extent, since the permeability around the concrete beams is expected to be high. A confirmation of the result from this case is thereafter sought in a number of larger hydraulic axis-symmetric 2D models.

The corresponding problem was not modelled in SR-Can.

1.13   Hydraulic modelling of the sealing ability of the tunnel plug

The objective of this task is to perform bounding calculations of the properties required for achieving an acceptable sealing ability.

The maximum allowed cumulative leakage through the plug is considered to be a certain fraction (e.g. 10%) of the available pore volume of the pellets-filled slot in the entire tunnel. Moreover, although the seal constitutes the main resistance, it will require both access to water and time to develop a high flow resistance. During this period the sealing ability will rely of the plug itself (or actually the low transmissivity between the concrete and the rock). These circumstances thus imply a relation between: i) the maximum allowed leakage, ii) the flow resistance of the plug and, iii) the time needed for the seal to become functional. The chosen approach is therefore to derive analytical expressions for this relation during different conditions. Support of these expressions is thereafter sought in a number of larger hydraulic axis-symmetric 2D models. Due to a limited ability to represent piping phenomena, these FEM models will only confirm a selection of temporary results concerning flows and pressure distribution, rather than complete analyses of the sealing process.

This process was not considered in SR-Can.
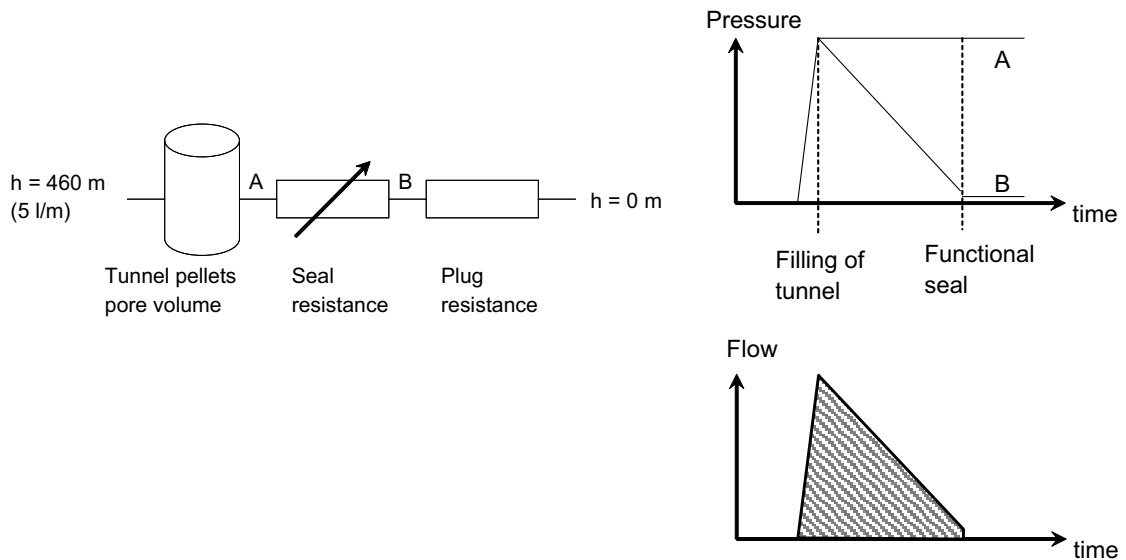
Figure 1-10. *Coupling scheme representing the main hydraulic components of the plug (left). Schematic evolution of pressures, upstream and downstream the seal, and leakage (right).*

1.14 Analysis of time-scale for hydration of central area, ramp, shaft and top seal

The objective of this task is to analyze the time-scale to saturate the central area and the ramp.

The chosen approach for this problem is to simplify the geometry as axis-symmetric. This is a fairly obvious simplification for the central area, but for the ramp it requires some further justifications and modifications. The inflow into the ramp can be assumed to be symmetric around the ramp. If the permeability of the backfill limits the inflow, it would be relevant to model the ramp as a vertical cylinder with the same section area as the tunnel. In this case, the pore volume would only be a tenth of the inclined ramp (the inclination is 10%). If, on the other hand, the permeability of the rock limits the inflow and the pore volume of the ramp thereby influences the time-scale, then it is more relevant to increase the section area with a factor of ten.
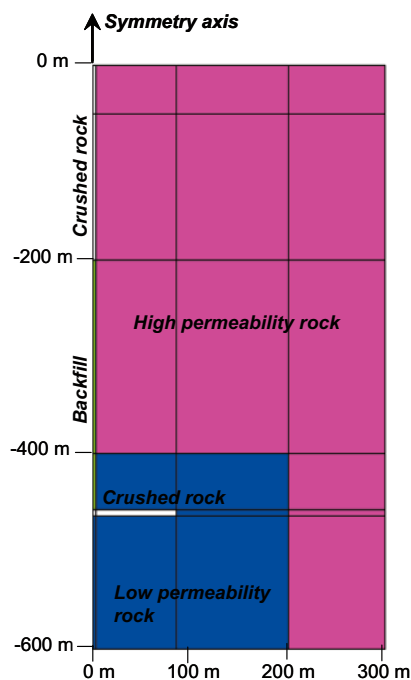
Figure 1-11. *Axis-symmetric geometry for central area and ramp.*

The task will thus be modelled with a number of large-scale hydraulic 2D models. The two extremes, with a correct ramp section area or with a correct ramp volume, will be investigated.

1.15 Analysis of the time-scale of bore-hole seal hydration

The objective is to estimate the time until full water saturation of the bore-hole seals.

The bore-hole seals consist of compacted bentonite in perforated copper tubes. Intersecting fractures will temporarily be secured with concrete fillings. At different depths the water pressure has different magnitude and will therefore pressurize the plug differently. Other conditions that may influence the saturation time are:

1. Rock hydraulic conductivity
2. Fracture frequency
3. Fracture transmissivity
4. The seal properties

The time-scale to saturate the bore-hole seals is analyzed with a number of hydraulic axisymmetric 2D Code_Bright models with or without fractures. If no fractures are considered the problem is assumed 1D axisymmetric, and if fractures are incorporated the problem become (using an assumption of a repeated representation) 2D axisymmetric, see Figure 1-12.
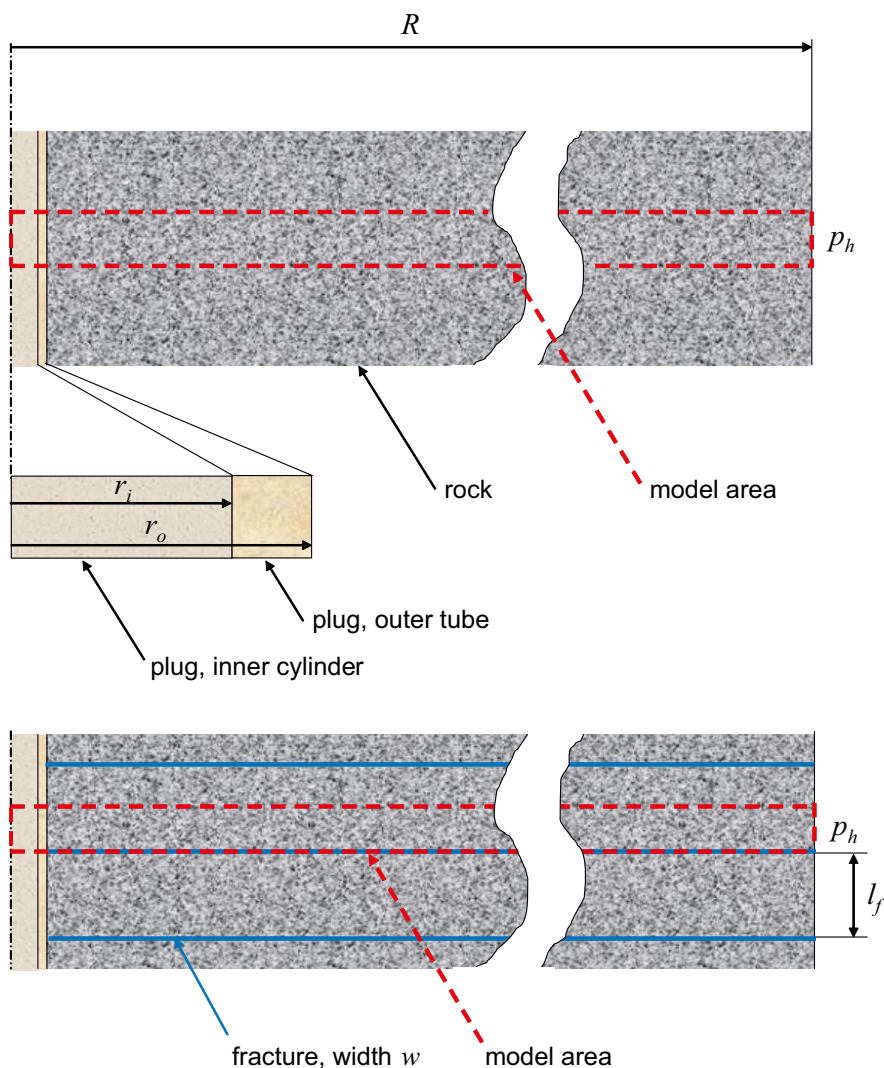
Figure 1-12. Geometry of the bore-hole seal models, without fractures (top) and with fractures (bottom).

The plug is represented by an inner cylinder (thought as located inside the copper tube) and an outer ring shaped volume (the bentonite pressed out through the perforated copper tube). The model properties are varied in terms of:

1. Depth (where the model is assumed to be located)
2. Rock conductivity
3. Plug representation (a higher or lower bound of the permeable representation)
4. Presence of fractures
5. Fracture transmissivity
6. Fracture frequency (distance between fractures)

The corresponding problem was not modelled in SR-Can.

1.16 Homogenisation of tunnel plug

The objective of this task is to analyze the homogenisation of the tunnel plug seal and to perform bounding calculations for achieving an acceptable swelling pressure on the plug.

The concrete plug is designed to withstand a swelling pressure of 2 MPa. The density of the backfill and the seal implies however a higher swelling pressure and the filter do therefore have to exhibit a certain thickness and compressibility.

The chosen approach is therefore to derive analytical relations for the required displacements of the interfaces toward the filter. A confirmation of these relations is thereafter sought in a number of hydro-mechanical axis-symmetric 2D models with controlled suction-evolution. These models are simplified is such a way that only backfill materials and filter material are included.

The corresponding problem was not modelled in SR-Can.

1.17 Backfill swelling after tunnel plug disintegration

With time the cement in the concrete plugs may be dissolved and transported away, which means that the stiffness and strength of the plugs will be dramatically reduced. This disintegration will affect the backfill material on both sides of the plug. When the plug cannot withstand the swelling pressure of the backfill it will be compressed and the backfill will swell, which leads to a loss in density and swelling pressure of the backfill. Since there is friction against the rock surface the loss in density may be significant close to the plug but will be reduced with distance from the plug. In order to understand how this affects the backfill and the location of the first deposition hole a number of FE calculations will be done.
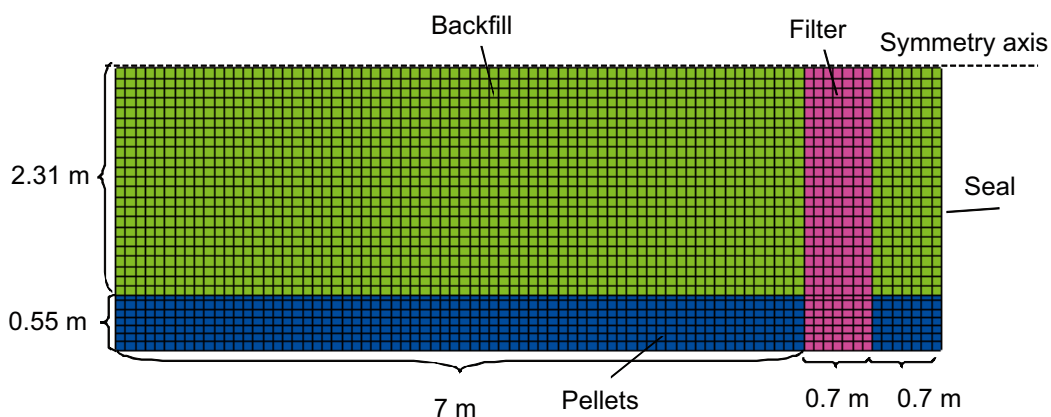
Figure 1-13. Tunnel plug model geometry (mechanical task).

The issue of penetration of bentonite into the central area will also be studied.

The corresponding problem was not modelled in SR-Can.

The main purpose of this task is to find how much the backfill density can been reduced in order to put a limit on how close to the plug the deposition hole can be located. Since no detailed knowledge of the plug status after disintegration is required only a very simplified model of the plug needs to be established. Therefore the whole plug including the clay and sand seal will be modelled as a unit with a compressibility corresponding to different plug designs. If the results appear to be critical a more detailed modelling will be performed.

The backfill will be modelled as completely homogenised and water saturated but different initial states that correspond to the expected variation in density caused mainly by the variation in rock contour will be studied. After release of initial locking the swelling of the backfill and compression of the plug will be modelled with reversed consolidation as function of time until full equilibrium is reached. The interaction between the rock and the backfill/plug will be modelled with contact elements with different friction angle.

1.18 Bottom plate 1 – Lifting of package

The objective of this task is to analyse the potential lifting of the buffer and canister package, especially during the period from the termination of the drainage to the installation of the backfill. A tailored solution will be developed for this analysis. The solution will be based on the following four assumptions:

i) The hydration of the pellets-filled slot is vertical and takes place as a distinct front, whereas the hydration of the block is radial and determined by the hydraulic properties. The hydration of blocks at a certain height starts when the slot hydration reaches this height.

ii) The build-up of swelling pressure is proportional to the extent of block hydration.

iii) The water pressure beneath the package will follow the swelling pressure at the bottom of the blocks (assumed threshold for piping). This pressure corresponds to a lifting force.

iv) The package will be lifted if this force exceeds the sum of the frictional force along the rock-wall and the weight of the package.

The problem was not modelled in SR-Can.

1.19 Bottom plate 2 – Buffer swelling after concrete disintegration

The cement in the thick concrete plate in the bottom of the deposition holes (see Figure 1-14) may with time be dissolved and transported away, which means that the stiffness and strength of the plugs will be dramatically reduced just as for the plugs. This will cause swelling and loss of density in the buffer.

The buffer swelling after concrete disintegration will be analysed in a similar way as the models with buffer upward swelling *at saturated conditions*, i.e. with Abaqus. This problem was not modelled in SR-Can.

The element model used for Task 8 (buffer upwards swelling) will also be used for this task. The modelling of case 2 in Task 8 will, after completion, be continued and also include a step with release of the bottom plate locking and continued reversed consolidation modelling. Different mechanical properties of the bottom plate will be included.
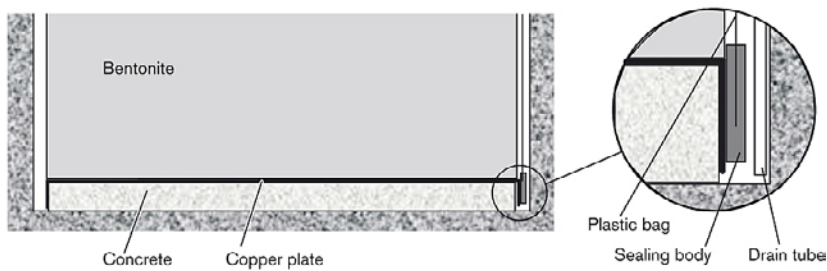
Figure 1-14. Bottom plate.

1.20 Homogenisation of bore-hole seals

The reference design of the bore-hole seals is to use highly compacted bentonite cylinders confined by a perforated copper tube in order to facilitate the installation. During wetting the bentonite will swell through the perforation and seal off the volume between tube and rock. Due to friction in the swelling bentonite the homogenization will be poor and the density of the bentonite outside the perforated tube lower than the average density. In order to study the bentonite penetration and resulting density and swelling pressure distribution outside the perforated tube analytical modelling will be done.

Theoretical models of force equilibrium for bentonite that has swelled through the perforated holes and further on between the tube and the rock surface will be derived. The models will be used to calculate the drop in density and swelling pressure at different parts of the plug.

The corresponding problem was not modelled in SR-Can.

1.21 Homogenisation of the bentonite in the bore-hole seals after loss of bentonite

If bentonite in a section of a bore-hole seal is lost to such an extent that the hole will be empty along a certain length the swelling ability of the bentonite will make the adjacent bentonite filled part swell and fill up the empty space. However, friction in the bentonite prevents complete homogenisation. The effect of such a loss needs to be investigated in order to ensure that the seal functions properly.

The swelling process will be analysed analytically in a similar way as for Task 20. A model will be derived and the results calculated for different mass lost. This process was not analysed in SR-Can.

1.22 Backfill swelling after tunnel plug disintegration 2 – omitted filling outside the plug

An improbable scenario that has been considered is that the backfilling of the central area and the transport tunnels that intersect the backfilled and plugged deposition tunnels is not executed. I.e. the plugs that end the backfilled deposition tunnels are left without any support for large parts of the life time of the repository. The consequence will be that the repository will be water filled, the plugs disintegrated and the backfill will swell without resistance from any backfill outside the plug.

After disintegration of the plug there will remain a substantial part of the components of the plug since both the sand filter and the concrete aggregate material will not dissipate but is expected to remain as a soil heap. However, since it is likely that the lack of support from a backfill outside the plug will make the particles fall down to some kind of angle of repose, there may be a large opening in the upper part of the plug where bentonite freely may swell out into the transport tunnel. Since the size of this opening is difficult to predict it will be conservatively assumed that the entire plug is lost.

The result of a free swelling of the backfill out of the deposition tunnel and into the transport tunnel will be driven by the swelling pressure of the backfill and counteracted by the friction between the backfill and the rock surface and the swelling of backfill from the other tunnels. The swelling is assumed to be similar from the other tunnels and thus stopped halfway between the deposition tunnels, i.e. the backfill cannot swell more than 20 m into the transport tunnel since the distance between the tunnels is 40 m.

There are two ways to tackle the problem. It can either be analysed in a simplified way with analytical solutions like the one used for tasks 20 and 21 or it can be modelled with FE. Attempts to do FE-calculations will be done but may encounter large problems caused by the extremely large swelling, large decrease in density and large element deformations, which may lead to numerical problems and lack of convergence.

2　Experience from SR-Can

This section gives a brief overview of the experiences from SR-Can. The description of the modelling (Section 2.1) and the sensitivity to assessment results (Section 2.2) was basically derived from the Data report for SR-Can /SKB 2006/. The limitations of SR-Can regarding these issues are summarized in Section 2.3.

2.1　Modelling in SR-Can

2.1.1　Thermal

The thermal properties of the buffer material were used in the thermal analysis for the repository where the temperature at the surface and in the interior of the canister is determined together with the temperature distribution in the bentonite and in the rock. These calculations were in SR-Can assessment performed by assuming isotropic thermal properties of the repository and considering the canister as a point source term /Hedin 2004/.

Thermal properties were also needed for analysis of the hydraulic and mechanical (THM) behaviour of the buffer and backfill material. These calculations required more detailed data than those used for the bounding calculations mentioned above.

2.1.2　Hydro-mechanical

The hydraulic and mechanical properties of the buffer and the backfill were included in the material models used for performance analyses in different calculations used for SR-Can. Example of such calculations are:

- Water saturation phase of buffer and backfill (see e.g. /Börgesson and Hernelind 1999, Hökmark 2004, Börgesson et al. 2006/).
- Canister displacement /Börgesson and Hernelind 2006A/.
- Rock shear through a deposition hole /Börgesson et al. 2003, Börgesson and Hernelind 2006C/.
- Homogenization of erosion damages /Börgesson and Hernelind 2006B/.
- Buffer upward swelling (see e.g. /Börgesson and Johannesson 2006, Johannesson and Nilsson 2006/).

Since different phenomena were studied and different assumptions were used in these calculations the material data may have differed. A common simplification was that no account was taken of the initial radial gaps between the buffer and the rock and canister and the resulting inhomogeneities. The buffer and the backfill were assumed to initially be completely homogeneous with exception of the upwards swelling calculations.

Slightly different data were needed depending on the code used for the analyses. Since the finite element program ABAQUS were used for most hydration calculations for SR-Can, the data was taken from the needs of the ABAQUS analyses.

2.2　Sensitivity to assessment results in SR-Can

2.2.1　Thermal

For the analysis performed it was clear that a higher conductivity of the buffer material will ideally lead to a lower temperature inside the canister (provided that the thermal properties of the rock are sufficient). The thermal properties of the buffer and the degree of saturation are coupled.

2.2.2 Hydro-mechanical

Sensitivity calculations have to some extent been performed concerning the influence of the buffer properties and the rock properties on the wetting rate of the buffer and the backfill.

Influence of buffer properties on the wetting rate of the buffer

/Hökmark 2004/ investigated the influence of some parameters in the models of CodeBright on the wetting rate of the buffer under the assumption that the hydraulic conductivity of the rock is high enough to supply the buffer with the required amount of water. The results are summarised in Table 2-1.

The influence was dominated by the retention curve and the hydraulic conductivity. The other variations are small in comparison. The high influence of the canister power is caused by the strong influence on water viscosity and thus hydraulic conductivity.

Influence of backfill properties on the wetting rate of the backfill

The influence of the backfill properties on the rate of backfill wetting has only been investigated in connection with the analysis of the influence of trapped air and in connection with the analysis of the difference between having 30/70 and Fridton /Börgesson et al. 2006/. The following conclusions can be drawn from these calculations:

* Trapped air influences the wetting rate of the backfill 30/70 significantly only when the rock hydraulic conductivity is high since the gas migration rate of the backfill will then govern the water inflow.

* The hydraulic conductivity and the retention curve of the backfill are (as for the buffer) the major regulators of the wetting rate if the water supply from the rock is large enough.

Influence of rock properties

The influence of the rock properties on the wetting rate has been investigated mainly in two reports /Börgesson et al. 2006/ and /Börgesson and Hernelind 1999/. Both rock modelled as homogeneous porous material with hydraulic properties corresponding to average values and rock with discrete fractures have been investigated. The influence of the rock is complex but some general conclusions are:

* For a fracture free rock the rate of wetting is determined mainly by the rock properties if the hydraulic conductivity of the rock is lower than the hydraulic conductivity of the buffer or backfill and vice versa.

* The water pressure in the boundary (or closest fracture) and the distance to the boundary (or closest fracture) has a clear but limited influence on the wetting rate. The influence is stronger for the backfill than for the buffer.

* The fracture frequency (intersecting the hole or tunnel) is the determining factor if the rock matrix hydraulic conductivity is lower than the hydraulic conductivity of the buffer or backfill.

* The fracture transmissivity seems to be of minor importance for the wetting of the backfill if it is higher than $\sim 10^{-10}$ m^2/s. For the buffer this limit is even lower ($< 10^{-11}$ m^2/s).

It should be noted that the backfill calculations are done with the assumption that no piping takes place. Piping will increase the wetting rate but also introduce other problems.

Table 2-1. Influence of a variation in buffer properties on the time to full saturation of the annulus between the rock and the canister (from /SKB 2006/).

Variation	Range of error or variation	Influence on the wetting rate	Magnitude in applicable range (roughly)	Comment
Retention curve	Factor 2	Strong influence	Proportional to the suction	
Hydraulic conductivity	Factor 4	Strong influence	Proportional	
δ	Factor 2	Small	10%	
D_{Tv}	Factor 10	Moderate		Strong influence on the saturation profile (water redistribution)
Gas confinement		Small		
Thermal conductivity	Factor 2	Small	10%	
Canister power	Factor 1.2	Moderate/strong	50%	Higher temperature yields higher K

2.3   Limitations of SR-Can

The modelling cases considered in SR-Can exhibited the following limitations:

- A single value was used for the buffer thermal conductivity value in the peak temperature calculations.
- No scenario with dry rock was considered in buffer models.
- No inner slot and pellets-filled gap were considered in buffer models.
- No case with backfill composed of blocks and pellets was considered in backfill models.
- No homogenization calculations were performed, except for erosion damages.
- Buffer upward swelling calculations were limited to cases with a homogenous backfill.
- Analyses were limited to buffer and backfill. No other system components were considered.

3 Supplier input on handling of data in SR-Site and SR-Can

The data supplier is part of the SR-Site Team, and information on the handling of data is given in Chapters 1 and 2.

4 Sources of information and documentation of data qualification

4.1 Introduction

This data qualification has focused on the bentonite material for buffer, backfill and the seals for tunnel plugs and bore-holes. All these system components are treated as if they were based on MX-80 bentonite. This material is however not planned to be used as backfill. The available data for the material devoted for this component (i.e. IBECO RWCBF) are limited at the moment, but exhibit many similarities to data for MX-80 (see Section 10.3.1). This observation can therefore justify the use of MX-80 data until more data for IBECO RWCBF is available.

Data for other materials are more or less well defined. Thermal data for copper and cast iron is very well defined and can be obtained from standard handbooks. The data for concrete and crushed rock fillings is in principle quite clear-cut. Their definitions have however not yet been decided upon. These materials are therefore assumed to exhibit the same properties as documented data for similar materials. Finally, the properties of the rock and the EDZ display a significant variability, especially regarding the hydraulic conductivity. It should be noticed that the modelling tasks are generally not site-specific and this variability is instead handled through sensitivity analyses of different parameters.

4.2 Documentation

4.2.1 Documentation for MX-80

The main documents for the process of acquiring, refining and qualifying data are listed in Table 4-1 and Table 4-2. The documentation for the acquisition and the refinement for each parameter are listed in Table 4-3 and Table 4-4.

Measurements of the *thermal conductivity* of MX-80 were presented by /Börgesson et al. 1994/ and /Kahr and Müller-Vonmoos 1982/. The refinement of this data for use in Code_Bright is given in this document (see Section 10.2.1). The refinement of this data for use in Abaqus was given in /Börgesson and Hernelind 1999/.

Measurements of *specific heat* for MX-80 have recently been presented by /Gailhanou et al. 2007/. This data does not require any further refinement. However, the measured value is close to the value used by /Börgesson and Hernelind 1999/ and it is shown in Section 10.2.1 that the latter value can be regarded as qualified.

Table 4-1. Main sources in SKB technical and international progress reports.

Reference	Report no.	Description
/Börgesson 2001/	IPR-01-34	Temperature gradient tests and water uptake tests.
/Börgesson and Hernelind 1999/	TR-99-41	Refinement of several Abaqus parameters.
/Börgesson et al. 1994/	TR-94-29	Measurement of thermal conductivity.
/Börgesson et al. 1995/	TR-95-20	Measurement and evaluation of hydraulic conductivity, swelling pressure, shear strength, compression tests etc.
/Dueck et al. 2010/	TR-10-32	Measurement of shear strength.
/Dueck and Nilsson 2010/	TR-10-55	Measurement of shear strength, retention properties, swelling tests and compression tests.
/Johannesson et al. 1995/	TR-95-19	Compaction tests.
/Karnland et al. 2000/	TR-00-22	LOT A1: Measurement of hydraulic conductivity, swelling pressure, shear strength, tensile strength.
/Karnland et al. 2006/	TR-06-30	Measurement of hydraulic conductivity, swelling pressure, particle density.
/Karnland et al. 2009/	TR-09-29	LOT A0;A2: Measurement of hydraulic conductivity, swelling pressure, shear strength.

Table 4-2. Other main sources.

Reference	Description
/Dueck 2004/	Measurement of retention properties
/Hökmark 2004/	Refinement of vapour diffusion tortuosity
/Kahr et al. 1990/	Measurement of retention properties
/Kahr and Müller-Vonmoos 1982/	Measurement of thermal conductivity
/Wadsö et al. 2004/	Measurement of retention properties
/Gailhanou et al. 2007/	Measurement of specific heat

Table 4-3. Acquisition and refinement of Code_Bright parameters.

Main parameter		Acquisition	Refinement
Thermal conductivity		/Börgesson et al. 1994/ /Kahr and Müller-Vonmoos 1982/	This document, Chapter 10
Specific heat		/Gailhanou et al. 2007/	This document, Chapter 10
Intrinsic permability		/Börgesson et al. 1995/ /Karnland et al. 2000/ /Karnland et al. 2006/ /Karnland et al. 2009/	This document, Chapter 10
Relative permability		/Börgesson 2001/	/Börgesson and Hernelind 1999/
Vapor diffusion tortuosity		/Börgesson 2001/	/Hökmark 2004/
Retention properties		/Dueck 2004/ /Dueck and Nilsson 2010/	This document, Chapter 10
Swelling pressure		/Börgesson et al. 1995/ /Dueck 2004/ /Karnland et al. 2000/ /Karnland et al. 2006/ /Karnland et al. 2009/	This document, Chapter 10
Shear strength		/Börgesson et al. 1995/ /Dueck et al. 2010/ /Dueck and Nilsson 2010/ /Karnland et al. 2000/ /Karnland et al. 2009/	This document, Chapter 10
Tensile strength		/Karnland et al. 2000/	This document, Chapter 10
Elastic	κ_i	/Dueck and Nilsson 2010/ /Börgesson et al. 1995/	This document, Chapter 10
	κ_s	/Dueck and Nilsson 2010/	This document, Chapter 10
	ν	/Dueck and Nilsson 2010/	This document, Chapter 10
Plastic	λ	Swelling pressure relation (this doc.)	This document, Chapter 10
	M	Swelling pressure relation (this doc.)	This document, Chapter 10
	p_s	Shear strength relation (this doc.)	
	p_0	Tensile strength relation (this doc.)	
	α	–	This document, Chapter 10
Particle density	ρ_s	/Karnland et al. 2006/	This document, Chapter 10

Measurements of the *hydraulic conductivity* of MX-80 were presented in /Börgesson et al. 1995/ together with evaluated void-ratio dependence. Since then, new measurements have been made, e.g. /Karnland et al. 2000, Karnland et al. 2006/ and /Karnland et al. 2009/. These measurements have been used for a new evaluation which is given in this document (see Section 10.2.2). Darcy's law is used in Abaqus as well as Code_Bright. The hydraulic conductivity is applied directly in Abaqus, whereas the *intrinsic permeability* is specified in Code_Bright. (At 20°C, the ratio between the intrinsic permeability and the hydraulic conductivity is approx. 10^{-7} m·s.)

The *relative permeability*, which is used in Abaqus as well as Code_Bright, can not be measured directly and this has instead been evaluated indirectly from water uptake tests in /Börgesson and Hernelind 1999/.

Table 4-4. Acquisition and refinement of Abaqus parameters (not rock shear models).

Main parameter	Acquisition	Refinement
Thermal conductivity, λ	/Börgesson et al. 1994/	/Börgesson and Hernelind 1999/
Specific heat, c	/Gailhanou et al. 2007/	This document, Chapter 10
Hydraulic conductivity, K	/Börgesson et al. 1995/	/Börgesson and Hernelind 1999/
Relative permability	/Börgesson 2001/	/Börgesson and Hernelind 1999/
Thermal vapour flow diffusivity, D_{Tv}	/Börgesson 2001/	/Börgesson and Hernelind 1999/
Isothermal vapour flow diffusivity	/Börgesson 2001/	/Börgesson and Hernelind 1999/
Water retention curve	/Dueck 2004/ /Dueck and Nilsson 2010/	Part of Task 5
Porous elasticity	/Börgesson et al. 1995/	/Börgesson et al. 1995
Moisture swelling data	/Börgesson et al. 1995/ /Dueck and Nilsson 2010/	/Börgesson and Hernelind 1999/ Part of Task 5
Poisson ratio	/Börgesson et al. 1995/	/Börgesson et al. 1995/
Friction angle in p-q plane	/Börgesson et al. 1995/	/Börgesson and Hernelind 1999/
Cohesion in p-q plane	/Börgesson et al. 1995/	/Börgesson and Hernelind 1999/
Dilation angle	/Börgesson et al. 1995/	/Börgesson and Hernelind 1999/
Yield function	/Börgesson 2001/	/Börgesson and Hernelind 1999/
Particle density	/Karnland et al. 2006/	This document, Chapter 10

The *thermal vapour flow diffusivity,* which is used in Abaqus, can not be measured directly and this has instead been evaluated indirectly from temperature gradient tests in /Börgesson and Hernelind 1999/. The *isothermal vapour flow diffusivity* has been assumed to be zero in /Börgesson and Hernelind 1999/.

The *vapour diffusion tortuosity*, used in the constitutive laws of Code_Bright, can not be measured directly and this has instead been evaluated indirectly from temperature gradient tests in /Hökmark 2004/.

Measurements of *retention properties* of MX-80 were presented in /Dueck 2004/. The refinement of this data for use in Code_Bright is given in this document (see Section 10.2.4). The corresponding refinement for use in Abaqus is completed but will be reported as a part of Task 5.

A fairly large number of parameters are used for the description of the mechanical behaviour, in Code_Bright as well as in Abaqus. Some of these parameters are highly related to the *swelling pressure* and its void ratio dependence, although it isn't applied directly in these descriptions. The swelling pressure is routinely measured together with the hydraulic conductivity, and therefore the same sources used for the hydraulic conductivity have been used for the swelling pressure, (see Section 10.2.5) In addition, measurements of retention properties (from /Dueck 2004/) have also been used for adoption of swelling pressure relations.

A second important mechanical property is the *shear strength* of compacted MX-80. Information on this property has been obtained through triaxial compression tests presented in /Börgesson et al. 1995/. A refinement, in the form of a parameterized relation between the deviatoric stress and the mean effective stress at the point of failure, was also given in /Börgesson et al. 1995/. This relation has been re-evaluated from more recent measurements presented by /Karnland et al. 2000, Karnland et al. 2009, Dueck et al. 2010/ and /Dueck and Nilsson 2010/ (see Section 10.2.6).

A third property which is used for the adoption of the mechanical parameters in Code_Bright is the *tensile strength* (or the tensile yield stress). This has been measured through beam tests /Karnland et al. 2000/. A parameterized relation between the tensile yield stress and the dry density is presented in Section 10.2.7.

The *elastic parameters* used for Code_Bright is based on experimental results presented in /Dueck and Nilsson 2010/ and /Börgesson et al. 1995/, as well as the evaluated swelling pressure relation. The *plastic parameters* used for Code_Bright is based on the evaluated relations for the swelling pressure, the shear strength and the tensile strength. The refinement of this data is given in Section 10.2.8.

All *mechanical parameters* used for the water-unsaturated buffer in Abaqus are based on measurements presented in /Börgesson et al. 1995/, with the exception for unconfined uniaxial compression tests presented in /Börgesson 2001/. The refinement of this data is given in /Börgesson et al. 1995/ and /Börgesson and Hernelind 1999/. Additional evaluations of the moisture swelling will be performed as a part of Task 5.

The *particle density* (or solid phase density) is used in Abaqus as well as in Code_Bright. This property has been measured by /Karnland et al. 2006/. The refinement of this data is given in Section 10.2.11.

4.2.2 Documentation for other materials

The main documents for the adoption of parameter values for other material are listed in Table 4-5 and Table 4-6. No rigorous qualification process is attempted and not actually motivated due to the various degrees of definition for these other materials (with very well known properties of copper and cast iron; with a rock which exhibits a significant variability; and with concrete and crushed rock components which haven't been defined yet).

Table 4-5. Main sources for data on concrete, crushed rock, copper and cast iron.

Material	Reference	Description
Concrete	/Dahlström et al. 2009/	Data on hydraulic conductivity and elasticity
Concrete	/Betonghandbok 1994/	Data on porosity and aggregates
Concrete	/Hedenblad 1996/	Data on retention properties
Crushed rock	/Bear 1972/	Data on porosity and retention properties
Crushed rock	/Gunnarsson et al. 2001/	Data on porosity from BFP-test
Crushed rock	/Åkesson 2006/	Data from compression tests on construction sand
Copper/Cast iron	/TEFYMA 1982/	Data on density, thermal conductivity and specific heat

Table 4-6. Main sources for data on granite rock.

Reference	Description
/Byegård et al. 2006/	Porosity data from Laxemar
/Follin et al. 2007/	ECPM hydraulic conductivity for Forsmark
/Vilks 2007/	Hydraulic conductivity data for Forsmark core samples
/Vidstrand 2003/	Hydraulic conductivity data for Äspö rock blocks
/Bäckblom 2008/	Hydraulic conductivity data for EDZ
/Finsterle and Pruess 1995/	Retention data for crystalline rock
/TEFYMA 1982/	Data on density, thermal conductivity and specific heat

4.3 Data qualification for MX-80

The qualification has been performed through a motivated and transparent chain; from measurements, via evaluations, to parameter determinations. The measured data was selected to be as recent, traceable and independent as possible. The data sets from this process are thus regarded to be qualified. Corresponding sets, from earlier sources, are considered to be supportive (Table 4-7 and Table 4-8). Five of the Abaqus parameters are indicated with both qualified and supportive sets. This is due to that the presented qualification process basically has confirmed previously used sets.

Table 4-7. Qualified and supporting data sets for Code_Bright parameters.

Main parameter		Qualified sets	Supporting sets
Thermal conductivity		This document	
Specific heat		This document	
Intrinsic permability		This document	
Relative permability			/Börgesson and Hernelind 1999/ /Hökmark 2004/
Vapor diffusion tortuosity			/Hökmark 2004/
Retention properties		This document	
Swelling pressure		This document	
Elastic	κ_i	This document	
	κ_s	This document	
	ν	This document	
Plastic	λ	This document	
	M	This document	
	p_s	This document	
	p_0	This document	
	α	This document	
Particle density		This document	

Table 4-8. Qualified and supporting data sets for Abaqus parameters.

Main parameter	Qualified sets	Supporting sets
Thermal conductivity, λ	This document	/Börgesson and Hernelind 1999/
Specific heat, c	This document	/Börgesson and Hernelind 1999/
Hydraulic conductivity, K	This document	/Börgesson and Hernelind 1999/
Relative permability		/Börgesson and Hernelind 1999/ /Hökmark 2004/
Thermal vapour flow diffusivity, D_{Tv}		/Börgesson and Hernelind 1999/
Isothermal vapour flow diffusivity		/Börgesson and Hernelind 1999/
Water retention curve	Task 5	
Porous elasticity		/Börgesson et al. 1995/
Moisture swelling data	Task 5	
Poisson ratio		/Börgesson et al. 1995/
Friction angle in p-q plane	This document	/Börgesson and Hernelind 1999/
Cohesion in p-q plane		/Börgesson and Hernelind 1999/
Dilation angle		/Börgesson and Hernelind 1999/
Yield function		/Börgesson and Hernelind 1999/
Particle density	This document	/Börgesson and Hernelind 1999/

5 Conditions for which data is supplied

Data is generally available for all conditions, e.g. for unsaturated as well as saturated conditions, and a summary of laboratory conditions and field conditions are given in Table 5-1. Some exceptions can however be noticed.

Water unsaturated bentonite pellets is a complex material, which has implication for the hydraulic as well as the mechanical properties. Since unsaturated pellets display piping phenomena, the conventional description of water transport does not apply. This can be handled through adopting a high hydraulic conductivity (e.g. $> 10^{-10}$ m/s) with no saturation dependence. This value is replaced with the true conductivity as soon as saturation is reached. The mechanical behaviour of pellets is complicated in that it can be expected to reach plastic conditions sooner than a homogenous material with the same dry density. This can be handled through adopting a lower value of the initial hardening parameter (p_0^*).

The *mechanical parameters* provided for use in Code_Bright are given for cases with *no dehydration*. If such cases would occur (typically model task no 5 – Natural buffer homogenisation) it is advised that the values of α_i, α_{ils} and α_{ss} is reassessed.

The thermomechanical effects (e.g. the thermal expansion of buffer material) have been considered to be of minor significance and have thereby been neglected since it has been shown that there is virtually no influence of the temperature on the swelling pressure at buffer density /Börgesson et al. 1995/. However, the thermal expansion of water is included.

Finally, it can be remarked that the relevance of the parameter values may be limited at conditions with temperatures above 90°C.

Table 5-1. Summary of laboratory conditions and field conditions for buffer.

Parameter	Water saturation	Void ratio	Temperature	Salt content
Field conditions	16–100%	0.57–1.78	15–90°C	0.2 M (LOT)
Thermal conductivity	0–100%	0.44–1.4	20–35°C	–
Hydraulic conductivity	100%	0.65–4.4	20–130°C*	0–0.2 M
Swelling pressure	100%	0.65–4.4	20–130°C *	0–0.2 M
Shear strength	100%	0.8–1.2	20°C	0–0.2 M
Retention properties	Water content: 0–64%	Free swelling conditions**	20–50°C*	–

* Occasional analyses have been performed for the higher temperatures.

** Additional tests have been performed at other conditions.

6 Conceptual uncertainty

The constitutive laws used in the two codes that will be employed for the modelling task (Code_Bright and Abaqus) both display conceptual uncertainties. A description of these constitutive laws can be found in their manuals (/CIMNE 2002/ and the /Abaqus manual 2008/).

These two codes differ in some respect regarding the underlying conceptual models, which implies that the required data sets also differ. Whereas the codes are equivalent concerning heat transport, water transport, retention properties and to some extent also in the mechanical constitutive laws, they display significant differences concerning the vapour transport and stress invariants used in the mechanical model.

6.1 Vapour transport

In Code_Bright, the vapour diffusion is driven by a gradient in the vapour mass fraction of the gas phase (ω_g^w):

$$\vec{i} = -n \cdot \tau \cdot D \cdot (1 - S_r) \cdot \rho_g \cdot \nabla \omega_g^w \qquad (6\text{-}1)$$

where n is the porosity, S_r is the water saturation and ρ_g is the gas density. The molecular diffusion coefficient of vapour in air is calculated as:

$$D = 5.9 \cdot 10^{-6} \frac{(273.15 + T)^{2.3}}{P_g} \qquad (m^2/s) \qquad (6\text{-}2)$$

where T is the temperature (in °C) and P_g is the gas pressure (in Pa). The only remaining parameter to be quantified is the tortuosity factor (τ).

In Abaqus, the vapour flux is modelled as a diffusion process driven by the temperature gradient and the water vapour pressure gradient (at isothermal conditions) according to:

$$q_v = D_{Tv} \nabla T - D_{pv} \nabla p_v \qquad (6\text{-}3)$$

where q_v is the vapour flow, D_{Tv} is the thermal vapour flow diffusivity, T is the temperature, D_{pv} is the isothermal vapour flow diffusivity and p_v is the vapour pressure. The isothermal vapour flow is neglected and thus is D_{pv} equal to zero. The thermal water vapour diffusivity D_{Tv} is modelled with the following saturation dependence:

$$D_{Tv} = D_{Tvb} \qquad\qquad 0.3 \leq S_r \leq 0.7 \qquad (6\text{-}4)$$

$$D_{Tv} = D_{Tvb} \cdot \cos^a \left(\frac{S_r - 0.7}{0.3} \cdot \frac{\pi}{2} \right) \qquad S_r \geq 0.7 \qquad (6\text{-}5)$$

$$D_{Tv} = D_{Tvb} \cdot \sin^b \left(\frac{S_r}{0.3} \cdot \frac{\pi}{2} \right) \qquad S_r \leq 0.3 \qquad (6\text{-}6)$$

a and *b* are factors that regulate the decreased vapour flux at high and low degree of saturation and are usually set to the value of 6. The only remaining parameter to be quantified is the D_{Tvb} factor, which has to be determined by indirect methods. The parameters *a* and *b* should also be checked in this way.

6.2   Stresses

The mechanical constitutive law used in Code_Bright (the BBM model) is defined for *net stresses* ($\boldsymbol{\sigma}$'), which in turn is defined as:

$$\boldsymbol{\sigma}' = \boldsymbol{\sigma} + \max(p_g, p_l)\mathbf{I} \tag{6-7}$$

where $\boldsymbol{\sigma}$ is the total stress (defined as < 0 for compressive stresses), p_g is the gas pressure, p_l is the liquid pressure and $\mathbf{I}$ is the unit tensor.

The corresponding law used in Abaqus (porous elastic and Drucker-Prager) is defined for *effective stresses* ($\boldsymbol{\sigma}^*$), which in turn is defined as:

$$\boldsymbol{\sigma}^* = \boldsymbol{\sigma} + \chi\, p_l \mathbf{I} \tag{6-8}$$

where χ is a saturation dependent factor, usually set to the degree of saturation (S_r).

The two stresses are identical at saturated conditions. For unsaturated conditions, however, the difference is significant. For instance, at unloaded conditions when the total stress is zero, the net stress is given by the gas pressure and is thereby also close to zero (0.1 MPa). The effective stress is on the other hand quite significant; for a buffer block in the order of 30 MPa. However, the effective stress has no meaning at unsaturated conditions in Abaqus since the Moisture swelling process, which is included in order to compensate for the shortcoming of the effective stress theory, has been calibrated in order to yield a correct total stress.

However, it is well established fact that the mechanical model of water unsaturated soils in general and swelling soils in particular is weaker and yields more problems than the thermal and hydraulic models. More knowledge is desirable.

7 Data uncertainty due to precision, bias, and representativity

7.1 Introduction

The selected data is to a large extent the same as was used in SR-Can. In order to strengthen the relevance of the parameter values and to confirm previously used relations, either newer or independent measurements have been taken into account.

Previously used relations for swelling pressures and hydraulic conductivities /Börgesson et al. 1995/ have been re-evaluated from more recent measurements /Karnland et al. 2000, Karnland et al. 2006, Karnland et al. 2009/. Similarly, the previously used relation for the shear strength /Börgesson et al. 1995/ has been re-evaluated from data from /Karnland et al. 2000, Karnland et al. 2009, Dueck et al. 2010/ and /Dueck and Nilsson 2010/. These re-evaluations have basically confirmed the previously used relations for these parameters.

Independent measurements of retention properties /Wadsö et al. 2004, Kahr et al. 1990/ and thermal conductivity /Kahr and Müller-Vonmoos 1982/ have demonstrated the coherence of the measured data sets (/Dueck 2004/; /Dueck and Nilsson 2010/ and /Börgesson et al. 1994/, respectively) on which the used parameters values and tables are based.

Generally, it can be remarked that all measurements have been performed on well-defined specimen and with methods dedicated for this type of application. Nevertheless the data exhibit some variability, which is discussed below.

The discussion below concerning precision, bias and representativity is focused on the main parameters mentioned above. Indirectly evaluated parameters, such as relative permeability, vapour diffusion parameters and mechanical parameters, are based on several additional properties and are much more complex to assess in this respect. The discussion has therefore not been pursued for those parameters.

Table 7-1. Summary of uncertainties of main parameters.

Parameter	Precision	Bias	Representatvity
Swelling pressure and hydraulic conductivity	Balance Volume measurement Force transducers Flow measurements Hydraulic pressure	Material and measurement techniques	Salt effects Temperature effects
Shear strength	Force transducers Cell pressure	–	Salt effects Temperature effects
Retention properties	Balance Salt solution Temperature control Disturbances	"Premature" closure	Free swelling conditions Temperature effects
Thermal conductivity	Heat power Temperature	Gap effects	Extrapolation for dry conditions

7.2 Swelling pressure and hydraulic conductivity

These measurements are usually performed successively on the same sample (see Figure 7-1). The swelling pressure is based on a *force measurement (F)*, while the hydraulic conductivity is based on a *flow measurement (Q)* and a *hydraulic pressure difference (Δp_l)* applied with a GDS pressure control. The *swelling pressure (p_swell)* and the *flux (q)* are given by the sample *area (A)*:

$$p_{swell} = \frac{F}{A} \qquad q = \frac{Q}{A} \qquad\qquad\qquad (7\text{-}1)$$

while the *hydraulic gradient (I)* and the *hydraulic conductivity (K)* are given by the sample *height (h)*:

$$I = \frac{\Delta p_l}{h \cdot \rho_w g} \qquad K = \frac{q}{I} \qquad\qquad\qquad (7\text{-}2)$$

After the measurements, the *density (ρ)* of the sample is given through mass measurement and volume measurement through submerging the sample in paraffin oil.

The flow measurements are performed through monitoring of the amount of percolate in a tube. At very low conductivity, this volume may be reduced through evaporation. This effect is minimized through covering the end of the tube, and checked through quantification of the loss in a separate tube.

The diameter of the sample is typically 20, 35 or 50 mm, while the height range from 5 mm up to 25 mm.

The *precision* of the measurements is largely given by the balance, the volume measurement, the force transducer, the flow measurement and the applied hydraulic pressure. This *precision* is reflected by the variability of hydraulic conductivity and swelling pressure (Figure 10-3 and Figure 10-10).

At lower densities the differences between different measurements of swelling pressure are more significant. Moreover, there appears to be differences between different sets of samples (different projects, see Figure 10-3 and Figure 10-10), and some analyses therefore appear to be *biased*. The reason for these deviations is however currently unknown. The results of hydraulic conductivity also display the same type of deviation at high density, although to a lesser extent. It has also been noticed that recently performed measurements yield significantly higher swelling pressure than earlier measurements; approx. 2 MPa (i.e. approx. 25%) at buffer density /Karnland et al. 2000/. A similar difference can be noticed for the hydraulic conductivity: earlier measurements have shown approx. 50% higher values than more recent measurements at buffer density. The reason for these differences may be due to changes in the delivered material and hysteresis effects revealed by different measurement techniques.

The measurements can be regarded as *representative* for the field conditions in that the measurements are performed at different salt solutions. The temperature dependence of the hydraulic conductivity is considered to be related to the temperature dependence of the viscosity of water. The temperature dependence of the swelling pressure has been shown to be of minor significance /Börgesson et al. 1995/ and has therefore not been addressed.
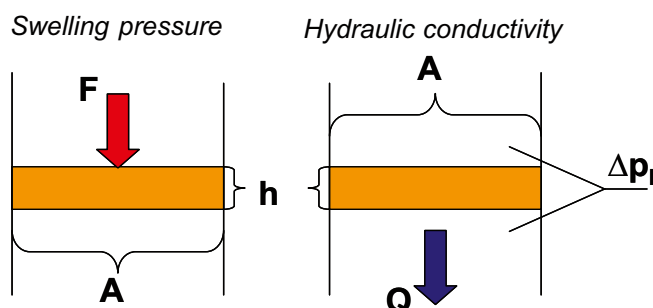

***Figure 7-1.** Schematic outline of measurement of swelling pressure and hydraulic conductivity.*

7.3   Shear strength

These measurements are usually performed via triaxial compression tests with un-drained conditions which for water saturated samples imply that the sample volume is constant throughout the test (see Figure 7-2). However, the tests performed with the purpose to investigate the influence of the shear rate on the shear strength for the rock shear model, are done as unconfined uniaxial compression tests, due to the complexity of the triax.

The first step is to allow the sample to equilibrate in a saturation device with free access of water. For the unconfined uniaxial compression tests the sample is then moved to a press and sheared to failure. For triaxial test the sample is moved to a triaxial cell with a cell pressure p_c applied by a GDS pressure control. The target for this pressure is set slightly above the swelling pressure measured in the saturation device in order to provide a *pore pressure (u)* in the sample. An *axial displacement (Δl)* is thereafter applied to the sample until failure is reached. At the same time, the increase in *axial force (ΔF_{ax})* and the sample pore pressure are measured.

The diameter of the samples is typically 35 mm, while the height is twice as high (i.e. 70 mm). Previously a larger sample diameter has been used (50 and 100 mm, respectively). The reason for choosing a smaller sample size is to enhance the water transfer within the sample.

The *deviatoric stress (q)* is given by the sample *area (A),* while the axial strain *(ε_{ax})* is are given by the sample *height (l):*

$$q = \frac{\Delta F_{ax}}{A} \qquad \varepsilon_{ax} = \frac{\Delta l}{l} \tag{7-3}$$

The *axial stress (σ_{ax})* and the mean effective stress (p') are given as:

$$\sigma_{ax} = q + p_c \qquad p' = \frac{\sigma_{ax} + 2 \cdot p_c - 3 \cdot u}{3} \tag{7-4}$$

The strength of the sample is characterized by p' and q at the point of failure. This point is evaluated as the highest registered deviatoric stress.

After the measurements, the *density (ρ)* of the sample is given through a mass measurement and a volume measurement through submerging the sample in paraffin oil.

The density is only of secondary interest, since the main results of the measurement is the point of failure in the p'-q plane. The *precision* of the measurements is thus largely given by the force transducer and the applied cell pressure. The available data suggests however that the measurement is not *biased* at low density as noticed for swelling pressure and hydraulic conductivity.

The measurements can be regarded as *representative* for the field conditions in that the measurements are performed at different salt solutions. The temperature dependence is considered to be of minor significance and has not been addressed.
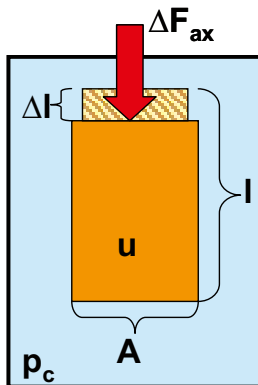

Figure 7-2. Schematic outline of a triax cell for measurement of shear strength.

7.4 Retention properties

Retention properties at free swelling conditions are usually measured via the glass jar method. With this method, a sample with an initial mass of approx. 10 g is placed in a glass jar where the relative humidity is set by a saturated salt solution. The sample is kept in the jar, which in turn is kept at 20°C (in some tests in a climate chamber) during the entire test. The mass of the sample is measured in place at regular intervals. After the water uptake has equilibrated, the sample is dried whereby the dry mass is quantified. The water content is calculated from the total mass and the dry mass.

The *precision* of the measurement is given by the balance, the salt solution, the temperature control and possible disturbances caused by the handling of the samples during drying. A possible *bias* of the measurement is the asymptotic behaviour during equilibration. Samples usually exhibit small changes even though the sample has been exposed for the salt solutions for very long time periods, e.g. three months. The deviation caused by such "premature" closure is regarded to be of minor significance.

The approach of measuring retention properties at free swelling condition is far from *representative* for field conditions with limited volumes. This is taken into account during the adoption of void ratio specific retention curves (see Section 10.2.4). The retention properties have also been noticed to exhibit a temperature dependence /Dueck and Nilsson 2010/. The available data is however still too limited for taking this effect into account.

7.5 Thermal conductivity

The thermal conductivity (λ) was measured with a dynamic technique by which a needle-shaped probe was inserted in the centre of a sample (diameter approx. 40–50 mm) and heated with a constant power (q). The temperature was measured continuously in the centre of the probe, and by considering the probe as a line source. The thermal conductivity can thereby be evaluated from the following relation:

$$T_2 - T_1 = \frac{q}{4\pi \cdot \lambda} \ln\left(\frac{t_2}{t_1}\right) \tag{7-5}$$

T_1 and T_2 are the temperature values at the time t_1 and t_2 (typically approx. 100 and 400 seconds, respectively).

The *precision* of the measurement is set by the heating equipment and the thermocouple. In /Börgesson et al. 1994/, the accuracy was estimated to be $\pm 10\%$.

The measurements can be *biased* by a transition zone between the probe and the sample. This effect was investigated by /Börgesson et al. 1994/, in which it was proposed that the effect could be counteracted through limitation of the temperature increase and through application of heat paste on the probe.

Measurements presented by /Börgesson et al. 1994/ were made on samples with fairly high saturation degree ($S_r \geq 43\%$). The *representativity* of the measurements was therefore limited to wet conditions. Extrapolations of the thermal conductivity for dryer conditions were based on different empirical models. Only one of these models were actually based on measurements of completely dry MX-80 samples /Kahr and Müller-Vonmoos 1982/ and the data from this report have therefore been directly used in the current evaluation. From this it can be noticed that the previously used data for dry conditions have underestimated the thermal conductivity.

8 Spatial and temporal variability

Several parameters are dependent on the void ratio or the degree of water saturation. These variables will vary in time and space, due to the initial heterogeneities and unsaturated conditions at installation, and the subsequent homogenization and hydration process. One of the goals of the modelling tasks is to describe these processes. Apart from this, there is no spatial and temporal variability in the parameter values for the different system components. The boundary conditions (i.e. the rock properties) display however a variability, which is taken into account through different modelling cases and sensitivity analyses.

9 Correlations

Several correlations can be identified, e.g. between swelling pressures and hydraulic conductivities, and several parameters display a dependence of void ratio or saturation degree. Such correlations are however mainly of concern for probabilistic data and not really of interest for these models.

10 Results of supplier's data qualification

10.1 Introduction

The purpose of the following parameter value evaluation is to provide data for deterministic models of the repository evolution. Only limited emphasis is therefore put on error estimations.

The most important parameters are the same as were discussed in the Chapter 7, i.e. hydraulic conductivity, swelling pressure, shear strength, retention properties and thermal conductivity. These parameters are highly significant for calculations of the hydration process, homogenisation and peak temperatures. For these parameters, the approach has been to evaluate new measurements (hydraulic conductivity, swelling pressure and shear strength), and to demonstrate coherence with independent measurements (thermal conductivity and retention properties).

Special emphasis has been put on adoption of BBM mechanical parameters used in Code_Bright. The aim has been to develop a general and clear-cut method to quantify the parameters for all relevant dry densities (void ratio 0.57–1.78). It should be remarked however that the BBM model has certain limitation for expansive soils, and one of the restrains of the presented approach is that some parameters, to some extent has to be based on a homogenized target void ratio. The elastic parameters are pragmatically based on results from compression and swelling tests with uniaxial strain. One important innovation is also introduced into the pressure dependence of the swelling modulus. The plastic stress-strain modulus values are based on the swelling pressure relation. Moreover, the suction dependence of this modulus is regarded to be insignificant. The other parameters describing the yield surface is based on relations for swelling pressure, shear strength and tensile strength. A few deviations from this approach are foreseen in cases with dehydration and for pellets.

10.2 Evaluation of parameter values

10.2.1 Thermal conductivity and specific heat

Measurements of thermal conductivity were reported in /Börgesson et al. 1994/ and were given for different void ratios and degrees of saturation. Results from this study are presented together with independent determined conductivity data /Kahr and Müller-Vonmoos 1982/ in Figure 10-1 and Figure 10-2. It can be noticed that the first set (from /Börgesson et al. 1994/) is limited to saturation degrees higher than 43%, whereas the highest saturation degree in the second set is 86%. The sets were obtained with similar methods and they are apparently in good agreement at mid-range saturation degrees.

In Abaqus, the saturation dependence and the void ratio dependence of the thermal conductivity can be defined in tables (Figure 10-1). For specific conditions during calculation, the conductivity is interpolated between these values. It can be noticed that adopted tables appear to underestimate the conductivity at low saturation degrees.

The constitutive law of Code_Bright enables a saturation dependence specified by a linear function:

$$\lambda(S_r) = \lambda_{dry}(1 - S_r) + \lambda_{sat} \cdot S_r \qquad (10\text{-}1)$$

A distinction has been made between the parameter values for blocks and pellets. High density blocks exhibit a higher conductivity than low density material. The lower end value (λ_{dry}), has therefore been set to 0.7 W/mK for blocks and 0 W/mK for pellets. The top end value (λ_{sat}) has in both cases been set to 1.3 W/mK (Figure 10-2). These parameters should be reassessed if a modelled block would display significant de-hydration (S_r below 50%).

Another dependence of thermal conductivity on saturation can be used to improve the representation at lower degree of saturation:

$$\lambda(S_r) = \lambda_{sat}^{S_r^n} \lambda_{dry}^{(1-S_r)^{\frac{1}{n}}} \qquad (10\text{-}2)$$
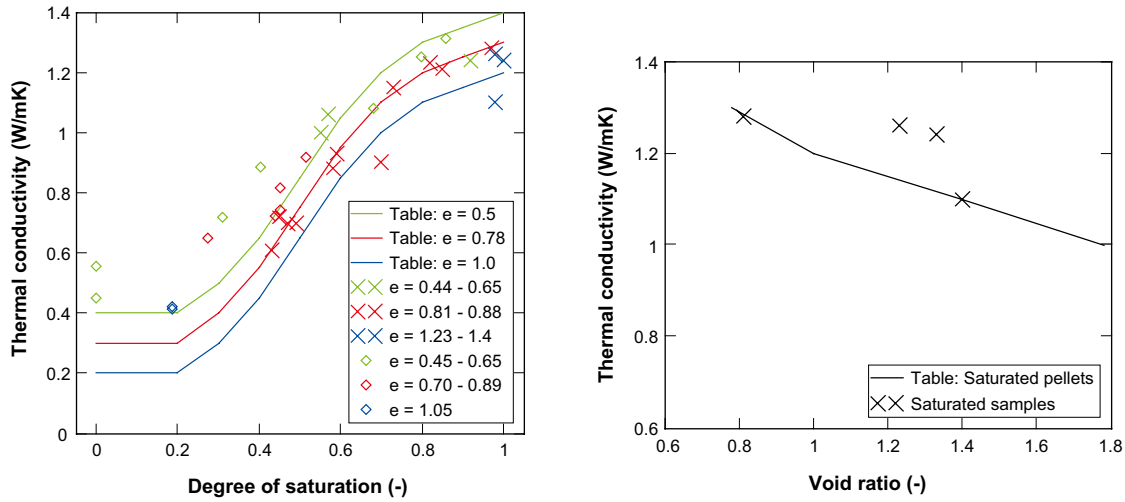
Figure 10-1. *Measured thermal conductivity for MX-80 (/Börgesson et al. 1994/: ×; /Kahr and Müller-Vonmoos 1982/: ◊) and adopted tables for Abaqus (lines). Blocks (left) and saturated pellets (right).*
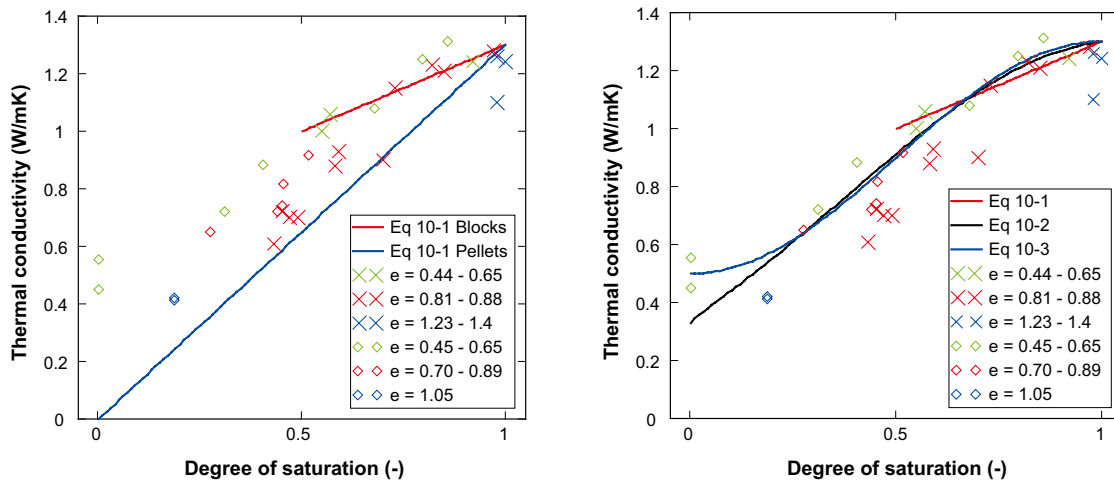
Figure 10-2. *Measured thermal conductivity for MX-80 (/Börgesson et al. 1994/: ×; /Kahr and Müller-Vonmoos 1982/: ◊) and adopted relations for Code_Bright (lines).*

The following parameter setting can be used to represent blocks and homogenised buffer materials: $\lambda_{sat} = 1.3$ W/mK; $\lambda_{dry} = 0.33$; and n = 0.5 (Figure 10-2).

A third relation could potentially be even more suitable for representing the saturation dependence:

$$\lambda(S_r) = \lambda_{dry} \cos^2\left(\pi S_r / 2\right) + \lambda_{sat} \sin^2\left(\pi S_r / 2\right) \tag{10-3}$$

This has been proposed by /Chen and Ledesma 2009/ with the parameters $\lambda_{sat} = 1.3$ W/mK and $\lambda_{dry} = 0.3$ (Figure 10-2). In Figure 10-2, this relation is illustrated for λsat=1.3 and λdry=0.5 W/mK. This relation is however not yet implemented in the source code and therefore not applicable.

The specific heat of MX-80 has recently been measured by /Gailhanou et al. 2007/. With a molar specific heat value of 326.13 J/molK and a molar mass of 378.787 g/mol, this yields a value of 861 J/kgK. This value is less than 10% higher than the 800 J/kgK stated in /Börgesson and Hernelind 1999/. This deviation is quite small and the latter value is therefore regarded to be qualified.

10.2.2 Hydraulic conductivity

Measurements of the hydraulic conductivity (K) with distilled water and at different densities were presented in /Börgesson et al. 1995/. A relation between K and the void ratio e were adopted on the following form:

$$K(e) = K_0 \cdot \left(\frac{e}{e_0}\right)^{\eta} \qquad (10\text{-}4)$$

where K_0 is the hydraulic conductivity at reference void ratio e_0 and η is a fitted exponent. In /Börgesson et al. 1995/, the following parameter setting was adopted for conditions with room temperature, distilled water and void ratios between 0.5 and 2.0:

$K_0 = 3 \cdot 10^{-13}$ (m/s)

$e_0 = 1.0$ (–)

$\eta = 4.64$ (–)

New measurements have recently been presented in /Karnland et al. 2000/ (LOT A1 reference material); /Karnland et al. 2006/ and /Karnland et al. 2009/ (LOT A0 and A2 reference material), both for de-ionized water and for different salt contents. A compilation of results are shown in Figure 10-3. It can be noticed that the values are fairly well gathered and appears to be unaffected by the salt. One exception though is the measurements in /Karnland et al. 2006/. These values are generally lower than the other measurements (probably due to a special experimental procedure) and are therefore neglected in the new evaluation. Among the remaining measurements all data for dry densities below 1,000 kg/m³ are also neglected, since this limit corresponds to the density of pellets and lower densities should therefore not occur in a repository. A new relation on the same form as (10-4) has been adopted with least-square regression for the remaining data. The following parameters have been found:

$K_0 = 2.4 \cdot 10^{-13}$ (m/s)

$e_0 = 1.0$ (–)

$\eta = 5.33$ (–)

This relation is used for the adopted Code_Bright parameters. It should be noticed however that there are no new measurements for dry densities above 1,681 kg/m³, corresponding to a void ratio of 0.65. It is therefore recommended that the scatter exhibited by the experimental data is taken into account through sensitivity analysis in which the K_0 is reduced with 40% and increased with 100%. This span covers the adopted line in /Börgesson et al. 1995/.
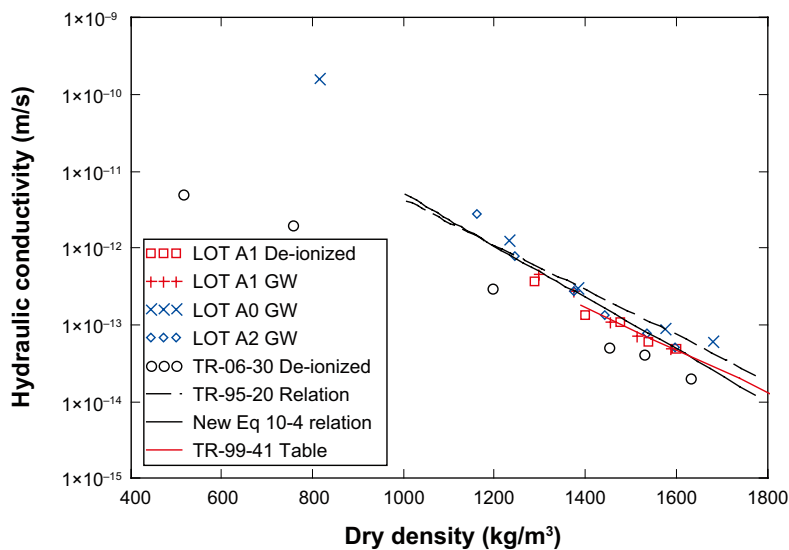

Figure 10-3. *Hydraulic conductivity versus dry density. LOT A1 /Karnland et al. 2000/, LOT A0 and A2 /Karnland et al. 2009/, TR 06-30 /Karnland et al. 2006/.*

The void ratio dependence of the hydraulic conductivity is in Abaqus handled with a specified table. The previously used table is shown in Figure 10-3 and the agreement is apparently good. In Code_ Bright the corresponding porosity dependence of the intrinsic permeability is normally described by Kozeny's law. An exponential porosity dependence of the intrinsic permeability can however also be adopted in Code_Bright:

$$k(n) = k(n_0) \cdot \exp\left[b \cdot (n - n_0)\right] \tag{10-5}$$

It can be shown that the value of the parameter b can be estimated as $4 \cdot \eta$.

10.2.3 Relative permeabilty and vapour diffusion coefficents

The relative permeability cubic power law (S_r^3), which is used in Code_Bright as well as Abaqus, and the thermal vapour flow diffusivity (used in Abaqus) were indirectly evaluated from water uptake tests and temperature gradient tests in /Börgesson and Hernelind 1999/. The influence of the exponent in the power law on the hydration time scale was investigated by /Hökmark 2004/. The alternative exponents 2 and 4 were examined. For an initial saturation degree of 80%, it was found that the influence was negligible. A vapour diffusion tortuosity value (used in Code_Bright) of 1 was indirectly evaluated by /Hökmark 2004/. Similarly, a D_{Tvb}-value (used in Abaqus) of $0.7 \cdot 10^{-11}$ m^2/s,K was indirectly evaluated by /Börgesson and Hernelind 1999/.

It should be noted that the relevance of the relative permeability model is clearly limited in the case of pellets fillings. This material exhibits piping phenomena by which the unsaturated permeability is much larger than the permeability for saturated conditions. The power law is therefore apparently not applicable for pellets. Instead, it is suggested that a high intrinsic permeability (e.g. set by numerical conveniences), and a perfectly mobile law (i.e. $k_r=1$) is used during unsaturated conditions. These parameter values are changed manually when saturation is reached.

10.2.4 Retention properties

Measurements of retention properties for MX-80 have been reported in /Dueck 2004/ and /Dueck and Nilsson 2010/. These measurements are based on a method with free swelling powder in jars, and by relating the properties to the initial water content, thereby addressing the hysteretic effects. Results from such measurements are shown together with data determined with the sorption balance method in Figure 10-4 and Figure 10-5. It can be noticed that the independent measurements are in agreement, especially regarding the hydration line.
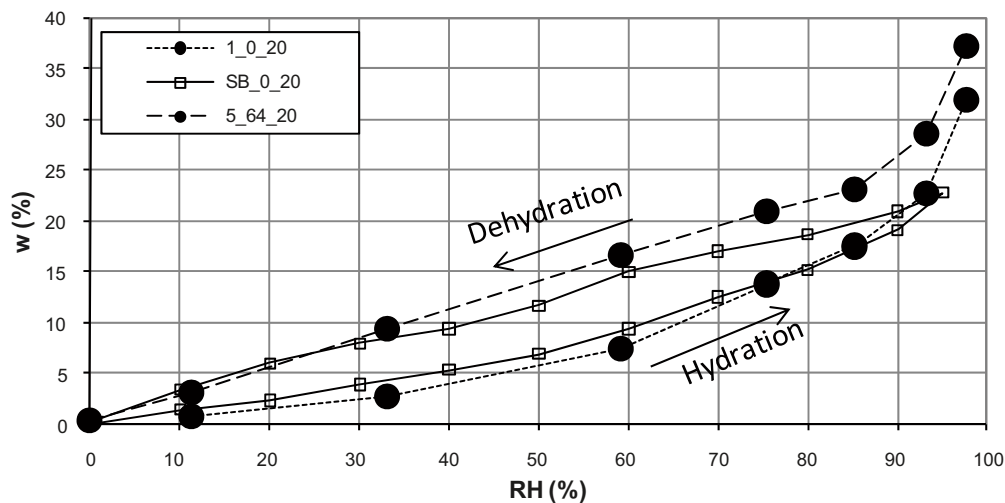

Figure 10-4. *Retention curves at 20°C determined with the sorption balance (□) and jars (●) with w_{ini} = 0% and 64% (data from /Dueck and Nilsson 2010/).*
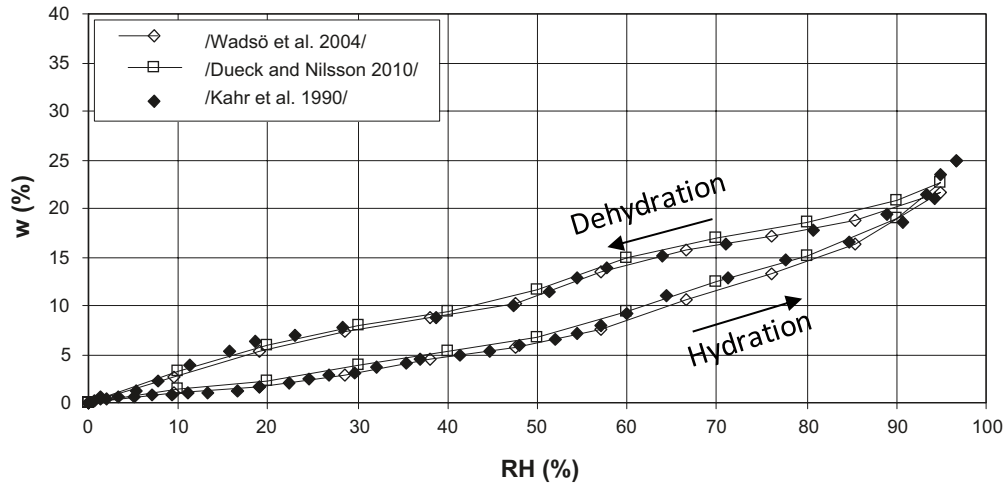
Figure 10-5. *Retention curves determined with sorption balances. The result SB_0_20 /Dueck and Nilsson 2010/ are presented together with results from /Wadsö et al. 2004/ and /Kahr et al. 1990/.*

Sets of data points, i.e. relative humidity and water content, have been produced for the following initial water contents: 0, 7.5, 9.4, 9.8, 15, 17.5, 27 and 64%. Among these, the sets for 17.5, 9.8 and 7.5 have been used for the different materials in the buffer, backfill and the bore-hole seals. The buffer and the backfill blocks as well as the backfill pellets will have an initial water content of 17%. The pellets in the buffer will have 10%, while the bore-hole seals will have 6%.

The retention curve used in Code_Bright follows the van Genuchten expression:

$$S_r(s) = \left(1 + \left(\frac{s}{P_0}\right)^{\frac{1}{1-\lambda}}\right)^{-\lambda} \tag{10-6}$$

Two parameters, P_0 and λ, are therefore determined for each material. The adoption of these parameter values are made in two steps.

The first step is to determine the initial point: the initial suction is derived from the initial relative humidity and Kelvin's law. The values are 46, 100 and 179 MPa for water contents of 17, 10 and 6%, respectively. The initial degree of saturation is derived as:

$$S_r = \frac{w \cdot \rho_s}{e \cdot \rho_w} \tag{10-7}$$

A relation between P_0 and λ can thus be derived, since the sought retention curve should intersect this point.

The second step is to calibrate the shape of the retention curve in order to match the experimental data points as closely as possible. Close to full saturation, the curve should be lower than the data points, representing the influence of the build-up of swelling pressure.

Parameters and graphs for eleven different van Genuchten curves are shown in Table 10-1, Figure 10-6 and Figure 10-7. For three materials, corresponding tables have been adopted for the use in Abaqus (see also Table 12-7).

Additional retention curves have been adopted for adhering to the measured data during conditions with dehydration, and for sensitivity analyses. For the former purpose an extended van Genuchten law has been employed:

$$S_r(s) = \left(1 + \left(\frac{s}{P_0}\right)^{\frac{1}{1-\lambda}}\right)^{-\lambda} \left(1 - \frac{s}{P_1}\right)^{\lambda_1} \tag{10-8}$$
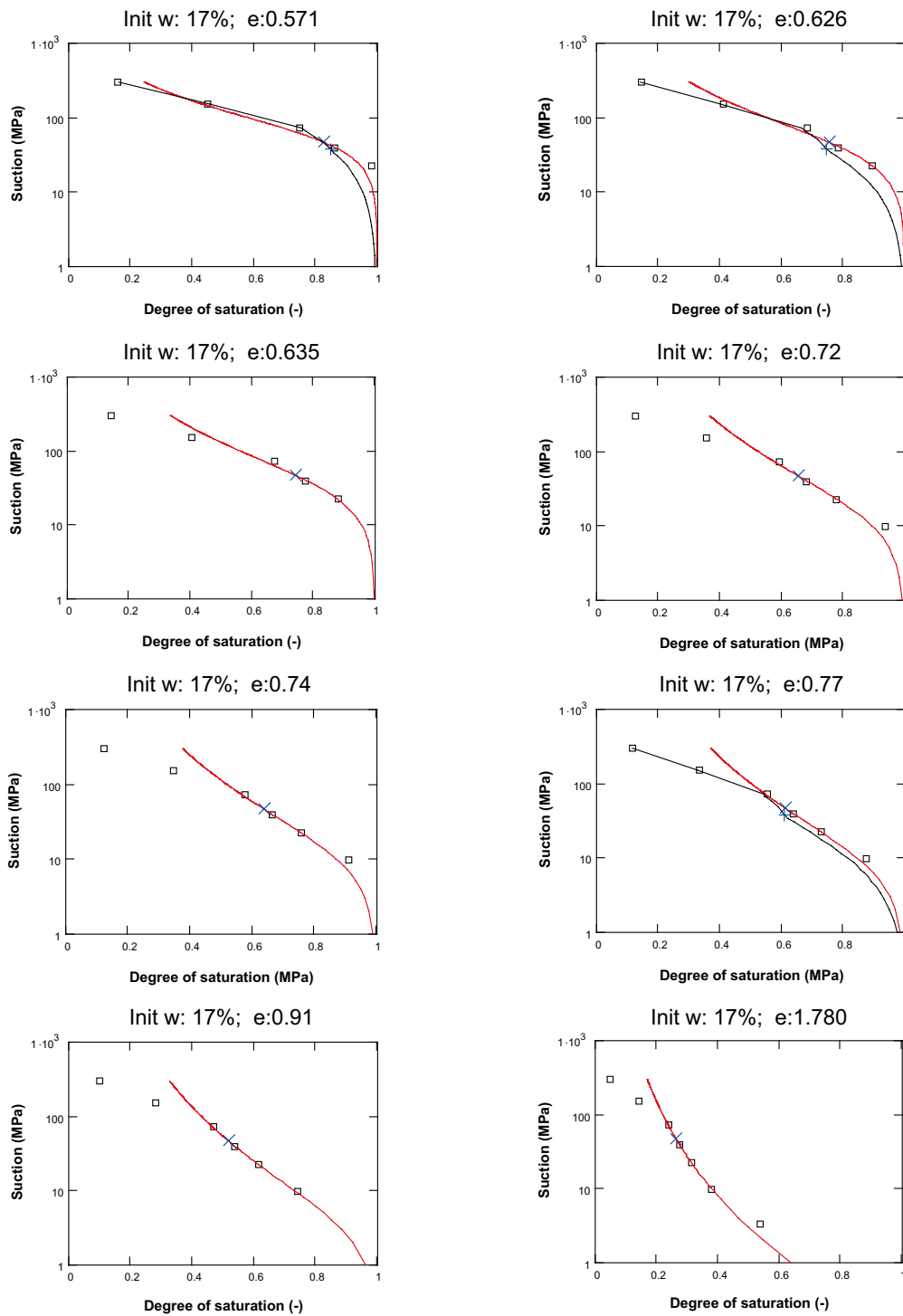
Figure 10-6. *Retention curves for different water contents and void ratios. Red lines: Code_Bright relations; Black lines: Abaqus relations; □: measured data at free swelling; ×: initial condition Code_Bright; +: initial condition Abaqus.*
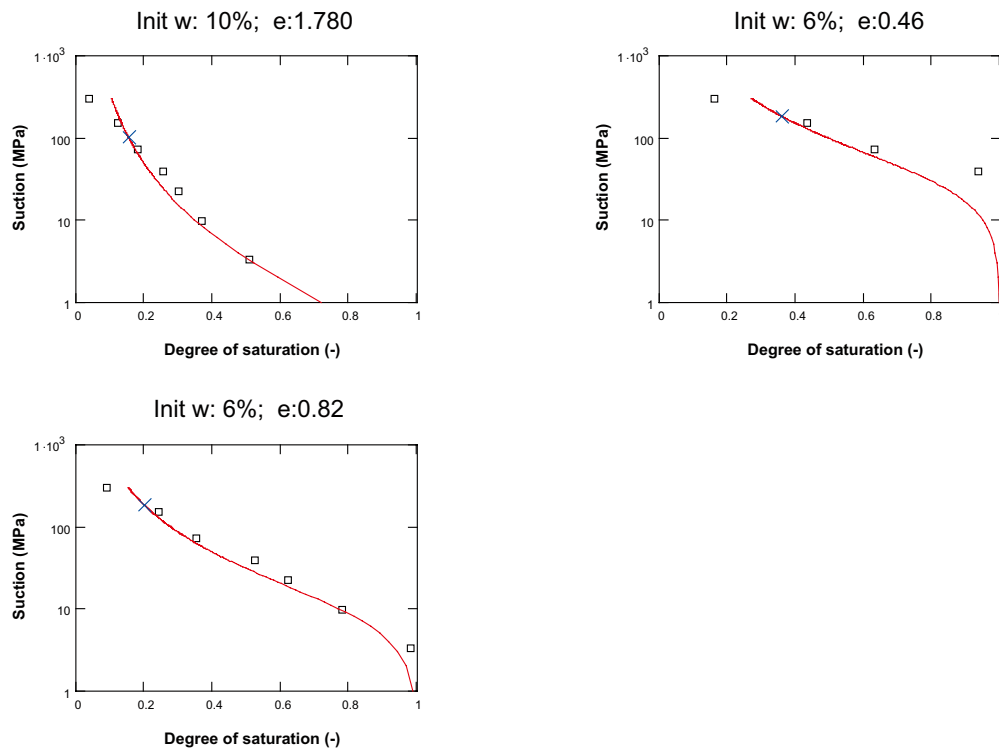
Figure 10-7. *Retention curves for different water contents and void ratios. Red lines: Code_Bright relations; □: measured data at free swelling; ×: initial condition Code_Bright.*

Table 10-1. Parameters for retention curves for different water contents and void ratios.

Material	Water content (%)	Void ratio (–)	P_0 (MPa)	λ (–)	Init. S_r (–)	Init. suction (MPa)
Buffer – ring shaped blocks	17	0.571	67.2	0.48	0.828	46
Buffer – solid blocks	17	0.626	43.5	0.38	0.755	46
Backfill – blocks	17	0.635	37.2	0.34	0.744	46
Homogenized buffer – blocks	17	0.72	15.2	0.25	0.656	46
Homogenized backfill – lower limit	17	0.74	11.6	0.23	0.639	46
Homogenized buffer – rings	17	0.77	8.93	0.22	0.614	46
Homogenized backfill – upper limit	17	0.91	3.45	0.20	0.519	46
Backfill – pellets	17	1.78	0.162	0.19	0.266	46
Buffer – pellets	10	1.78	0.508	0.26	0.156	100
Bore-hole seal – block	6	0.46	33.3	0.37	0.363	179
Bore-hole seal – homogenized	6	0.82	9.39	0.35	0.203	179

Parameter values for retention curves on this form have been adopted for initial buffer blocks void ratios and homogenized buffer void ratios (Table 10-2; Figure 10-8). For sensitivity analyses, steeper retention curves have been adopted in accordance with the model by /Dueck 2004/. This has been made for buffer blocks (Table 10-2; Figure 10-8), as well as backfill blocks and pellets (Table 10-3; Figure 10-9).

Figure 10-8. *Additional retention curves for buffer. Lines: Code_Bright relations; □: measured data at free swelling; ×: initial condition Code_Bright.*

Table 10-2. Parameters for additional retention curves for buffer.

Material	Water content (%)	Void ratio (–)	P_0 (MPa)	λ (–)	P_1 (MPa)	λ_1 (–)	Init. S_r (–)	Init. suction (MPa)
Buffer – ring shaped blocks	17	0.571	47.651	0.05	320	1.0	0.828	46
Buffer – solid blocks	17	0.626	5.222	0.05	280	0.9	0.755	46
Homogenized buffer – blocks	17	0.72	15.56	0.19	400	1.0	0.656	46
Homogenized buffer – rings	17	0.77	8.176	0.165	350	0.9	0.614	46

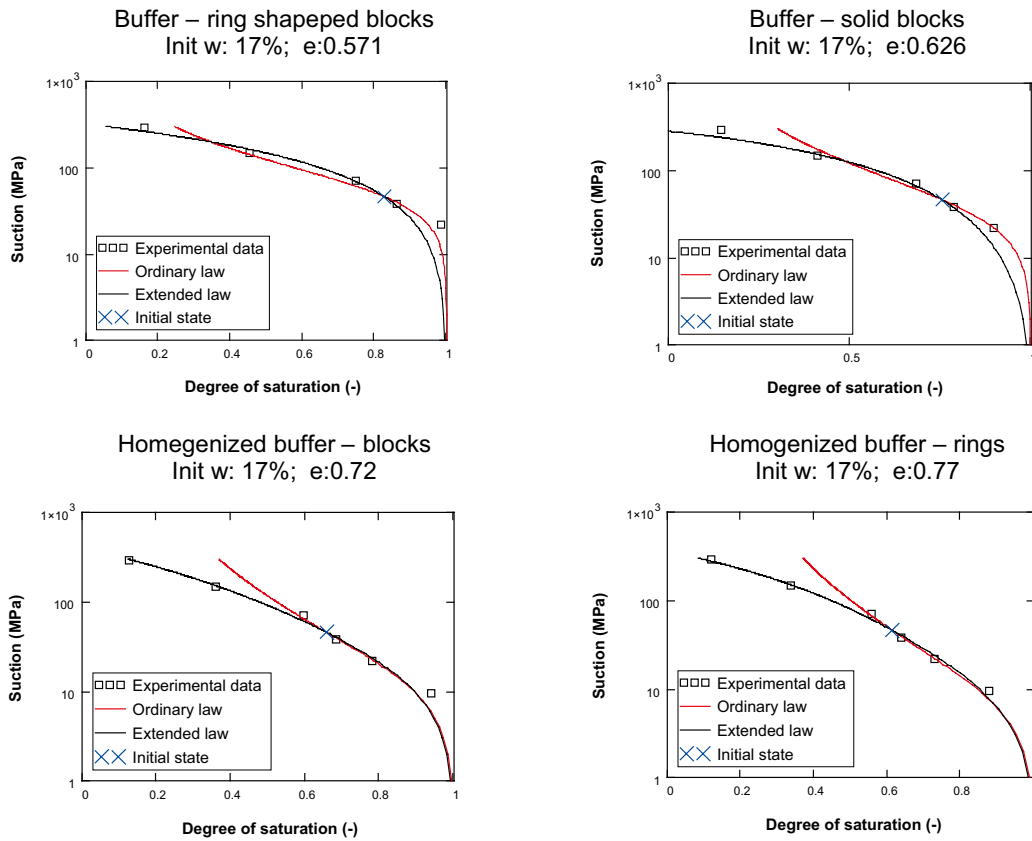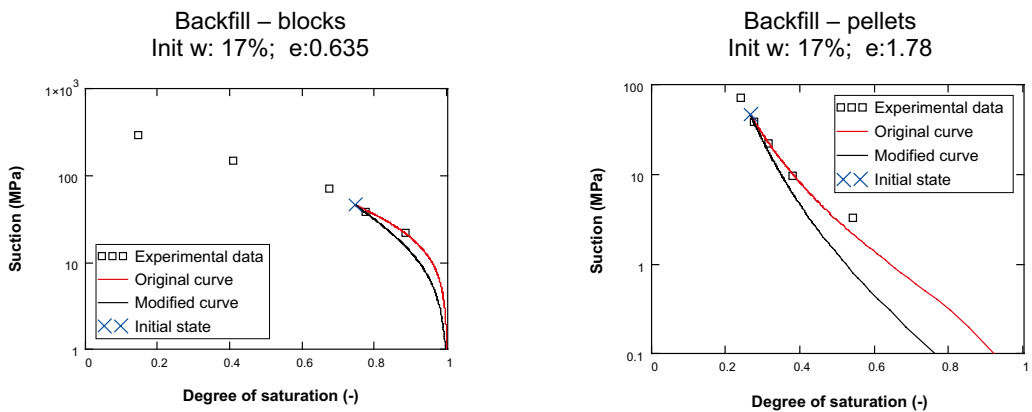**Figure 10-9.** *Additional retention curves for backfill. Lines: Code_Bright relations; □: measured data at free swelling; ×: initial condition Code_Bright.*

Table 10-3. Parameters for additional retention curves for backfill.

Material	Water content (%)	Void ratio (–)	P_0 (MPa)	λ (–)	Init. S_r (–)	Init. suction (MPa)
Backfill – blocks	17	0.635	17.4	0.2	0.744	46
Backfill – pellets	17	1.78	0.0251	0.15	0.266	46

10.2.5 Swelling pressure

Measurements of the swelling pressure (p_{swell}) with distilled water and at different densities were presented in /Börgesson et al. 1995/. A relation between p_{swell} and the void ratio e were adopted on the following form:

$$p_{swell}(e) = p_{swell\,0} \cdot \left(\frac{e}{e_0}\right)^{\frac{1}{\beta}}$$

(10-9)

where $p_{swell\,0}$ is the swelling pressure at the reference void ratio e_0 and β is a fitted exponent. In /Börgesson et al. 1995/, the following parameter setting was adopted for conditions with room temperature, distilled water and void ratios between 0.5 and 1.5:

$p_{swell\,0} = 1$ (MPa)
$e_0 = 1.1$ (–)
$\eta = -0.19$ (–)

The swelling pressure is routinely measured together with the hydraulic conductivity, and therefore the same sources used for the hydraulic conductivity have been used for the swelling pressure. A compilation of measured swelling pressures is shown in Figure 10-10 and Figure 10-11.

It can be noticed that the values from /Karnland et al. 2006/ are generally higher than other measurements, especially at dry densities below 1,300 kg/m³. There is apparently a significant deviation in two branches below this limit. This can to some extent be explained by the difference in salt content, although other results from /Karnland et al. 2006/ obtained at 0.1 and 0.3 M NaCl concentration are only marginally lower than the data shown in Figure 10-10 and Figure 10-11. The lower branch is supported by other measurements of swelling pressure for typical pellets densities /Karnland et al. 2008/. On the other hand, the higher branch is supported by results from saturated oedometer tests reported in /Börgesson et al. 1995/. Measurements on Na-converted and purified samples in /Karnland et al. 2006/ are also in more agreement with theoretical calculations /Karnland et al. 2005/. Due to this ambiguity, two types of expressions have been evaluated.

The first relation is evaluated in the same way as for the hydraulic conductivity: by neglecting data from /Karnland et al. 2006/ and other data below 1,000 kg/m³. A new relation on the same form as (10-9) has been adopted with least-square regression for the remaining data. The following parameters have been found:

$p_{swell\,0} = 2.4$ (MPa)
$e_0 = 1.0$ (–)
$\eta = -0.185$ (–)

A second relation is evaluated from data from /Karnland et al. 2006/ on the form:

$$\log^{10}(p_{swell}) = c_2 \cdot \rho_d{}^2 + c_1 \cdot \rho_d + c_0$$

(10-10)

The following coefficients have been derived with least-square regression (p_{swell} in kPa):

$c_0 = 1.23$
$c_1 = 7.97 \cdot 10^{-4}$
$c_2 = 5.95 \cdot 10^{-7}$

The adopted polynomial function (10-10) has some advantages in comparison to the simple power function (10-9). For instance, the power function clearly overestimates the swelling pressure at high densities (above dry densities of 1,600 kg/m³). Moreover, the polynomial function appears to be fairly representative for all measurements above dry densities of 1,400 kg/m³. Finally, it may also be numerically more convenient (for Code_Bright) to apply the polynomial function, with its considerable swelling pressures at pellets density. It is therefore recommended that the (10-10) relation based on the data from /Karnland et al. 2006/ is used in the parameter evaluation.

An additional swelling pressure curve has also been adopted from measured retention data for an initial water content of 17.5% /Dueck 2004/. The curve follows the (10-10) relation and was fitted by hand in order to approximate the retention data as well as the lower end of the scatter of swelling pressure data (Figure 10-10 and Figure 10-11). It should be noted that the point in the retention data for RH 97.6% (corresponding to a swelling pressure of approx. 3.3 MPa) represents a short equilibration time of only approx. 3 weeks. The following coefficients have been adopted (p_{swell} in kPa):

$c_0 = -1.74$

$c_1 = 4.12 \cdot 10^{-3}$

$c_2 = -3.94 \cdot 10^{-7}$

It can be noticed that this line is very close to the relation adopted by /Börgesson et al. 1995/ for void ratios higher than 0.8. This curve has also been used in some Code_Bright calculations and this will be reported as part of Task 5.

10.2.6 Shear strength

The shear strength is quantified through triaxial compression test during which the sample is driven to failure. The main results from such tests are the mean effective stress (p') and the deviatoric stress (q) at the point of failure. Results from triaxial tests with different densities were presented in /Börgesson et al. 1995/, and a compilation showed that the failure points in the p-q plane can be described as:

$$q = a \cdot p'^b \tag{10-11}$$

The value of a and b are 2.45 and 0.77, respectively, if the stresses are given in kPa.
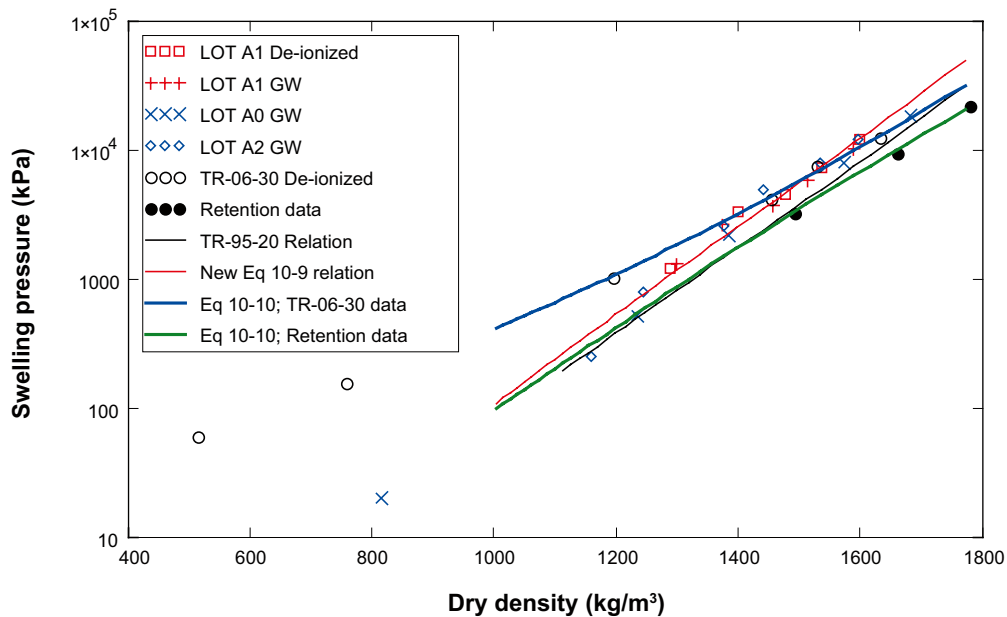
Figure 10-10. *Swelling pressure versus dry density.*
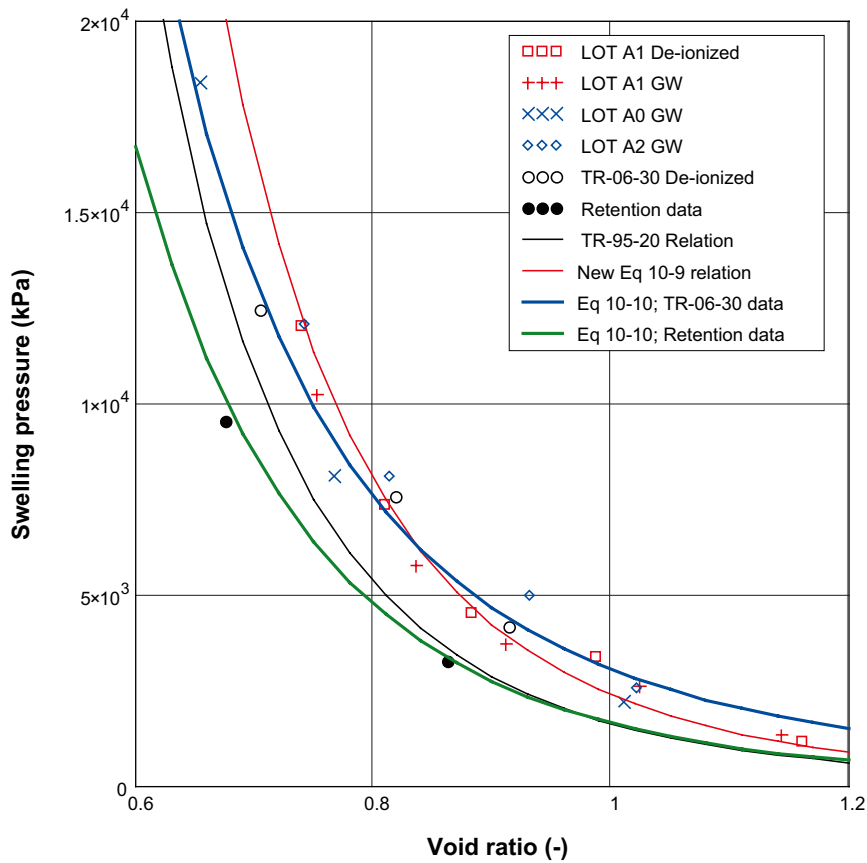
Figure 10-11. *Swelling pressure versus void ratio.*

Newer measurements have been presented by /Karnland et al. 2000, Karnland et al. 2009, Dueck and Nilsson 2010/ and /Dueck et al. 2010/. A compilation of results are shown in Figure 10-12. A new relation on the same form as (10-11) has been adopted with least-square regression for these points. The following parameters have been found: a=2.68 and b=0.76.
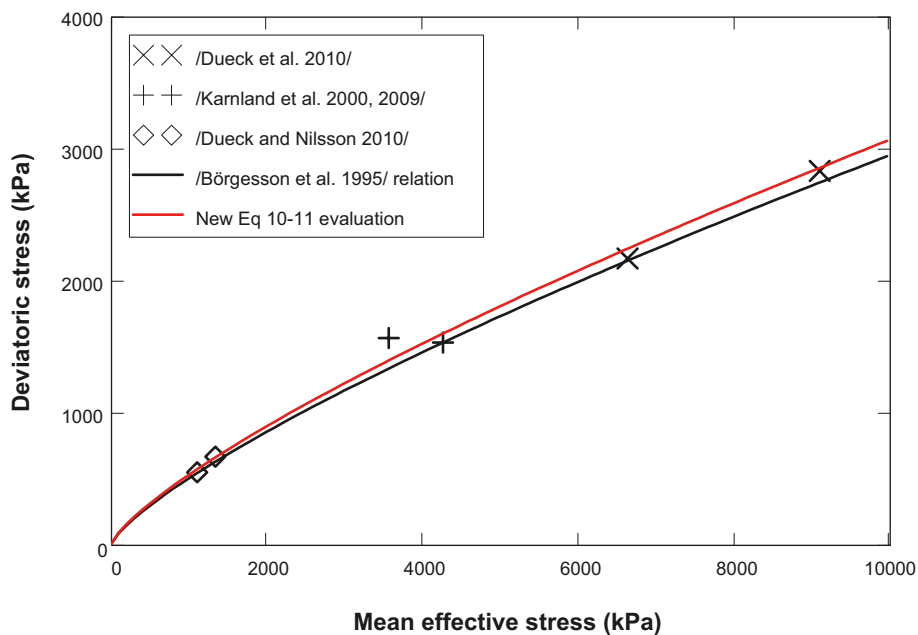
Figure 10-12. *Deviatoric stress versus mean effective stress at points of failure.*

It can be noticed that the original curve is very similar to the relation evaluated from the recent measurement. The former relation is therefore used in the evaluation of mechanical parameters in Section 10.2.8.

Some analytical calculations in the modelling tasks will be based on the friction angle of the bentonite. The failure points in the p-q plane correspond to friction angles (φ) in the σ-τ plane according to the following relation:

$$\sin \phi = \frac{3q}{q + 6p'} \qquad\qquad (10\text{-}12)$$

Based on this and Equation (10-11), a relation between the friction angle and the mean effective stress can be derived (Figure 10-13).

10.2.7 Tensile strength

An indication of the tensile strength can be obtained from beam tests. This type of test results in a major principal stress σ_{tf} at yielding. Since the two minor principal stresses are zero, all such results fall on a straight line in the p-q plane ($-\sigma_{tf}/3$, σ_{tf}). Results from such tests with saturated samples and different dry densities are given in /Karnland et al. 2000/.

A relation, similar to the one used for the swelling pressure (10-10), is adopted for the tensile yield stress. The relations are shown together with experimental data in Figure 10-14. The following coefficients have been adopted (in kPa):

$c_0 = -2.26$

$c_1 = 5.40 \cdot 10^{-3}$

$c_2 = -1.24 \cdot 10^{-6}$
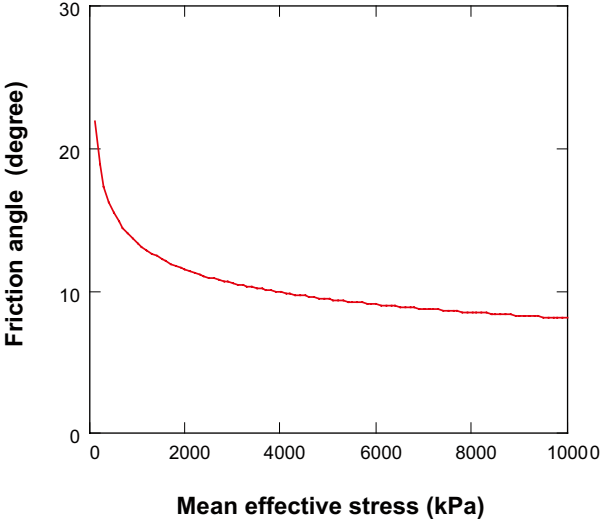
Figure 10-13. *Friction angle versus mean effective stress.*
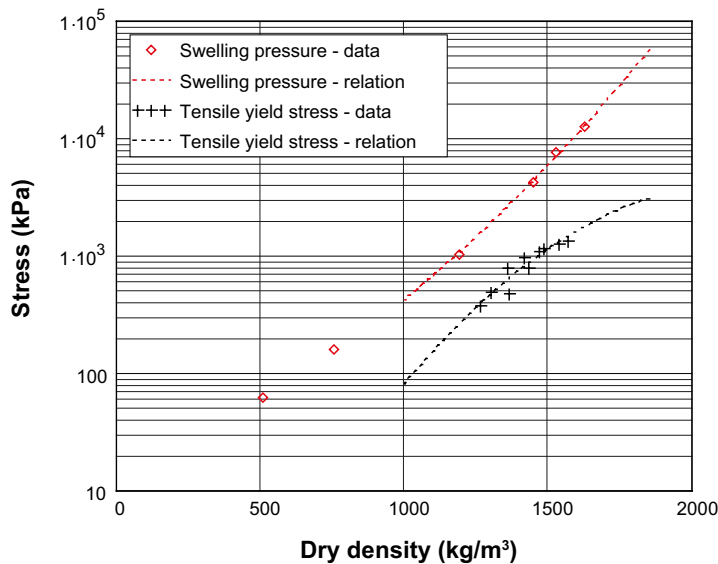
Figure 10-14. Experimental data and adopted relations for swelling pressure and tensile yield stress.

10.2.8 Mechanical parameters – Code_Bright

An in-depth description of the thermo-elastoplastic (TEP) constitutive laws, which are based on the Barcelona Basic Model (BBM) and used in Code_Bright, is given in /Kristensson and Åkesson 2008/ together with evaluations of experimental results from test performed with MX-80. A summary is also given in Appendix D. Below a strategy for a general parameter adoption for different void ratios is given.

A key mechanical property is the swelling pressure. In principal, it would be possible to apply either one of the relations derived in Section 10.2.5. As stated before, it may however be numerically more convenient to apply the one following (10-10) and this is therefore used in the following parameter adoption.
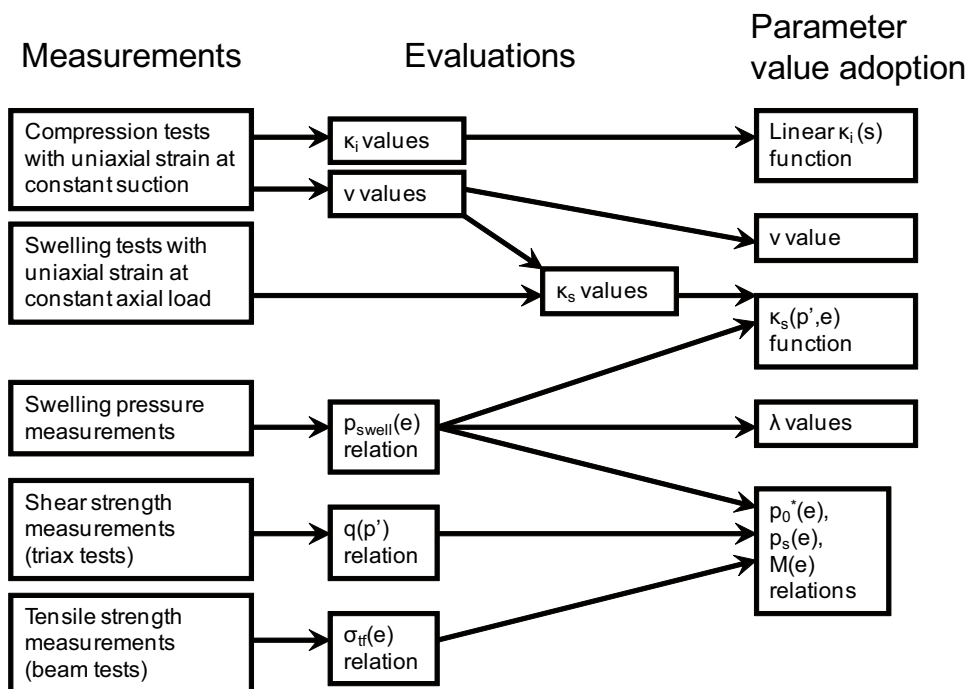
Figure 10-15. Strategy for adoption of mechanical parameters.

κ_i

This is the porous-elastic stiffness parameter. The parameter can be directly evaluated from compression tests with uniaxial strain at constant suction if both axial and radial stresses are measured. Unsaturated samples at buffer density generally show parameter values between 0.001 and 0.06 (see Appendix B). Unloading of saturated oedometers at similar densities and with free access of water show values of 0.12–0.15.

The TEP laws enable the adoption of a κ_i for zero suction and a suction dependence (both linear and logarithmic). Moreover, the specification of a minimum bulk modulus (K_{min}) replaces the κ_i-value at low stress levels. The relation between the bulk modulus and the κ_i is given by $K = p'\cdot(1+e)/\kappa_i$.

To model a water uptake test with fairly constant volume, it can be relevant to adopt a linear suction dependence so that κ_i is close to (although not lower than) zero for the initial suction value (s_i), and that it assumes the experimentally determined value (i.e. 0.12–0.15) at zero suction. The α_i is thus set according to:

$$\alpha_i \approx -\frac{1}{s_i} \tag{10-13}$$

Still, it should be observed that this is only an illusory suction dependence: With the decrease of suction follows the build-up of stresses. And with an increasing κ_i value, this corresponds to a fairly constant bulk modulus.

The K_{min} value is set low (e.g. ≤ 20 MPa), in order to adhere to the BBM model as far as possible.

κ_s

This is a modulus that describes the swelling and shrinking behaviour and is defined in a similar way as the κ_i modulus. Swelling tests with uniaxial strain for unsaturated samples at low constant axial stress and buffer density generally show values around 0.3, under the assumption that the Poisson's ratio (ν) is 0.2 (Appendix B). It should be noted that no unique κ_s value can be evaluated from a swelling test with constant axial stress and uniaxial strain, unless either κ_i or ν is known beforehand. Similar swelling tests performed at higher axial stress levels results in lower κ_s value, e.g. for an axial load of 9 MPa, the modulus is approx. 0.07.

The TEP laws enable the adoption of a κ_s for zero suction and an exponential suction dependence and a logarithmic stress dependence. The suction dependence can describe the shrinkage limit at high suction levels and is therefore important to take this into account if dehydrating conditions is being modelled. The pressure dependence can fairly well describe the κ_s-values that have been evaluated from swelling tests performed at different levels in axial stress.

The pressure dependence, described by α_{sp} and p_{ref}, implies a stress level for which κ_s and the swelling strain is zero, and the final swelling pressure is more or less given by this stress level. The α_{sp} can thus be set according to the swelling pressure for the current void ratio:

$$\alpha_{sp} = -\frac{1}{\ln\left(\dfrac{p_{swell}(e)}{p_{ref}}\right)} \tag{10-14}$$

This approach is fairly unambiguous if the volume is constant. If the material will expand to a higher void ratio however, it is necessary to modify the α_{sp}-value in order to correspond to the lower swelling pressure. A swelling pressure relation, such as (10-10), has therefore been incorporated by Clay Technology AB in the source code (see Appendix C). This would thereby replace the use of a constant specified α_{sp}-value.

The reference pressure p_{ref} is set to a level below the final swelling pressure for the void ratio in question. For pellets, a value of 0.1 MPa is appropriate, whereas a value of 1 MPa is chosen for blocks.

v

The Poisson's ratio (v) is the conventional elastic parameter, defined as the negative ratio between the transverse strain and the axial strain for uniaxial compression tests. Compression tests with uniaxial strain for unsaturated samples at constant suction and buffer density show values between 0.1 and 0.4 (Appendix B). In general, the value tends to increase for increasing stress levels. However, the highest v values reflect plastic strains and should therefore not be adopted. A general value of 0.2 therefore appears to be appropriate.

λ

This is a stress-strain modulus for *plastic* deformation defined in the same way as the κ_i modulus. An indication of the value of this modulus can be gained through direct evaluation of compression tests. For compression tests on unsaturated samples with uniaxial strain and constant suction at buffer density, such evaluations show values between 0.10 and 0.16 (Appendix B). However, under uniaxial and triaxial conditions, the true value, which can be obtained through calibration modelling, tends to be slightly lower than the directly evaluated value.

The modulus for saturated conditions can be argued to correspond to the swelling pressure curve. And for buffer density this should correspond to the range 0.15 to 0.20.

The TEP laws enable and prescribe the adoption of a λ-value for zero suction and an exponential suction dependence. And this suction dependence is one of the corner stones of the loading-collapse (LC) yield curve. The convex shape of this curve is basically a result of the suction dependence of λ. If λ *decreases* with increasing suction then the p_0 *increases* with increasing suction.

However, the experimental data for buffer density show that the value of lambda for a given void ratio is only slightly lower at unsaturated conditions. Moreover, compaction curves for different water contents show that the final void ratio at a load of 25 MPa is approx. 0.71 and virtually independent of the water content /Johannesson et al. 1995/. Above 25 MPa the final void ratio actually tends to increase slightly with increasing water content. This suggests that the LC-curve, at buffer density, is basically a straight line in the s-p plane. Still, at lower compaction loads and higher void ratios, it may be relevant to apply a convex LC curve, since in this case the final void ratio tends to decrease with increasing water contents (see compaction data in /Börgesson 2001/).

The general approach for the determination of lambda is to calculate it as the average module between two points on the swelling pressure curve, representing the initial void ratio (e_i) and the homogenized target void ratio (e_f) (Figure 10-16).

$$\lambda = -\frac{e_i - e_f}{\ln(p_{swell}(e_i)) - \ln(p_{swell}(e_f))} \qquad (10\text{-}15)$$

It should be noted that material undergoing a successive swelling and compression cycle (typically outer parts of blocks) can reach an intermediary void ratio that is higher than the final void ratio. This can motivate a higher value of the modulus (Figure 10-16).

The lambda value is made independent of the suction level by setting r and β to zero.

$p_0{}^*$, p_s and M

The yield surface is described by three parameters: p_0, p_s and M. The first parameter, p_0, is the pre-consolidation stress; p_s is the tensile strength and M is the critical state line parameter, which describes the slope of the line between the tensile strength point (p_s) and the failure point of the yield surface in the p'-q plane.

The pre-consolidation stress for zero suction conditions, denoted $p_0{}^*$, is set initially and acts as a hardening parameter which changes during plastic deformations. As was mentioned above, p_0 can be given a suction dependence through the treatment of lambda. But the pre-consolidation stress will be independent of suction if lambda is made independent of suction.
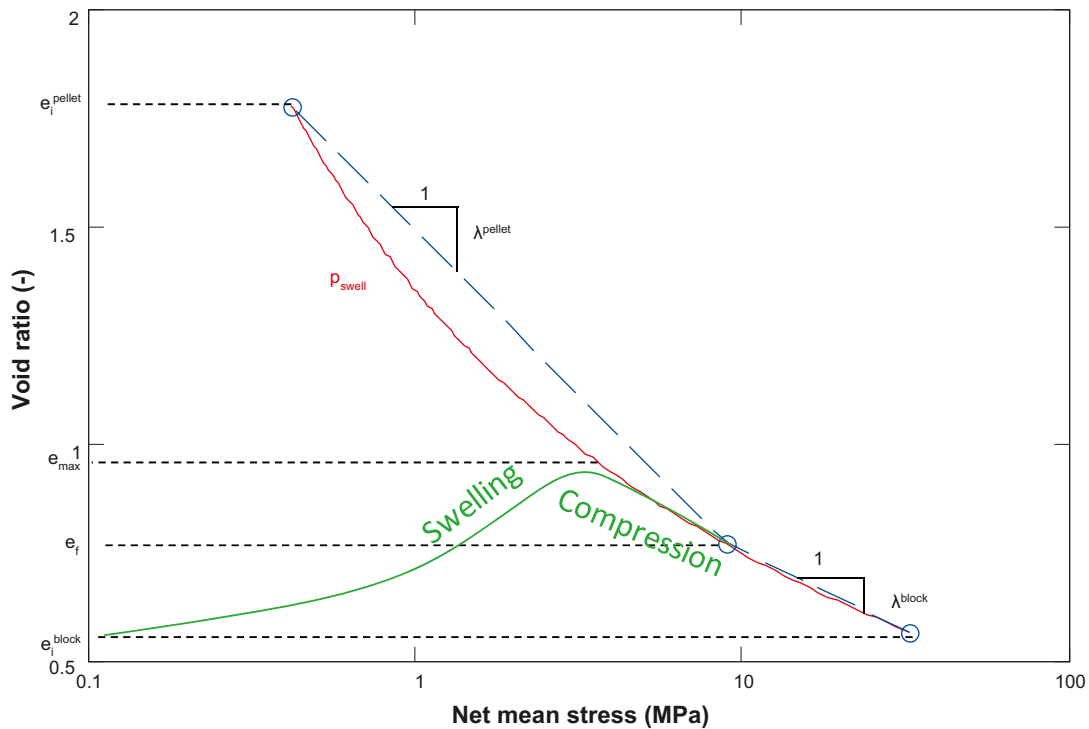
Figure 10-16. *Adoption of lambda values for initial and homogenized target void ratios. Note the stress path for swelling/compression.*

The tensile strength can be given a linear suction dependence. Experimental data suggests however that the *shear strength* of MX-80 is more dependent on void ratio than on the degree of saturation /Dueck 2010/. The suction dependence is therefore not used in this approach.

Void ratio dependences for these three parameters (p_0^*, p_s and M) can be derived under the assumption that *the net mean stress at the failure point is equal to the swelling pressure for the void ratio in question* (Figure 10-17). This is a fairly relevant approach since an undrained triaxial test exhibit a constant p'-value and in principle ends at the point of failure. The value of p_0^* will thus be slight more than twice as high as the swelling pressure. This may very well correspond to the relation between the compaction pressure and the swelling pressure for a given density.

There are thus three relations: $\sigma_{tf}(e)$, $p_{swell}(e)$ and q(p') at failure, and if treated as an equation system, the three parameters (p_0^*, p_s and M) can be derived.

First, the yield surface is described by the following relation:

$$q^2 = M^2(p' + p_s)(p_0^* - p') \qquad (10\text{-}16)$$
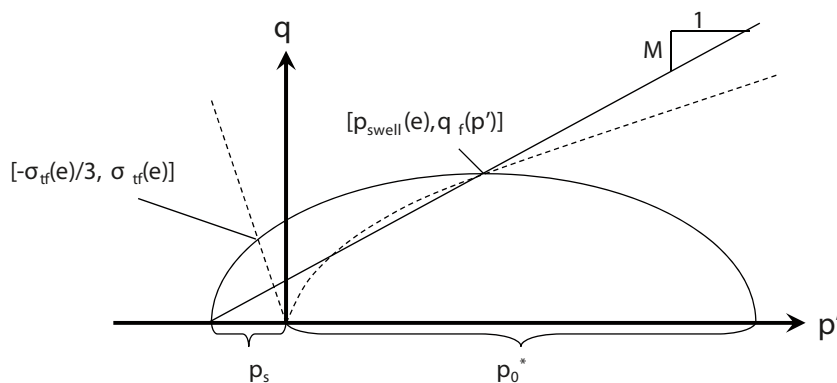
Figure 10-17. *Determination of plastic parameters p_s, p_0^* and M from shear strength relation and void ratio dependences of swelling pressure and tensile strength.*

The net mean stress at the critical state point is equal to the swelling pressure, ($p'= p_{swell}$). From this it follows that:

$$p_0^* = p_s + 2 \cdot p_{swell}$$

(10-17)

The deviatoric stress q at the critical state point (q_f) is given by (10-11):

$$q_f = a \cdot p_{swell}^{\ b}$$

(10-18)

If Equations (10-16)–(10-18) are taken together, a relation between M and p_s can be derived as:

$$M = \frac{a \cdot p_{swell}^{\ b}}{p_{swell} + p_s}$$

(10-19)

Secondly, the yielding point in the beam tests is defined as:

$$q = \sigma_{tf} \qquad p' = -\frac{\sigma_{tf}}{3}$$

(10-20)

If this is substituted into the yield surface relation (10-16) one gets:

$$\sigma_{tf}^{\ 2} = M^2 \left(p_s - \frac{\sigma_{tf}}{3} \right) \left(p_0^* + \frac{\sigma_{tf}}{3} \right)$$

(10-21)

And if p_0^* is substituted according to (10-17), one gets a second relation between M and p_s:

$$M = \frac{\sigma_{tf}}{\sqrt{\left(p_s + 2 \cdot p_{swell} + \frac{\sigma_{tf}}{3} \right) \left(p_s - \frac{\sigma_{tf}}{3} \right)}}$$

(10-22)

Equations (10-19) and (10-22) can be combined so that an expression for p_s can be derived:

$$p_s = -p_{swell} + \sqrt{ p_{swell}^{\ 2} + \frac{\frac{\sigma_{tf}}{3} \left(2 \cdot p_{swell} + \frac{\sigma_{tf}}{3} \right) + \left(\frac{\sigma_{tf}}{a \cdot p_{swell}^{\ b-1}} \right)^2}{1 - \left(\frac{\sigma_{tf}}{a \cdot p_{swell}^{\ b}} \right)^2} }$$

(10-23)

And with p_s known, p_0^* and M can be calculated from (10-17) and (10-19), respectively. Calculated values of p_s, M, p_0^* and p_{swell} are shown in Figure 10-18. The void ratio dependence of the yield surface is illustrated in Figure 10-19.
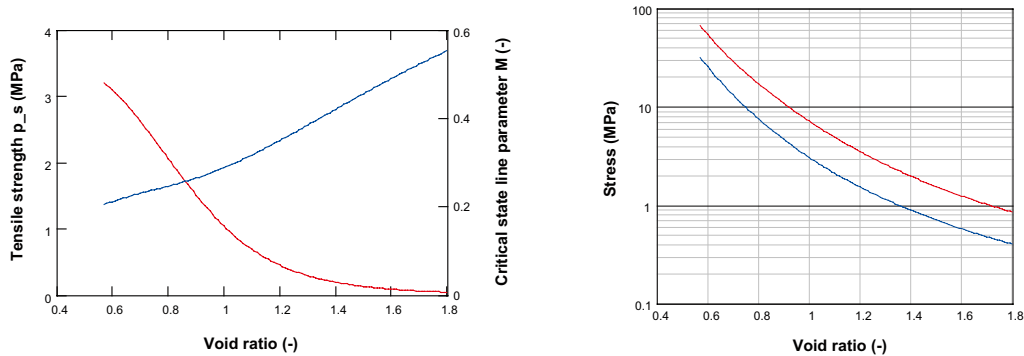
Figure 10-18. *Evaluated parameters for different void ratios. Left: p_s (red) and M (blue); right: p_0^* (red) and p_{swell} (blue).*
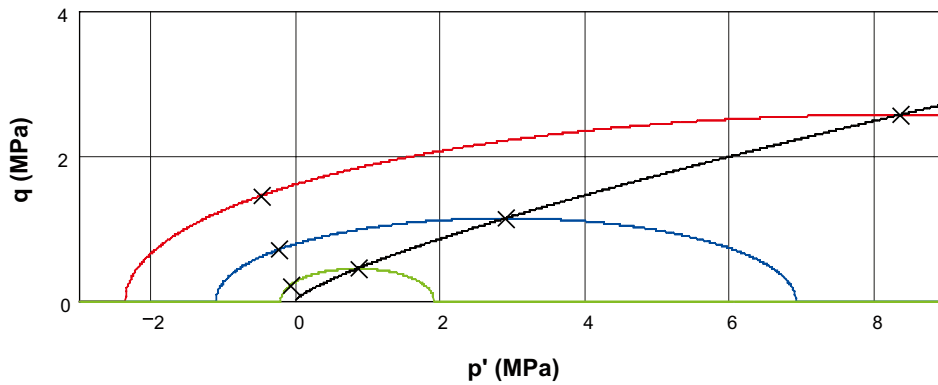
Figure 10-19. *Examples of evaluated yield surfaces for different void ratios: 0.77 (red), 1 (blue) and 1.4 (green). The black line is the failure points described by (10-11).*

α

Finally, α is the non-associativity parameter, which describes the difference between the yield surface and the plastic potential. The value of this falls, by definition, in the interval between 0 and 1. A general value of 0.5 appears to be appropriate. This value has been found to give good agreement with some experimental results (see /Kristensson and Åkesson 2008/).

Considerations for general parameter settings

As shown in Figure 10-19, the size of the yield surface is reduced during isotropic swelling. This behaviour has been addressed in the development of the Barcelona Expansive Model (BExM), but cannot be captured by BBM. Instead, it is suggested that the parameters for the materials that expands (e.g. blocks) are set to correspond to the homogenized target void ratio.

Table 10-4. General mechanical parameter setting for MX-80.

Parameter			
Elastic	κ_i	κ_{i0}	0.12–0.15
		α_i	Set from initial suction
		α_{ils}	0
		K_{min}	≤ 20 MPa
	κ_s	κ_{s0}	0.3
		α_{ss}	0
		α_{sp}	Replaced with inbuilt swelling pressure relation
		p_{ref}	0.1 MPa (pellets) 1 MPa (blocks)
	v	v	0.2
Plastic	λ	λ_0	Set from initial and target void ratio
		r	0
		β	0
	M	M	Set from initial void ratio (pellets) Set from target void ratio (blocks)
	p_s	p_{s0}	Set from initial void ratio (pellets) Set from target void ratio (blocks)
		k	0
	p_0	p_0^*	Set from initial void ratio or lower (pellets) Set from target void ratio (blocks)
		p_c	1 MPa
	α	α	0.5

Pellet material, on the other hand, is compressed during homogenization. Moreover, close to the water supply it also reaches water saturation much faster than large blocks. It can therefore be foreseen that the possibility to capture the mechanical behaviour of the pellets relies heavily on the consistency between the initial swelling pressure (given by the inbuilt pressure dependence of κ_s) and the applied stress-strain relation (given by the specified lambda modulus). Moreover, the dual-porosity character of pellets materials can be foreseen to display some deviating behaviour. For example, the stress level at which plastic conditions begin, i.e. the pre-consolidation stress, can be expected to be significantly lower than for a homogenous sample with the same density. It may therefore be appropriate to apply a significantly lower p_0^*-value for pellets than for a homogenous sample, in order to enable that the yield surface is reached before the material is water saturated.

10.2.9 Mechanical parameters – Abaqus

Porous elasticity

The *Porous Elastic Model* implies a logarithmic relation between the void ratio e and the average effective stress p according to Equation (10-24).

$$\Delta e = \kappa \Delta \ln p \tag{10-24}$$

where

κ = porous bulk modulus = 0.20

The value of κ has been derived from oedometer and swelling pressure tests /Börgesson et al. 1995/.

Poisson's ratio

Poisson's ratio (ν) is the conventional elastic parameter, defined as the negative ratio between the transverse strain and the axial strain for uniaxial compression tests. A value of 0.4 has been chosen.

Drucker Prager Plasticity

Drucker Prager Plasticity model contains the following parameters:

β = friction angle in the *p-q* plane
d = cohesion in the *p-q* plane
ψ = dilation angle
q = $f(\varepsilon^d_{pl})$ = yield function

The yield function is the relation between Mises' stress q and the plastic deviatoric strain ε^d_p at a specified stress path. The dilation angle determines the volume change during shear.

The following data will be used for the *Drucker Prager Plasticity* model

$\beta = 0.001°$
$d = 2,500$ kPa for $e{=}0.78$
$\psi = 2°$

Table 10-5. Yield function.

q (kPa)	ε_{pl}
1	0
50	0.005
100	0.02
150	0.04
200	0.1

The low friction angle and high cohesion are motivated by the fact that the strength of unsaturated bentonite depends almost entirely of the void ratio independently of the degree of saturation and not by the effective stress /Dueck 2010/. This plasticity data will be used for modelling the saturation phase. Other values of β and d will be used for modelling swelling and homogenization when only fully saturated bentonite is considered since for those cases the effective stress theory is valid:

$\beta = 17°$

$d = 100$ kPa

Mechanical coupling between the structure and the pore water

The mechanical behavior is modelled to be governed by the effective stress theory and a procedure called moisture swelling.

Effective stress theory

The effective stress concept according to Bishop is used for modelling the mechanical behavior of the water-unsaturated buffer material:

$$s_e = (s - u_a) + \chi(u_a - u_w) \tag{10-25}$$

Equation (10-25) is simplified in the following way:

$u_a = 0$ (no account is taken to the pressure of enclosed air)

$\chi = S_r$

Moisture swelling

The shortcomings of the effective stress theory can be compensated in ABAQUS by a correction called "*moisture swelling*". This procedure changes the volumetric strain ε_v by adding a strain that can be made a function of the degree of saturation S_r.

The effective stress theory decomposes the total stress into pore pressure and effective stress (which only depends on deviatoric strains). However, the effective strain can be made dependent on saturation by using the concept of *moisture swelling* which modify the effective strain by this user defined saturation dependent volumetric strain (*moisture swelling*). In this application the moisture swelling contribution is calibrated by using the measured swelling pressure and assuming that the effective strain (after adding the moisture swelling) should be zero. Neglecting moisture swelling will imply an effective strain defined by the elastic material (porous elastic) and thus the moisture swelling strain can be calculated from Equations (10-26) and (10-27).

$$\Delta\varepsilon_v = f(S_r) = \ln(p_0/p)\cdot\kappa/(1+e_0) \tag{10-26}$$

$$p = p_{tot} - u_w\cdot S_r \tag{10-27}$$

where
ε_v = volumetric strain
p_0 = initial effective stress taken from the initial conditions
p = actual effective stress
κ = porous bulk modulus
e_0 = initial void ratio
p_{tot} = actual total stress
u_w = pore water pressure
S_r = degree of water saturation

The moisture swelling relation (*M.S.*) that is needed as input is the logarithmic volumetric strain according to Equation (10-24) where $\Delta\varepsilon_v$ is taken from Equation (10-26).

$$M.S.= \ln(1+\Delta\varepsilon_v) \qquad\qquad (10\text{-}28)$$

The data for the *moisture swelling procedure* is derived from the assumption that the relation between total stress and degree of saturation of a confined sample (constant volume) is linear when the degree of saturation is increased from its initial value to 100% /Dueck 2004/.

The moisture swelling procedure must be adapted to the initial conditions (void ratio and degree of saturation) of the bentonite. Two examples are given here:

1. An increase in degree of saturation from the initial values S_r=69% and e=0.55 to S_r=100% the total pressure increases from 0 to 40 MPa.

2. An increase in degree of saturation from the initial values S_r=82.6% and e=0.60 to S_r=100% yields an increase in total pressure from 0 to 25 MPa.

M.S. as a function of degree of saturation for the two cases is shown in Figure 10-20.

10.2.10 Mechanical properties for special cases – Abaqus

Creep behaviour

Creep processes in the bentonite buffer must be considered since the weight of the canister will cause excess remaining uneven stresses in the bentonite and make the canister move due to creep effects. The effect of creep on the canister displacement is investigated as Task 9.

General

The definition of creep is according to normal soil mechanics terminology a strain that will increase with time at a constant load and constant pore water pressure. The latter requirement is necessary in order to distinguish creep from consolidation. The rate of creep is thus controlled by viscosity related deformations in the structure while consolidation is controlled by the rate of the pore water flux out from (or into) the soil pore system. Creep processes take place also when the material is volumetrically confined and will at constant volume yield a change in stress with time (stress relaxation).
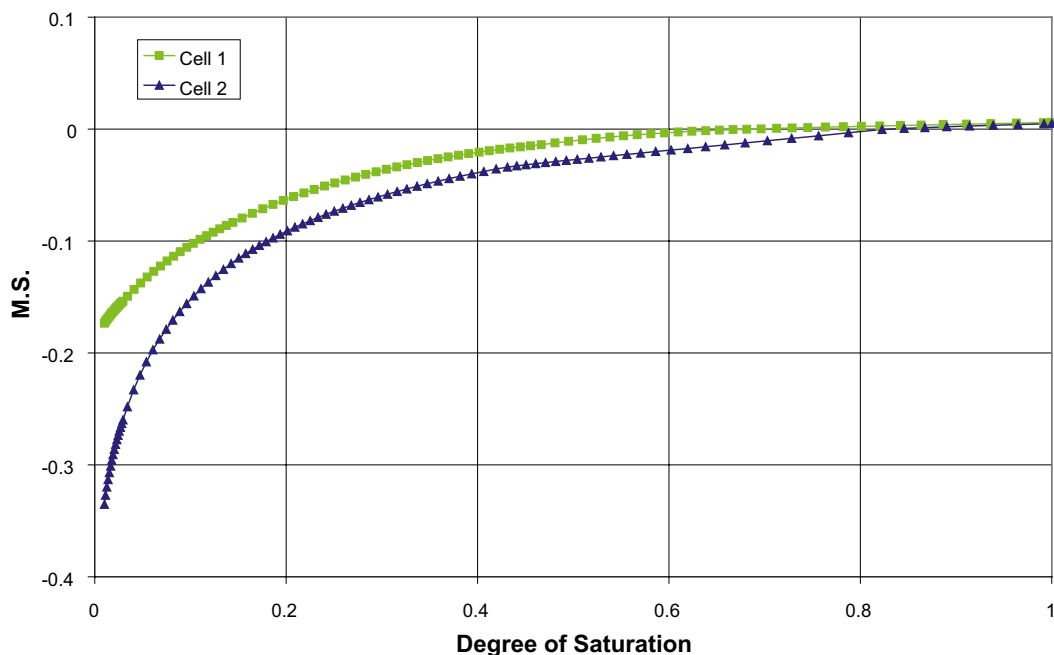
Figure 10-20. Moisture swelling functions derived for the two examples.

Creep at constant stress can be divided into two main processes, namely the volumetric creep and the deviatoric creep with the following symbols:

Volumetric creep strain: $\qquad\qquad \varepsilon_{cv}$

Volumetric creep rate: $\qquad\qquad \dot{\varepsilon}_{cv} = d\varepsilon_{cv}/dt$

Deviatoric creep strain: $\qquad\qquad \varepsilon_{cd}$

Deviatoric creep rate: $\qquad\qquad \dot{\varepsilon}_{cd} = d\varepsilon_{cd}/dt$

Deviatoric creep is developed after a change in deviatoric stress at constant average stress, while volumetric creep rate is caused by a change only in average stress. Only deviatoric creep is considered in the creep model since volumetric creep will not cause mass reduction but only increased density.

Deviatoric creep

The creep theory and the creep tests made for validating the theory and evaluate the parameters are described by /Börgesson et al. 1995/. The proposed creep theory states that the creep rate can be modelled according to Equation (10-29).

$$\dot{\varepsilon}_{cdt} = \dot{\varepsilon}_{cdo} \cdot e^{\alpha D_r} \cdot e^{-\alpha D_{ro}} \cdot \left[\frac{t}{t_o}\right]^{-n} \qquad\qquad (10\text{-}29)$$

where

$\dot{\varepsilon}_{cdt}$ $\qquad$ = deviatoric creep rate ($d\varepsilon_{cd}/dt$) at any time

$\dot{\varepsilon}_{cdo}$ $\qquad$ = deviatoric creep rate ($d\varepsilon_{cd}/dt$) at $t=t_0$

t $\qquad$ = time

t_o $\qquad$ = reference time

e $\qquad$ = 2.7183

D_r $\qquad$ = degree of mobilised strength $(\sigma_1-\sigma_3)/(\sigma_1-\sigma_3)_f$

$(\sigma_1-\sigma_3)$ = deviatoric stress

$(\sigma_1-\sigma_3)_f$ = deviatoric stress at failure

D_{ro} $\qquad$ = reference degree of mobilised strength $(\sigma_1-\sigma_3)_o/(\sigma_1-\sigma_3)_f$

α $\qquad$ = inclination of the relation between $\dot{\varepsilon}_{cdo}$ and D_r plotted in a semi-logarithmic diagram

n $\qquad$ = inclination of the relation between $\dot{\varepsilon}_{cdt}$ and t plotted in a double-logarithmic diagram

The reference parameters are

t_r $\quad$ = 10,000 s

D_{ro} = 0.5

The validity of Equation (10-29) rests on two observations. The first one is that the relation between $\dot{\varepsilon}_{cdo}$ and D_r is a straight line in a semi-logarithmic diagram. As indicated in Figure 10-21 this is not true for low values of D_r and of course not for $D_r=0$. It is neither true for high values of D_r. and of course not for $D_r=1$. Instead the relation shown in Figure 10-21 is used. The second observation is that the relation between $\dot{\varepsilon}_{cdt}$ and t is a straight line in a double-logarithmic diagram. Figure 10-22 shows an example of measurements that confirm this for MX-80.

$0.1 < D_r < 0.9$

The following values were found for Equation (10-29) and the reference parameters:

$\dot{\varepsilon}_{cdo}$ = 4.4·10^{-8} 1/s

α $\quad$ = 4.15

n $\quad$ = 0.91

Equation (10-29) is thus only valid for $0.1 < D_r < 0.9$ and another relation is required outside this range.
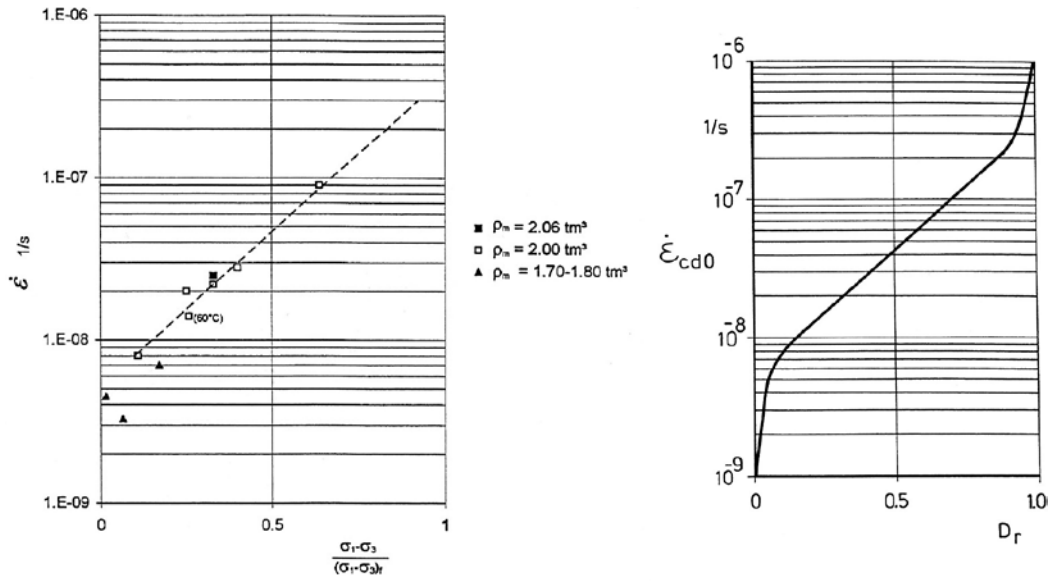
Figure 10-21. *Measured relation between creep rate $\dot{\varepsilon}_{cdt}$ and degree of mobilised strength D_r for MX-80 at different densities (left) and used in the model (right).*
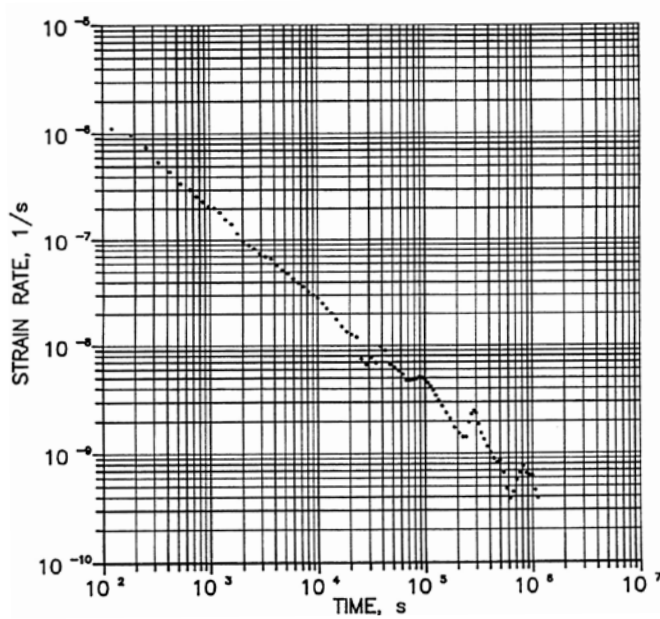
Figure 10-22. *Example of measured creep rate of a sample of MX-80 as a function of time. $\rho_m=1.99$ t/m³, $\sigma_3=4.83$ MPa, $u_i=0.75$ MPa, $D_r=0.40$.*

$D_r < 0.1$

The following equation based on Figure 10-21 and Equation (10-29) is proposed:

$$\dot{\varepsilon}_{cdt} = A \cdot D_r{}^a \cdot \left[\frac{t}{t_o}\right]^{-n} \tag{10-30}$$

with the following parameters

$t_o = 10{,}000$ s

$n = 0.91$

$A = 8.0 \cdot 10^{-8}$ 1/s

$a = 1.0$

$D_r > 0.9$

The following equation also based on Figure 10-21 and Equation (10-29) is proposed:

$$\dot{\varepsilon}_{cdt} = B \cdot \left[1 - D_r\right]^{-b} \cdot \left[\frac{t}{t_o}\right]^{-n}$$
(10-31)

with the following parameters

t_o = 10,000 s
n = 0.91
B = 2.3·10⁻⁸ 1/s
b = 1.0

ABAQUS application

The creep theory has been implemented in ABAQUS. Since the theory according to Equations (10-29) to (10-31) is derived in two dimensions it assumes that the intermediate principle stress σ_2 is equal to the minimum principle stress σ_3, which is the case for the triaxial tests. In the 3D space, which is treated by ABAQUS, σ_2 usually differs from the two other principle stresses. The deviatoric stress D is more generally expressed with von Mises' stress q that takes the intermediate principal stress into account according to Equation (10-32).

$$q = \left(\left((\sigma_1 - \sigma_3)^2 + (\sigma_1 - \sigma_2)^2 + (\sigma_2 - \sigma_3)^2\right)/2\right)^{1/2}$$
(10-32)

If $\sigma_2 = \sigma_3$ Mises stress will be equal to the deviatoric stress ($q = D$)

In ABAQUS the degree mobilized deviatoric strength D_r is exchanged for the degree of mobilized Mises' strength Q_r.

$$Q_r = q / q_f$$

where

q = actual Mises' stress
q_f = Mises' stress at failure

Stress-strain properties at very fast shear

The effect of a rock shear on the buffer and canister is part of the modelling work for the canister and the models and data are described in the data report of the canister.

10.2.11 Phase properties

Particle density

/Karnland et al. 2006/ have reported results from measurements of particle density in different liquids (see Table 10-6). It can be noted that density values obtained from measurements in kerosene are significantly lower than those obtained with different salt solutions and should therefore be disregarded. Values obtained from the different solutions fall in a narrow interval between 2,750 and 2,780 kg/m³. The latter value has been used in all evaluations of void ratios and saturation degrees in this qualification process and should therefore be used in the modelling tasks.

Table 10-6. Compilation of measured particle density (kg/m³) in various liquids (from /Karnland et al. 2006/).

Sample	Kerosene	1 M CaCl2	1 M NaCl	3 M NaCl
1	2,621	2,761	2,776	2,754
2	2,625	2,777	2,777	2,752

Treatment of phase properties in Code_Bright

The density of water (ρ_l) is in Code_Bright treated as a function of the water pressure (P_l), the temperature (T in °C) and the mass fraction of dissolved air (ω_l^h):

$$\rho_l(P_l,T) = \rho_{l0} \cdot \exp\left[\beta \cdot (P_l - P_{l0}) + \alpha \cdot T + \gamma \cdot \varpi_l^h\right] \tag{10-33}$$

where ρ_{l0} is the reference density (1,002.6 kg/m³ as default), β is the compressibility of water ($4.5 \cdot 10^{-4}$ MPa^{-1} as default), P_{l0} is a reference pressure (0.1 MPa as default), α is the volumetric thermal expansion coefficient of water ($-3.4 \cdot 10^{-4}$ °C^{-1} as default), and γ is the solute variation (0.6923 as default).

Treatment of phase properties in Abaqus

Abaqus includes modelling of the separate phases of water and particles, both stress-strain behaviour and thermal expansion.

The water and the particles are mechanically modelled as separate phases with linear elastic behavior. The pore air is not mechanically modelled. The following standard values have been used for the *properties of the water and solid phases*:

$B_w = 2.1 \cdot 10^6$ kPa (bulk modulus of water)

$B_s = 2.1 \cdot 10^8$ kPa (bulk modulus of solids)

$\rho_w = 1,000$ kg/m³ (density of water)

$\rho_s = 2,780$ kg/m³ (density of solids)

The volume change caused by the thermal expansion of water and particles can be modelled with the parameters

α_s = coefficient of thermal expansion of solids

α_w = coefficient of thermal expansion of water

Only the expansion of the separate phases is taken into account. The possible change in volume of the structure by thermal expansion (not caused by expansion of the separate phases) is not modelled. However, a thermal expansion in water volume will change the degree of saturation which in turn will change the volume of the structure. The following values have been used:

$\alpha_w = 3.0 \cdot 10^{-4}$
$\alpha_s = 0$

10.3 Other materials

10.3.1 IBECO RWCBF

Different characterisations and tests have been performed on IBECO RWCBF concurrently with the production of this data report /Johannesson et al. 2010/. The first evaluations of these tests indicate that this material exhibit many similarities with MX-80. Measured values of hydraulic conductivity and swelling pressure are shown in Figure 10-23 together with relations presented in Section 10.2. A retention curve for IBECO RWCBF (initial water content: 19%) is shown in Figure 10-24 together with a corresponding curve for MX-80 (initial water content: 17.5%). The differences between MX-80 and IBECO RWCBF are apparently quite small, except for the hydraulic conductivity at dry densities below approx. 1,400 kg/m³. This can therefore justify the use of MX-80 data for the backfill in the modelling tasks until more data is available for IBECO RWCBF. Some differences may nevertheless be foreseen (given that IBECO RWCBF is a calcium bentonite), such as concerning the hydraulic conductivity and the swelling pressure at low densities and concerning the shear strength. This should be addressed in the modelling tasks.
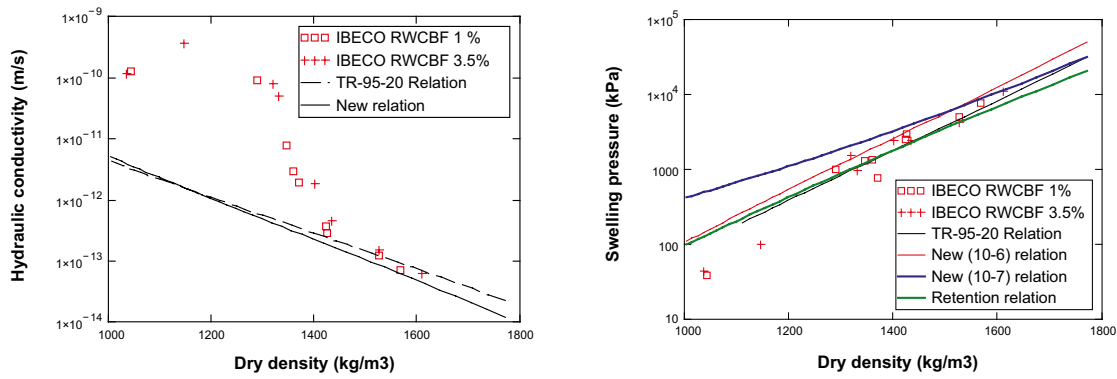
Figure 10-23. *Experimental data for IBECO RWCBF (symbols) and adopted relations for MX-80 (lines) for hydraulic conductivity (left) and swelling pressure (right).*
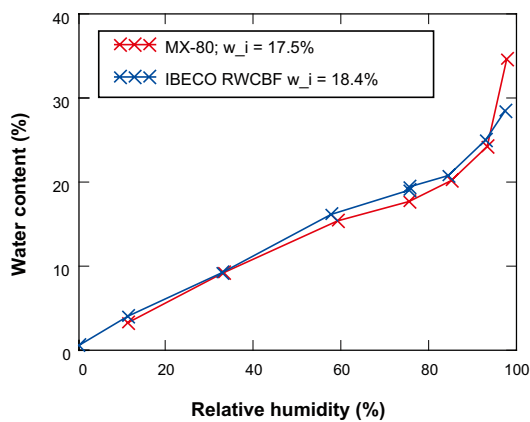
Figure 10-24. *Retention curves for MX-80 and IBECO RWCBF.*

10.3.2 Concrete

Three components of concrete are foreseen in the modelling tasks: i) the tunnel plug, ii) the prefab beams in the plug construction, and iii) the bottom plate. These materials are assumed to exhibit the same properties which are summarized in Table 10-7.

The hydraulic conductivity and the elastic parameters are the most important hydromechanical parameters for the concrete. These have been obtained from the dimensioning of the plug /Dahlström et al. 2009/. The porosity and the aggregates are assumed to be representative for a K40 concrete with a water-cement ratio of 0.5 and was obtained from /Betonghandbok 1994/. The retention properties were also assumed to be representative for a concrete with a water-cement ratio of 0.5 and was obtained from /Hedenblad 1996/. The adoption of van Genuchten parameters are shown in Figure 10-25. A cubic power law was assumed for the relative permeability law.

Table 10-7. Data used for concrete components.

Parameter		Tunnel plug	Bottom plate	Prefab beams
Porosity	n (–)	0.135	0.135	0.135
Intrinsic permeability	k (m²)	5E–19	5E–19	1E–15
Relative permeability	k_r (–)		S_r^3	
Water retention curve	P_0 (MPa)		9	
	λ (–)		0.3	
Elastic parameters	E (GPa)		35	
	v (–)		0.27	
Aggregates	(–)	0.67	0.67	–

Figure 10-25. Adoption of van Genuchten retention curve. Left: for concrete with data from /Hedenblad 1996/. Right: for fine sand (after /Bear 1972/).

10.3.3 Crushed rock

Two components of crushed rock are foreseen in modelling tasks: i) the filter in the plug construction, and ii) the filling of the central area and the upper parts of the ramp and the shafts. These materials are assumed to differ with respect to the porosity. The filter porosity is assumed to have a fairly high porosity representing a well sorted material (see /Bear 1972/), whereas the crushed rock filling is regarded to be a poorly sorted material. The value chosen for the filling material was also obtained in the Backfill and Plug Test /Gunnarsson et al. 2001/.

The retention curves for both materials are assumed to be similar to the properties of fine sand with a plateau at 3 kPa /Bear 1972/ see Figure 10-25 (right). The hydraulic conductivity is assumed to be very high, while a perfectly mobile law is assumed for the relative permeability.

The adoption of elastic parameters for the filter material was based on results from compression tests with construction sand /Åkesson 2006/. Two alternative sets of initial porosity and Young modulus are adopted (Figure 10-26).
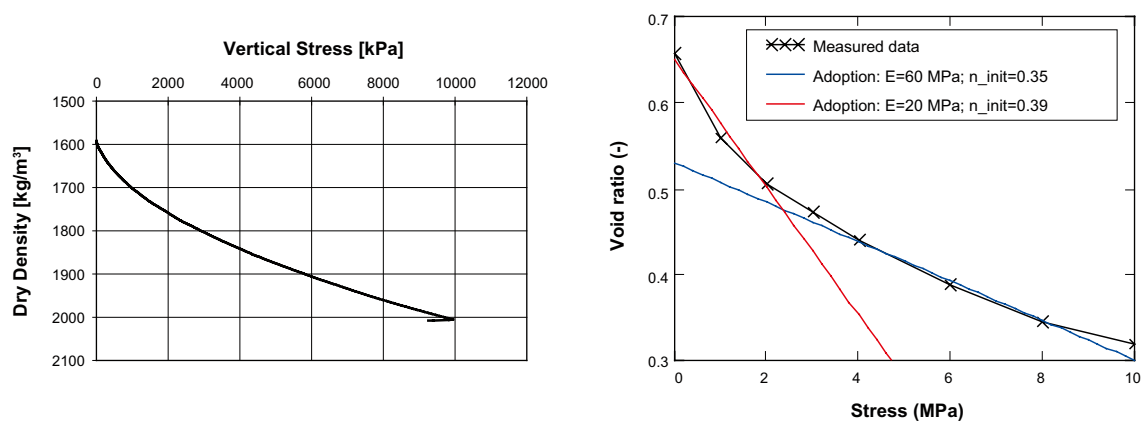
Figure 10-26. Adoption of elastic parameters for construction sand. Measured data from /Åkesson 2006/.

Table 10-8. Data used for crushed rock components and rock materials.

Parameter		Crushed rock		Rock materials		
		Plug filter	Filling	Rock matrix	Fracture material	EDZ
Porosity	n (–)	0.35/0.39	0.18	0.003	0.003	0.003
Intrinsic permeability	k (m^2)	1E–15	1E–15	1E–18 – 1E–20	Specified	1E–15
Relative permeability	k_r (–)	1	1	vG: λ=0.6	vG: λ=0.6	vG: λ=0.6
Water retention curve	P_0 (MPa) λ (–)	3E–3 0.9	3E–3 0.9	1.74 0.6	1.74 0.6	1.74 0.6
Elastic parameters	E (MPa) v (–)	60/20 0.2	–	–	–	–

10.3.4 Rock

The parameter value adoption for rock material is special in the sense that the properties display a significant spatial variability and that they are largely site-specific. These parameters also have special roles in the modelling tasks.

For example, the thermal evolution around a deposition hole can not be truly modelled unless in principle all canisters in the repository are represented in the model. For efficiency however, models for calculation of the hydration time only include one canister. And in order to model a relevant thermal evolution, the boundary conditions have to be set from a large-scale analytical thermal model. This procedure may also necessitate a calibration of the thermal transport properties, i.e. thermal conductivity, specific heat and density. There is thus no motive for the prescription of such properties. Standard values (from /TEFYMA 1982/) for density, thermal conductivity and specific heat are therefore given in Table 10-10.

The hydraulic transport properties display an even larger variability (and scale dependence) than the thermal properties. For example, profiles of evaluated equivalent continuous porous medium (ECPM) hydraulic conductivity from the Forsmark area, presented by /Follin et al. 2007/, in general shows values down to 10^{-11} (m/s) below a depth of 400 m. This value is also used as a minimum value for the hydraulic rock domain (HRD) within the fracture domains in hydraulic conductor domain (HCD) models. In contrast, measurements on core samples from the Forsmark area /Vilks 2007/, in general show values in the range 10^{-13}–10^{-12} (m/s). On the other hand, evaluated hydraulic conductivities from so-called "rock blocks" at Äspö /Vidstrand 2003/ in general show values in the range 10^{-8}–10^{-6} (m/s). This variability thus requires a sensitivity analysis, and it is left to the modelers to analyze relevant ranges for the *un-fractured rock matrix*, at least between 10^{-13} and 10^{-11} (m/s).

Two other types of rock material are foreseen in the modelling tasks: *fractures* (a material representing a single fracture with a given transmissivity), and *excavation damaged zone (EDZ)*. These materials are assumed to exhibit the same properties, except regarding the intrinsic permeability, and are summarized in Table 10-8. The fracture transmissivity is treated as a part of the boundary condition (yielding a certain inflow) and should thereby be analysed for the different task. The hydraulic conductivity for the EDZ has been found to be in the order of 10^{-8} m/s /Bäckblom 2008/.

Reported retention curves and relative permeability parameters are shown in Table 10-9 and Figure 10-27. Among these, only the data given by /Finsterle and Pruess 1995/ appears to be based on actual measurements (in Grimsel). These data are therefore proposed for the modelling tasks. The porosity chosen for all rock material (Table 10-8) is representative for experimental data from Laxemar /Byegård et al. 2006/.

Table 10-9. Reported retention and relative permeability data for granitic rock.

Source	P_0 (MPa)	λ (–)	Relative permeability
/Börgesson and Hernelind 1999/	4	0.65	Power law; δ=3
/Thomas et al. 2003/	0.7	0.33	van Genuchten law; λ=0.33
/Finsterle and Pruess 1995/	1.74	0.60	van Genuchten law; λ=0.60
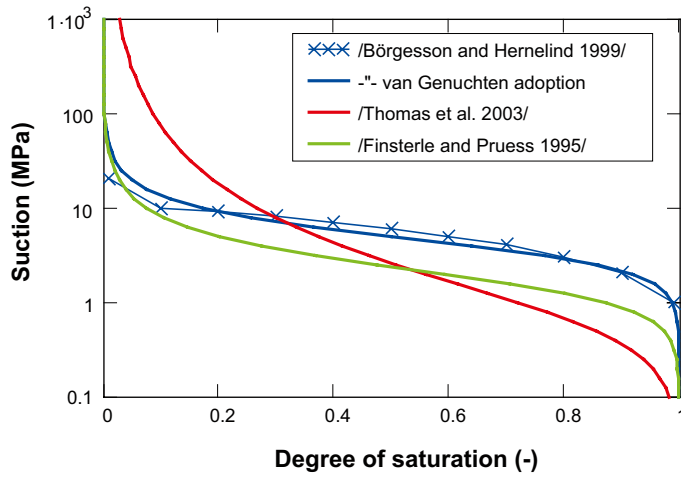
Figure 10-27. *Reported retention curves for granitic rock.*

10.3.5 Copper and cast iron

Only the density and the thermal properties are of relevance for copper and cast iron. These parameters are summarized in Table 10-10 and were taken from /TEFYMA 1982/.

Table 10-10. Thermal data for copper, cast iron and rock.

Parameter		Copper	Cast iron	Rock
Density	ρ (kg/m^3)	8,930	5,700–7,200	2,700
Specific heat	c (J/kgK)	390	500	800
Thermal conductivity	λ (W/mK)	390	30–50	3.5

11 Judgement of the SR-Site team

In this chapter the data supplied is examined by the SR-Site team.

- Sources of information and documentation of data qualification

There are many very well qualified sources of information regarding the thermo-hydro-mechanical properties of the reference buffer material MX-80. A problem might be that many of them are reports, which are not examined according to the new QA system of SKB. Another problem might be that some of the reports are not printed yet, but those reports will undergo such examination before approval.

There is a lack of information regarding the new reference backfill Milos Backfill. The reason is of course that it has recently been appointed reference material. Laboratory tests are ongoing and unpublished data indicate that the thermo-hydro-mechanical properties are very similar to those of MX-80. On this reason the data of MX-80 adapted to the initial conditions of the backfill will be used for the SR-Site modelling. The lack of information can partly be compensated by doing sensitivity analyses. If the ongoing tests reveal that there are some critical data used that are not covered by those analyses new analyses have to be done.

- Conditions for which data are supplied

The data supplied for MX-80 is considered to cover the relevant conditions in a repository regarding temperature, water content, density and chemical conditions. There are however, a few exceptions, which are commented in Chapter 5. In addition the following can be mentioned:

Long time creep data are lacking for the canister sinking calculations. However, this will be compensated by a very wide sensitivity analysis that will show the small influence of creep on the sinking.

The effect of possible but not probable long time chemical influences on the mechanical properties of the buffer is not known. Since the water saturation and homogenisation are completed long before any chemical effects will take place, the influence is for most cases not important. It may however affect the homogenisation after chemical erosion of bentonite colloids and the stiffness of the bentonite during a rock shear through a deposition hole. Those uncertainties may induce problems that have to be considered in SR-Site.

- Conceptual uncertainty

As noted in Chapter 6 the main conceptual uncertainties are the vapour transport model and the mechanical model for unsaturated materials. The models of Code_Bright and Abaqus also differ substantially in those cases. Especially the mechanical models are uncertain. Although, better understanding is desirable the impact of these uncertainties is not strong on the long term safety. Regarding the water transport uncertainty, it is widely governed by the rock hydrology and the vapour transport is only important at very dry rock conditions. The uncertainty of the mechanical models is mainly affecting the path to full saturation and the final state after full saturation and homogenisation but the final state can also be modelled with the assumption that the material is saturated since the stress path does not affect the final state very much.

- Data uncertainty due to precision, bias, and representativity

The uncertainty of some important parameters that can be directly measured has been thoroughly discussed in Chapter 7. As mentioned the uncertainty of the parameters that need to be indirectly evaluated is larger and those uncertainties have not been considered, which of course is a problem. All parameters in general and especially the indirectly measured ones need to be validated by modelling both small scale tests and large scale tests and compare modelled results with measured results. Such validation is ongoing e.g. in the Äspö Task Force for Engineered Barrier Systems and needs to be continued.

The data uncertainty is mainly treated in SR-Site by sensitivity analyses and conservative assumptions where appropriate.

- Spatial and temporal variability

According to Chapter 8 there is no spatial and temporal variability in the parameter values. The reason is the extensive control program at delivery and manufacturing of the buffer and backfill materials, which guarantees that the variation is small and within the acceptance margins. However, there is a stronger variability in rock geometry and properties that may affect the modelling results. This variability is taken into account by sensitivity analyses and conservative assumptions where appropriate.

- Correlations

Since no probabilistic analyses are done such correlations are not considered. Any probabilistic variation in data is instead taken into account by sensitivity analyses and conservative assumptions where appropriate.

- Results of supplier's data qualification

In Chapter 10 the data supplier has (based on available data) made a very good analyses and choice of data that should be used in the SR-Site modelling regarding both parameters that are directly and indirectly measurable. It should be emphasised, as mentioned earlier, that (except for making more laboratory tests) the main tool for strengthening the data credibility is to do verification modelling and that uncertainties are treated with sensitivity analyses and conservative assumptions where appropriate.

12 Data recommended for use in the SR-Site modelling

12.1 Code_Bright data for MX-80

Table 12-1. Data used for different MX-80 buffer materials (Code_Bright).

		Buffer ring e=0.571 w=17%	Buffer block e=0.626 w=17%	Buffer pellets e=1.780 w=10%
Thermal conductivity†	λ_{dry} λ_{sat} (W/mK)	0.7 1.3	0.7 1.3	0 1.3
Specific heat for solid	c (J/kgK)		800	
Intrinsic permeability	k_0 (m^2) n_0 (–) b (–)	1.2E–21 0.363 21.3	2.0E–21 0.385 21.3	5.2E–19 0.64 21.3
Relative permeability	k_r (–)	S_r^3	S_r^3	*
Vapour diffusion tortuosity	τ (–)		1	
Water retention curve	P_0 (MPa) λ (–)	67.2 0.48	43.5 0.38	0.508 0.26
Target void ratio		0.77	–	0.77
Porous elasticity	κ_{i0} (–) α_i α_{ils} K_{min} (MPa)	0.12–0.15 –0.02 0 ≤20	–	0.12–0.15 –0.01 0 ≤20
Swelling modulus	κ_{s0} (–) α_{ss} (–) α_{sp} p_{ref} (MPa)	0.3 0 ** 1	–	0.3 0 ** 0.1
Poisson's ratio	v (–)		0.2	
Plastic stress strain modulus	λ_0 (–) r (–) β (MPa^{-1})	0.156‡ 0 0	–	0.330 0 0
Critical state line parameter	M (–)	0.24	–	0.55
Tensile strength	p_{s0} (MPa) k (MPa^{-1})	2.2 0	–	0.05 0
Pre-consolidation stress	p_0^* (MPa) p_c (MPa)	20 1	–	≤0.88 1
Non-associativity parameter	α (–)		0.5	
Partice density	ρ_s (kg/m^3)		2,780	

* An alternative approach should be applied for pellets material.

** The α_{sp}-parameter is replaced with an inbuilt swelling pressure relation.

† Alterative parameter values and saturation dependence should be used if the degree of saturation is found to be below 50% (see Section 10.2.1).

‡ Higher values can be motivated (see Section 10.2.8).

Table 12-2. Data used for different MX-80 backfill materials (Code_Bright).

Parameter	Symbol	Backfill block e=0.635 w=17%			Backfill Pellets e=1.780 w=17%		
Thermal conductivity†	λ_{dry}	0.7			0		
	λ_{sat} (W/mK)	1.3			1.3		
Specific heat for solid	c (J/kgK)	800					
Intrinsic permeability	k_0 (m²)	2.1E–21			5.2E–19		
	n_0 (–)	0.388			0.64		
	b (–)	21.3			21.3		
Relative permeability	k_r (–)	S_r^3			*		
Vapour diffusion tortuosity	τ (–)	1					
Water retention curve	P_0 (MPa)	37.2			0.162		
	λ (–)	0.34			0.19		
Target void ratio		0.74	0.83	0.91	0.74	0.83	0.91
Porous elasticity	κ_{i0} (–)	0.12–0.15			0.12–0.15		
	α_i	–0.02			–0.02		
	α_{ils}	0			0		
	K_{min} (MPa)	≤20			≤20		
Swelling modulus	κ_{s0} (–)	0.3			0.3		
	α_{ss} (–)	0			0		
	α_{sp}	**			**		
	p_{ref} (MPa)	1			0.1		
Poisson's ratio	ν (–)	0.2					
Plastic stress strain modulus	λ_0 (–)	0.161‡	0.171‡	0.182‡	0.323	0.346	0.367
	r (–)	0	0	0	0	0	0
	β (MPa⁻¹)	0	0	0	0	0	0
Critical state line parameter	M (–)	0.24	0.25	0.27	0.55	0.55	0.55
Tensile strength	p_{s0} (MPa)	2.4	1.9	1.5	0.05	0.05	0.05
	k (MPa⁻¹)	0	0	0	0	0	0
Pre-consolidation stress	p_0^* (MPa)	23	15	10	≤0.88	≤0.88	≤0.88
	p_c (MPa)	1	1	1	1	1	1
Non-associativity parameter	α (–)	0.5					
Partice density	ρ_s (kg/m³)	2,780					

* An alternative approach should be applied for pellets material.

** The α_{sp}-parameter is replaced with an inbuilt swelling pressure relation.

† Alterative parameter values and saturation dependence should be used if the degree of saturation is found to be below 50% (see Section 10.2.1).

‡ Higher values can be motivated (see Section 10.2.8).

Table 12-3. Data used for homogenized MX-80 materials, only thermal and hydraulic parameters (Code_Bright).

Parameter		Homog. Buffer e=0.72 w=17%	Homog. Buffer e=0.77 w=17%	Homog. Backfill e=0.74 w=17%	Homog. Backfill e=0.91 w=17%	Bore-hole seal (block) e=0.46 w=6%	Bore-hole seal (hom) e=0.82 w=6%
Thermal conductivity†	λ_{dry}	0.7	0.7	0.7	0.7	0.7	0.7
	λ_{sat} (W/mK)	1.3	1.3	1.3	1.3	1.3	1.3
Specific heat for solid	c (J/kgK)			800			
Intrinsic permeability	k_0 (m²)	4.2E–21	6.0E–21	4.8E–21	1.5E–20	3.8E–22	8.3E–21
	n_0 (–)	0.419	0.435	0.425	0.476	0.315	0.451
	b (–)	21.3	21.3	21.3	21.3	21.3	21.3
Relative permeability	k_r (–)			S_r^3			
Vapour diffusion tortuosity	τ (–)			1			
Water retention curve	P_0 (MPa)	15.19	8.93	11.6	3.45	33.26	9.38
	λ (–)	0.25	0.22	0.23	0.20	0.37	0.35

† Alterative parameter values and saturation dependence should be used if the degree of saturation is found to be below 50% (see Section 10.2.1).

12.2 Abaqus data for MX-80

Table 12-4. Data used for the buffer in the water saturation phase analyses (ABAQUS).

Parameter/variable	Value	Comment
Thermal conductivity, λ	f(Sr, e)	1)
Specific heat, c	c = 800/(1+w)+4,200w/(1+w)	
Hydraulic conductivity, K	f(Sr, e, T)	2)
Thermal vapour flow diffusivity, DTv	f(Sr, e, T)	3)
Isothermal vapour flow diffusivity	Dpv = 0	
Water retention curve	u = f(Sr)	4)
Porous elasticity	κ = 0.2	
Moisture swelling data	f(Sr)	5)
Poisson ratio	v = 0.4	
Friction angle in p-q plane	β = 16°	Drucker Prager Plasticity model
Cohesion in p-q plane	d = 100 kPa	Drucker Prager Plasticity model
Dilation angle	ψ = 2°	Drucker Prager Plasticity model
Yield function	$\varepsilon_{pl} = f(q)$	6)
Particle density	2,780 kg/m³	

1) The thermal conductivity of the buffer material is a function of both e and S_r. The values used in the modelling of the saturation phase are shown in Table 12-5.

2) The hydraulic conductivity is at full water saturation a function of the temperature and the void ratio. Table 12-6 shows the values used in the model.

3) The water vapour flux is modelled as a diffusion process driven by the temperature gradient and the water vapour pressure gradient (at isothermal conditions) according to (6-3). The thermal water vapour diffusivity D_{Tv} is modelled according to Equations (6-4)–(6-6). D_{Tv} is also depending on the void ratio and the temperature. For the conditions of the reference material the following values have been used:

$D_{Tvb} = 0.7 \cdot 10^{-11}$ m²/s,K

4) The relation between suction and degree of saturation (water retention curve) is important for the wetting modelling. The actual relation is also a function of the void ratio and has been adapted to three different void ratios, corresponding to buffer rings, buffer blocks and homogenized buffer (Table 12-7).

5) The data for the moisture swelling procedure includes a long list of volumetric strain corrections $\Delta\varepsilon_v$. Figure 12-1 shows the relations derived for the rings (e=0.56), the blocks (e=0.636) and the brick filling on top of the canister (e=0.72).

6) The yield function describes the plastic strain as a function of von Mises stress q in the Drucker Prager plasticity model (Table 12-8).

Table 12-5. Thermal conductivity λ of the buffer material as a function of the degree of saturation Sr for three different void ratios.

Sr	λ (W/m,K) (e=0.5)	λ (W/m,K) (e=0.78)	λ (W/m,K) (e= 1.0)
0	0.4	0.3	0.2
0.2	0.4	0.3	0.2
0.3	0.5	0.4	0.3
0.4	0.65	0.55	0.45
0.5	0.85	0.75	0.65
0.6	1.05	0.95	0.85
0.7	1.2	1.1	1.0
0.8	1.3	1.2	1.1
0.9	1.35	1.25	1.15
1.0	1.4	1.3	1.2

Table 12-6. Hydraulic conductivity K at full saturation as a function of void ratio e and temperature T.

Void ratio	$K \cdot 10^{13}$ (m/s) (T=20°C)	$K \cdot 10^{13}$ (m/s) (T=40°C)	$K \cdot 10^{13}$ (m/s) (T=60°C)	$K \cdot 10^{13}$ (m/s) (T=80°C)
0.4	0.035	0.05	0.07	0.1
0.6	0.2	0.31	0.44	0.55
0.8	0.65	1.0	1.45	1.8
1.0	1.75	2.75	3.85	4.9

Table 12-7. Retention curves adopted for Abaqus calculations.

Suction (MPa)	Sr (–) e=0.56	Sr (–) e=0.636	Sr (–) e=0.78
295.1	0.163	0.143	0.117
149.7	0.458	0.403	0.328
71.2	0.755	0.665	0.542
65.4	0.770	0.680	0.555
54.5	0.800	0.700	0.570
47.5	0.820	0.720	0.590
37.0*	0.849	0.747	0.610
33.6	0.861	0.763	0.625
30.2	0.873	0.780	0.642
25.2	0.892	0.806	0.671
22.0	0.904	0.825	0.694
14.3	0.936	0.877	0.762
11.3	0.949	0.899	0.796
8.4	0.961	0.923	0.836
6.9	0.968	0.935	0.858
5.5	0.974	0.947	0.882
4.1	0.981	0.960	0.908
2.7	0.987	0.973	0.936
1.4	0.994	0.986	0.967
0.7	0.997	0.993	0.983
0	1	1	1

* = Initial value.

Table 12-8. Yield function.

q (kPa)	ε_{pl}
1	0
50	0.005
100	0.02
150	0.04
200	0.1
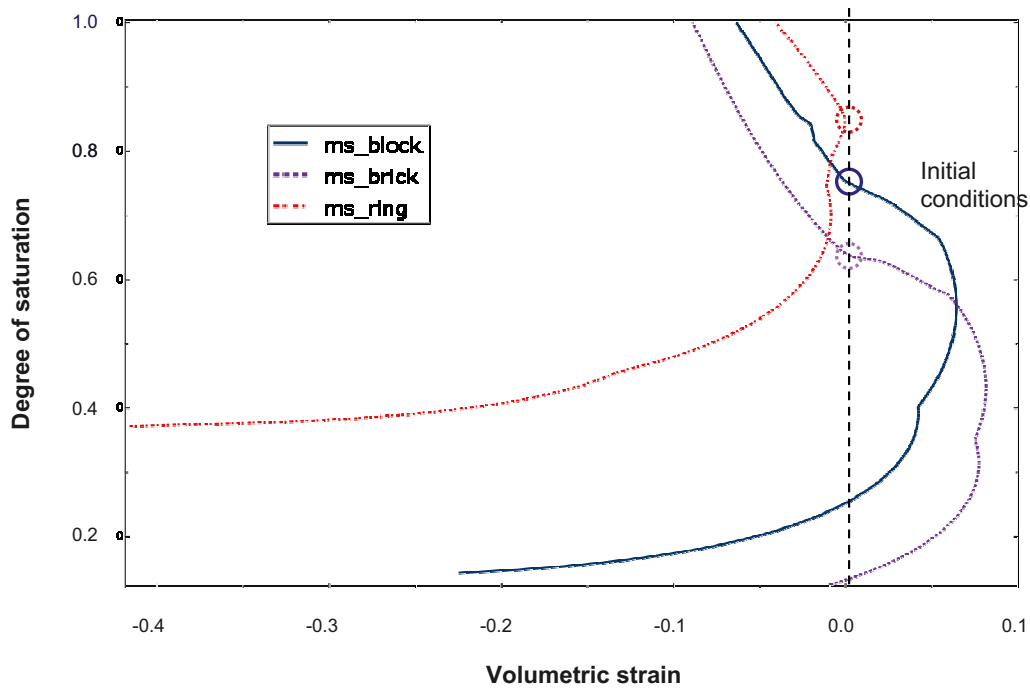
Figure 12-1. *Volume change correction $\Delta\varepsilon_v$ used in the moisture swelling procedure for the three different bentonite block types. The initial conditions are also noted in the figure.*

12.3 Data for other materials

Table 12-9. Hydro-mechanical data for concrete components.

Parameter		Tunnel plug	Bottom plate	Prefab beams
Porosity	n (–)	0.135	0.135	0.135
Intrinsic permeability	k (m²)	5E–19	5E–19	1E–15
Relative permeability	k_r (–)		S_r^3	
Water retention curve	P_0 (MPa)		9	
	λ (–)		0.3	
Elastic parameters	E (GPa)		35	
	v (–)		0.27	
Aggregates	(–)	0.67	0.67	–

Table 12-10. Hydro-mechanical data for crushed rock components and rock materials.

Parameter		Crushed rock		Rock materials		
		Plug filter	Filling	Rock matrix	Fracture material	EDZ
Porosity	n (–)	0.35/0.39	0.18	0.003	0.003	0.003
Intrinsic permeability	k (m²)	1E–15	1E–15	1E–18 – 1E–20	Specified	1E–15
Relative permeability	k_r (–)	1	1	vG: λ=0.6	vG: λ=0.6	vG: λ=0.6
Water retention curve	P_0 (MPa)	3E–3	3E–3	1.74	1.74	1.74
	λ (–)	0.9	0.9	0.6	0.6	0.6
Elastic parameters	E (MPa)	60/20	–	–	–	–
	v (–)	0.2				

Table 12-11. Thermal data for copper, cast iron and rock.

Parameter		Copper	Cast iron	Rock
Density	ρ (kg/m^3)	8,930	5,700–7,200	2,700
Specific heat	c (J/kgK)	390	500	800
Thermal conductivity	λ (W/mK)	390	30–50	3.5

13 References

ABAQUS manuals, 2008. Dassault Systems Simulia Corp, ABAQUS Inc.

Bear J, 1972. Dynamics of fluids in porous media. Dover Publications, New York.

Betonghandbok, 1994. Material. Utgåva 2, Svensk Byggtjänst, Solna.

Byegård J, Gustavsson E, Tullborg E-L, 2006. Bedrock transport properties. Data evaluation and retardation model. Preliminary site description. Laxemar subarea – version 1.2. SKB R-06-27, Svensk Kärnbränslehantering AB.

Bäckblom G, 2008. Excavation damage and disturbance in crystalline rock – results from experiments and analyses. SKB TR-08-08, Svensk Kärnbränslehantering AB.

Börgesson L, 1986. Model shear tests on canisters with smectite clay envelopes in deposition holes. SKB TR 86-26, Svensk Kärnbränslehantering AB.

Börgesson L, Fredrikson A, Johannesson L-E, 1994. Heat conductivity of buffer materials. SKB TR 94-29, Svensk Kärnbränslehantering AB.

Börgesson L, Sandén T, 2006. Piping and erosion in buffer and backfill materials. Current knowledge. SKB R-06-80, Svensk Kärnbränslehantering AB.

Börgesson L, Johannesson L-E, Sandén T, Hernelind J, 1995. Modelling of the physical behavior of water saturated clay barriers. SKB TR 95-20, Svensk Kärnbränslehantering AB.

Börgesson L, Hernelind J, 1999. Coupled thermo-hydro-mechanical calculations of the water saturation phase of a KBS-3 deposition hole. SKB TR-99-41, Svensk Kärnbränslehantering AB.

Börgesson L, 2001. Compilation of laboratory data for buffer and backfill materials in the Prototype repository. SKB IPR-01-34, Svensk Kärnbränslehantering AB.

Börgesson L, Johannesson L-E, Hernelind J, 2003. Earthquake induced rock shear through a deposition hole. Effect of the canister and the buffer. SKB TR-04-02, Svensk Kärnbränslehantering AB.

Börgesson L, Johannesson L-E, 2006. Consequences of upwards swelling from a wet deposition hole into a dry tunnel with backfill made of blocks – A preliminary study. SKB TR-06-12, Svensk Kärnbränslehantering AB.

Börgesson L, Hernelind J, 2006A. Canister displacement in KBS-3V – A theoretical study. SKB TR-06-04, Svensk Kärnbränslehantering AB.

Börgesson L, Hernelind J, 2006B. Consequences of loss or missing bentonite in a deposition hole. A theoretical study. SKB TR-06-13, Svensk Kärnbränslehantering AB.

Börgesson L, Hernelind J, 2006C. Earthquake induced rock shear through a deposition hole. Influence of shear plane inclination and location as well as buffer properties on the damage caused to the canister. SKB TR-06-43, Svensk Kärnbränslehantering AB.

Börgesson L, Fälth B, Hernelind J, 2006. Water saturation phase of the buffer and backfill in the KBS-3V concept. Special emphasis given to the influence of the backfill on the wetting of the buffer. SKB TR-06-14, Svensk Kärnbränslehantering AB.

CIMNE, 2002. Code_Bright user's guide, Departamento de Ingeniería del Terreno, Universidad Politécnica de Cataluña.

Chen G J, Ledesma A, 2009. Coupled Thermohydromechanical modeling of the Full-Scale In Situ Test "Prototype Repository". Journal of Geotechnical and Geoenvironmental Engineering, 135, 121–132.

Dahlström L-O, Magnusson J, Gueorguiev G, Johansson M, 2009. Feasibility study of a concrete plug made of low pH concrete. SKB R-09-34, Svensk Kärnbränslehantering AB.

Dueck A, 2004. Hydro-mechanical properties of a water unsaturated sodium bentonite. Laboratory study and theoretical interpretation. Ph. D. thesis, Lund University, Sweden.

Dueck A, 2010. Thermo-mechanical cementation effects in bentonite investigated by unconfined compression tests. SKB TR-10-41, Svensk Kärnbränslehantering AB.

Dueck A, Nilsson U, 2010. Thermo-Hydro-Mechanical properties of MX-80. Results from advanced laboratory tests. SKB TR-10-55, Svensk Kärnbränslehantering AB.

Dueck A, Börgesson L, Johannesson L-E, 2010. Stress-strain relation of bentonite at undrained shear – Laboratory tests to investigate the influence of material composition and test technique. SKB TR-10-32, Svensk Kärnbränslehantering AB.

Finsterle S, Pruess K, 1995. Solving the estimation-identification problem in two-phase flow modeling. Water Resour. Res. 31(4), 913–924.

Follin S, Johansson P-O, Hartley L, Jackson P, Roberts D, Marsic N, 2007. Hydrogeological conceptual model development and numerical modelling using CONNECTFLOW, Forsmark modelling stage 2.2. SKB R-07-49, Svensk Kärnbränslehantering AB.

Gailhanou H, van Miltenburg J C, Rogez J, Olives J, Amouric M, Gaucher E C, Blanc P, 2007. Thermodynamic properties of anhydrous smectite MX-80, illite IMt-2 and mixed-layer illite-smectite ISCz-1 as determined by calorimetric methods. Part I: Heat capacities, heat contents and entropies. Geochimica et Cosmochimica Acta, 71, 5463–5473.

Gunnarsson D, Börgesson L, Hökmark H, Johannesson L-E, Sandén T, 2001. Report on the installation of the Backfill and Plug Test. SKB IPR-01-17, Svensk Kärnbränslehantering AB.

Hedenblad G, 1996. Materialdata för fukttransportberäkningar. Byggforskningsrådet. T19:1996.

Hedin A, 2004. Integrated near-field evolution model for a KBS-3 repository. SKB R-04-36, Svensk Kärnbränslehantering AB.

Hökmark H, 2004. Hydration of the bentonite buffer in a KBS-3 repository. Applied Clay Science, 24, 219–233.

Hökmark H, Lönnqvist M, Kristensson O, Sundberg J, Hellström G, 2009. Strategy for thermal dimensioning of the final repository for spent nuclear fuel. SKB R-09-04, Svensk Kärnbränsle-hantering AB.

Johannesson L-E, Börgesson L, Sandén T, 1995. Compaction of bentonite blocks. SKB TR 95-19, Svensk Kärnbränslehantering AB.

Johannesson L-E, Nilsson U, 2006. Deep repository – Engineered barrier systems. Geotechnical behaviour of candidate backfill materials – Laboratory tests and calculations for determining performance. SKB R-06-73, Svensk Kärnbränslehantering AB.

Johannesson L-E, Sandén T, Dueck A, Ohlsson L, 2010. Characterization of backfill candidate material, IBECO-RWC-BF. Baclo project – phase 3, Laboratory tests. SKB R-10-44, Svensk Kärnbränslehantering AB.

Kahr G, Müller-Vonmoos M, 1982. Wärmeleitfähigkeit von bentonit MX80 und von Montigel nach der heizdrahtmethode. Nagra. NTB 82-06.

Kahr G, Kraehenbuehl F, Stoeckli H F, Müller-Vonmoos M, 1990. Study of the Water-Bentonite System by vapour adsorption, immersion calometry and X-ray techniques: II. Heats of immersion, swelling pressures and thermodynamic properties. Clay Minerals, 25, 499–506.

Karnland O, Sandén T, Johannesson L-E, 2000. Long term test of buffer material. SKB TR-00-22, Svensk Kärnbränslehantering AB.

Karnland O, Muurinen A, Karlsson F, 2005. Bentonite swelling pressure in NaCl solutions – Experimental determined data and model calculations. In: Alonso and Ledesma (Eds), Advances in Understanding Engineering Clay Barriers, London, 241–254.

Karnland O, Olsson S, Nilsson U, 2006. Mineralogy and sealing properties of various bentonites and smectite-rich clay materials. SKB TR-06-30, Svensk Kärnbränslehantering AB.

Karnland O, Nilsson U, Weber H, Wersin P, 2008. Sealing ability of Wyoming bentonite pellets foreseen as buffer material – Laboratory results. Physics and Chemistry of the Earth, 33, 472–475.

Karnland O, Olsson S, Dueck A, Birgersson M, Nilsson U, Hernan-Håkansson T, Pedersed K, Nilsson S, Eriksen T E, Rosborg B, 2009. Long term test of buffer material at the Äspö Hard Rock Laboratory, LOT project. Final report on the A2 test parcel. SKB TR-09-29, Svensk Kärnbränslehantering AB.

Kristensson O, Åkesson M, 2008. Mechanical modeling of MX-80 – Quick tools for BBM parameter analysis. Physics and Chemistry of the Earth, 33, 508–515.

SKB, 2006. Data report for the safety assessment SR-Can. SKB TR-06-25, Svensk Kärnbränslehantering AB.

SKB, 2010. Data report for safety assessment SR-Site. SKB TR-10-52, Svensk Kärnbränslehantering AB.

TEFYMA, 1982. Handbok för grundläggande teknisk fysik, fysik och matematik. Ingelstam, Rönneberg och Sjöberg. Sjöbergs förlag, Stockholm/Bromma.

Thomas H R, Cleall P J, Chandler N, Dixon D, Mitchell H P, 2003. Water infiltration into a large-scale in-situ experiment in an underground research laboratory. Geotechnique, 53, 207–224.

Vidstrand P, 2003. Update of hydrogeological model 2002. SKB IPR-03-35, Svensk Kärnbränslehantering AB.

Vilks P, 2007. Forsmark site investigation. Rock matrix permeability measurements on core samples from borehole KFM01D. SKB P-07-162, Svensk Kärnbränslehantering AB.

Wadsö L, Svennberg K, Dueck A, 2004. An experimentally simple method for measuring sorption isotherms. Drying Technology, 22(10), 2427–2440.

Åkesson M (ed), 2006. Temperature buffer test. Evaluation modelling – Field test. SKB IPR-06-10, Svensk Kärnbränslehantering AB.

Summary of modelling tasks

Table A-1. Models of buffer and backfill in SR-Site.*

	Objective	SR-Can model	SR-Site model
T	1. Peak temperature calculations	/Hedin 2004/	Several T models. /Hökmark et al. 2009/ STD report on review.
H	2. Analysis of time-scale of backfill hydration	/Börgesson et al. 2006/	2D axis symmetric H(M) model: Block and pellets or Homogenized bentonite. 2D plane strain H(M) model: Block and pellets or Homogenized bentonite. Possibly also diffusion of dissolved oxygen.
TH	3. Analysis of time-scale of buffer hydration	/Börgesson and Hernelind 1999/ /Börgesson et al. 2006/	2D axis symmetric TH model: Block and pellets or Homogenized bentonite.
	4. Analysis of moisture-redistribution in dry rock	No model	2D axis symmetric TH model: Block and pellets. Input to model 1. Analysis of dehydration of rock due to ventilation.
THM	5. Buffer homogenisation	No model	1D axis-symmetric THM models – CRT test (Code_Bright & Abaqus). Uneven pressure distributions.
HM	6. Homogenisation of erosion damages	/Börgesson and Hernelind 2006B/	Models from SR-Can will be updated. If ongoing tests imply that the material model should be modified. Possibly also with new input from erosion calculations (less mass erosion):
	7. Backfill homogenisation	No model	1D axis-symmetric HM model (if M is not included in model 2).
	8. Buffer upward swelling	/Börgesson et al. 2006/ /Börgesson and Johannesson 2006/	3D hydro-mechanical Abaqus models. (Possibly also axis-symmetric 2D mechanical Code_Bright models).
	9. Canister sinking	/Börgesson and Hernelind 2006A/	No new model.
	10. Rock shear through a deposition hole	/Börgesson et al. 2003/	This task is part of the modelling work for the canister.
	11. Piping and erosion	Brief description in /Börgesson and Sandén 2006/	A model of erosion rate is under development.

* The descriptions were prepared before the data qualification process and do not necessarily correspond exactly to the actual modeling work.

Table A-2. Models of other system components in SR-Site.*

	Objective	SR-Can model	SR-Site model
H	12. Analysis of time-scale of tunnel plug hydration	No	2D axis-symmetric H Code_Bright model. Time-scale: from plug completion to full saturation.
	13. Hydraulic modelling of the sealing ability of the tunnel plug	No	2D axis-symmetric H Code_Bright model. Influence of EDZ and fractures.
	14. Analysis of time-scale of central area etc and top seal hydration	No ?	Simplified 2D axis-symmetric H Code_Bright model. Time-scale: from top seal completion to full saturation.
	15. Analysis of time-scale of bore-hole seal hydration	No	2D axis-symmetric H Code_Bright model. Time-scale: from seal completion to full saturation.
HM	16. Homogenisation of tunnel plug	No	2D axis-symmetric HM Code_Bright model. Time-scale: from plug completion to full saturation.
	17. Backfill swelling after tunnel plug disintegration	No	2D axis-symmetric HM Abaqus model.
	18. Bottom plate 1 Lifting of package	No	Special/analytical analysis.
	19. Bottom plate 2 Buffer swelling after concrete disintegration	No	2D axis-symmetric HM Abaqus model.
	20. Homogenization of bore-hole seals	No	Special/Analytical analysis.
	21. Homogenization of bore-hole seals after loss of bentonite	No	Special/Analytical analysis.

* The descriptions were prepared before the data qualification process and do not necessarily correspond exactly to the actual modeling work.

Evaluated data from oedometer tests

Compression/unloading tests have been performed in oedometers kept at constant relative humidity /Dueck and Nilsson 2010/. Corresponding tests at saturated and drained conditions were presented by /Börgesson et al. 1995/. Different axial loads have been applied, while the deformation and the radial stress have been measured. The net mean stress, p', can thus be derived as $(\sigma_{ax}+2\cdot\sigma_{rad})/3$, where σ_{ax} and σ_{rad} are the measured axial and radial stresses, respectively.

Swelling/shrinkage /Dueck and Nilsson 2010/ tests have also been performed in oedometers kept at constant axial load. Different RH levels and axial stresses have been applied, while the deformation and the radial stress have been measured.

The porous-elastic module κ_i was evaluated by the relation:

$$\kappa_i = -\frac{\Delta e}{\Delta \ln p} \qquad (B-1)$$

The same relation was used for estimation of the plastic module λ, although this is only valid for isotropic conditions. Data on axial and radial stresses was used to evaluate the Poisson ratio, ν.

$$\nu = \frac{\Delta \sigma_{rad}}{\Delta \sigma_{ax} + \Delta \sigma_{rad}} \qquad (B-2)$$

The swelling module κ_s was evaluated by the relation:

$$\kappa_s = 3 \cdot \frac{1-\nu}{1+\nu} \cdot \frac{-\Delta e}{\Delta \ln(s + 0.1)} \qquad (B-3)$$

It can be noticed that the module is dependent on ν, since the test conditions are anisotropic. A value of 0.2 was used for ν. The factor $3(1-\nu)/(1+\nu)$ is thereby equal to 2.

Table B-1. Evaluation of porous-elastic modulus (κ_i). XMAR data from /Börgesson et al. 1995/, other data from /Dueck and Nilsson 2010/.

Test no	Value	Description
XMAR2	0.12	Unloading of saturated oedometer at void ratio 0.66
XMAR3	0.15	Unloading of saturated oedometer at void ratio 0.66
XMAR5	0.12	Unloading of saturated oedometer at void ratio 0.66
O4_0905	0.063, 0.063	Two of three load steps at 24 MPa suction
O4_1105	0.001, 0.062, 0.011, 0.009	Two of three load steps and two unload step at 28 MPa suction
O2_0905	0.054, 0.011	One of two load steps and one unload step at 41 MPa suction
O2_1005	0.069	One of two load steps at 6 MPa suction
O2_1105	0.017	One unload step at 17 MPa suction

Table B-2. Evaluation of swelling modulus (κ_s). Data from /Dueck and Nilsson 2010/.

Test no	Value	Description
O3_0905	0.025	Swelling at 20 MPa axial stress
O2_1205	0.057	Swelling (or shrinkage*) at 9 MPa axial stress
O2_1205*	0.064	–"–
O4_1005	0.080	–"–
O3_1105	0.073	–"–
O1_1005	0.281	Swelling at 1 MPa axial stress
O1_1105	0.213	–"–
O4_1205	0.334	Swelling at 0.24 MPa axial stress
O3_1005	0.289	Swelling (or shrinkage*) at 0.1–0.2 MPa axial stress
O3_1005*	0.192	–"–
O4_0705	0.366	–"–
O3_1205	0.261	–"–
O2_0705	0.300	–"–
O3_0705	0.376	–"–
O2_0905	0.280	–"–
O4_0905	0.299	–"–
O2_1005	0.288	–"–
O2_1105	0.259	–"–
O4_1105	0.265	–"–

Table B-3. Evaluation of Poisson's ratio (v). Data from /Dueck and Nilsson 2010/.

Test no	Value	Description
O4_0905	0.10, 0.25	Two of three load steps at 24 MPa suction
O4_1105	n.d., 0.25, 0.19, 0.35	Two of three load steps and two unload step at 28 MPa suction
O2_0905	0.17, 0.2	One of two load steps and one unload step at 41 MPa suction
O2_1005	0.18	One of two load steps at 6 MPa suction
O2_1105	0.26	One unload step at 17 MPa suction

Table B-4. Evaluation of plastic stress-strain modulus (λ). XMAR data from /Börgesson et al. 1995/, other data from /Dueck and Nilsson 2010/.

Test no	Value	Description
XMAR2	0.23	Loading of saturated oedometer at void ratio 0.89–0.78
XMAR5	0.18	Loading of saturated oedometer at void ratio 0.89–0.71
XMAR4	0.48	Loading of saturated oedometer at void ratio 2.1–1.5
XMAR4	0.34	Loading of saturated oedometer at void ratio 1.5–1.04
XMAR4	0.25	Loading of saturated oedometer at void ratio 1.04–0.77
O4_0905	0.127	One of three load steps at 24 MPa suction
O4_1105	0.110	One of three load steps at 28 MPa suction
O2_0905	0.115	One of two load steps at 41 MPa suction
O2_1005	0.107	One of two load steps at 6 MPa suction
O2_1105	0.125	One load steps at 17 MPa suction
O3_0705	0.157	One load step at 42 MPa suction
O2_0705	0.097	One load step at 42 MPa suction

Code modification for pressure dependence of kappa_s

```
*
********************************************************************
* Calculates the poroelastic parameter kappa_s in BBM
*
* Output: xk_s (kappa_s)
*
* Input: itycl_21 (not used)
*        parcl_21 (vector with parameters)
*        p_mean (net mean stress)
*        s (suction)
*        e (void ratio)
*
* Developed by UPC
* Modified by Ola Kristensson, Clay Technology, 2009-02-03
*
********************************************************************
      subroutine comp_ks(itycl_21,parcl_21,p_mean,s,e,xk_s)
c
      implicit real*8 (a-h,o-z)
      common /dimcl/mnp,ncl,npflux,nfluxtype,nvdvn,ndvn,ndve,nq
c
      dimension parcl_21(mnp)
c
c Unpack the parameters and set the solid density
      xk_s0=parcl_21(2)
      alphasp=parcl_21(9)
      pref=parcl_21(10)
      alphass=parcl_21(6)
      s_dens   = 2780             ! Read from parcl_10(2)in the future
c
c Calculate the pressure dependent term
      if (abs(alphasp).ge.1.0d-10) then
       aux=p_mean
       if (aux.lt.pref) then
         factorp = 1.0d0
       elseif (aux.gt.p_swell(e,s_dens)) then
         factorp = 1.0d-20
       else
         factorp = 1.d0 - dlog(aux/pref)/dlog(p_swell(e,s_dens)/pref)
       endif
c
c Old expression
c       if (aux.lt.1e-20)aux=1e-20
c       factorp=1.0d0+alphasp*dlog(aux/pref)
c       if (factorp.le.0.0d0) factorp=0.0d0
c
      else
       factorp=1.0d0
      endif
c
c Calculate the suction dependent term
      factors=dexp(alphass*s)
c
c Calculate kappa_s
      xk_s=xk_s0*factors*factorp
c
      return
      end
```

```
*
****************************************************************
* Swelling pressure function
*
* Output: p_swell (swelling pressure)
*
* Input: e (void ratio)
*        s_dens (solid density)
*
* Developed by Ola Kristensson, Clay Technology, 2009-02-03
*
****************************************************************
      real*3 function p_swell(e,s_dens)
      implicit real*8 (a-h,o-z)
c
c Parameters in the swelling pressure function
      c0 = 1.229
      c1 = 7.969d-4
      c2 = 5.95d-7
c
c Calculate the dry density
      d_dens = s_dens/(1.d0+e)
c
c Calculate the swelling pressure
      p_swell = c0 + c1*d_dens + c2*d_dens**2
      p_swell = 10**(p_swell)/1d3
c
      return
      end
```

Constitutive laws for Code_Bright

Table D-1. Summary of used constitutive laws and equilibrium restrictions.

Equation	Variable name	Equation	Parameter relationships
Constitutive equations			
Darcy's law	Liquid advective flux	$$\mathbf{q}_l = -\frac{\mathbf{k}k_{rl}}{\mu_l}(\nabla p_l - \rho_l \mathbf{g})$$	$$k = k_0 \frac{n^3}{(1-n)^2}\frac{(1-n_0)^2}{n_0^3}$$ $$k = k_0 \exp(b(n-n_0))$$ $$k_{rl} = S_r^3$$ $$k_{rl} = \sqrt{S_r}\left(1-(1-S_r^{1/\lambda})^\lambda\right)^2$$
Fick's law	Vapour non-advective flux	$$\mathbf{i}_g^w = -(n\rho_g(1-S_r)D_m^w)\nabla\omega_g^w$$	$$D_m^w = \tau \cdot 5.9 \cdot 10^{-6}\frac{(273.15+T)^{2.3}}{p_g}$$
Fourier's law	Conductive heat flux	$$\mathbf{i}_c = -\lambda\nabla T$$	$$\lambda(S_r) = \lambda_{sat}S_r + \lambda_{dry}(1-S_r)$$ $$\lambda(S_r) = \lambda_{sat}{}^{S_r^n}\lambda_{dry}{}^{(1-S_r)^{\frac{1}{n}}}$$
Retention curve	Liquid degree of saturation	$$S_r(s) = \left(1+\left(\frac{s}{P_0}\right)^{\frac{1}{1-\lambda}}\right)^{-\lambda}$$ $$S_r(s) = \left(1+\left(\frac{s}{P_0}\right)^{\frac{1}{1-\lambda}}\right)^{-\lambda}\left(1-\frac{s}{P_1}\right)^{\lambda_1}$$	
Phase density	Liquid density Gas density	$$\rho_l(P_l,T) = \rho_{l0}\cdot\exp\left[\beta\cdot(P_l - P_{l0}) + \alpha\cdot T + \gamma\cdot\varpi_l^h\right]$$ $$\rho_g : ideal\ gas\ law$$	
Phase viscosity	Liquid viscosity	$$\mu_l = 2\cdot 10^{-12}\exp\left(\frac{1808.5}{273.15+T}\right)$$	
Mechanical constitutive model	Stress tensor	$$d\varepsilon = d\varepsilon^e(d\boldsymbol{\sigma}) + d\varepsilon^P(dp_0^*) + d\varepsilon^h(ds)$$	
Equilibrium restrictions			
Kelvin's law	Vapour pressure	$$RH = \frac{p_v}{p_v^{sat}} = \exp\left(\frac{-s\ M_w}{R(273.15+T)\rho_l}\right)$$	$$p_v^{sat} = 136075\exp\left(-\frac{5239.7}{273.15+T}\right)$$

Table D-2. Summary of used elasto-plastic laws (based on BBM).

Elastic strain increment:	$$d\boldsymbol{\varepsilon}^e = -\frac{1}{3}d\varepsilon_v^e \mathbf{I} + d\mathbf{e}^e$$
Elastic volumetric strain increment:	$$d\varepsilon_v^{\,e} = \frac{dp'}{K}, \quad K = \max\left\{\frac{(1+e)p'}{\kappa_i(s)}, K_{min}\right\}$$
Suction dependence of κ_i :	$$\kappa_i(s) = \kappa_{i0}\left[1+\alpha_i s\right]$$
Elastic deviatoric strain increment:	$$d\mathbf{e}^e = \frac{d\mathbf{s}}{2G}, \quad G = \frac{3(1-2\nu)}{2(1+\nu)}K$$

Plastic strain increment:	$$d\boldsymbol{\varepsilon}^p = d\Lambda\frac{\partial g}{\partial \boldsymbol{\sigma}}$$
Yield surface:	$$f = q^2 - M^2(p'+p_s)(p_0 - p')$$
Plastic potential:	$$g = \alpha q^2 - M^2(p'+p_s)(p_0 - p')$$
Tensile strength:	$$p_s(s) = ks$$
LC-curve:	$$p_0(s, p_0^{\;*}) = p^c\left(\frac{p_0^{\;*}}{p^c}\right)^{\frac{\lambda_0 - \kappa_{i0}}{\lambda(s) - \kappa_{i0}}}$$
Suction dependence of λ:	$$\lambda(s) = \lambda_0\left((1-r)\exp(-\beta s) + r\right)$$
Hardening law:	$$dp_0^{\;*} = \frac{1+e}{\lambda_0 - \kappa_{i0}}p_0^{\;*}d\varepsilon_v^p$$

Hydraulic strain increment:	$$d\boldsymbol{\varepsilon}^h = -\frac{1}{3}d\varepsilon_v^h \mathbf{I}$$
Hydraulic volumetric strain increment:	$$d\varepsilon_v^{\,h} = \frac{\kappa_s(p',e)}{(1+e)(s+p_{atm})}ds$$
Void ratio and pressure dependence of κ_s:	$$\kappa_s(p',e) = \kappa_{s0}f(p',e)$$

$$f(p',e) = \begin{cases} 1 & \text{if } p' < p_{ref} \\ 10^{-20} & \text{if } p' > p_{swell}(e) \\ 1 - \dfrac{\ln p' - \ln p_{ref}}{\ln(p_{swell}(e)) - \ln p_{ref}} & \text{otherwise} \end{cases}$$

$$p_{swell}(e) = 10^{\left[c_0 + c_1\frac{\rho_s}{1+e} + c_3\left(\frac{\rho_s}{1+e}\right)^2\right] - 3}$$